Turbidity Monitoring on Minnesota Construction Sites:

Insight into the Factors Influencing the Turbidity and TSS Relationship

A THESIS
SUBMITTED TO THE FACULTY OF THE GRADUATE SCHOOL OF THE
UNIVERSITY OF MINNESOTA
BY

REBEKAH LYNN PERKINS

IN PARTIAL FULFILLMENT OF THE REQUIREMENTS
FOR THE DEGREE OF
MASTER OF SCIENCE

Bruce N. Wilson
John S. Gulliver

May, 2013

Acknowledgements

First and foremost, I would like to thank the Minnesota Department of Transportation for funding this project and providing us with access to many of their talented employees for technical support. I am also very grateful that we were allowed to extend our project to their Arden Hills and Bloomington sites to gain more insight into the topic. I would like to thank the University of Minnesota as well, specifically the Department of Bioproducts and Biosystems Engineering, for the use of their laboratory facilities.

I would like to offer a sincere thank you to my two extremely talented graduate advisers, Bruce Wilson and John Gulliver. Your experience, guidance, and overall support throughout this project were invaluable. From the day I started this project to the day I finished, I know that I have grown as an engineer because of the resources you provided. For that, I will always be grateful.

To my parents, Bob and Joyce, thank you for the constant support and encouragement throughout my life. Thank you for always pushing me to be my best and guiding me through life's challenges. Thank you for being my biggest fans. To my brother Matt, thank you for the encouragement to further my education and the interest you took in my research. Also, thank you Aunt Carol for the support and encouragement during my time in Minnesota.

I would like to give a big thank you to Brad Hansen for providing technical support throughout the laboratory and field experiments. Because of your guidance, I was able to increase my knowledge of construction site practices, monitoring equipment, and equipment set up that will be useful in my future career.

Finally, a special thank you Dwayne Stenlund from the Minnesota Department of Transportation for taking time out of your busy schedule to collect the soil used in the laboratory experiment and guiding us through the Arden Hills construction site.

Abstract

Stormwater runoff from construction sites can transport eroded sediment to nearby water bodies degrading water quality and impairing biotic communities. The United States Environmental Protection Agency (EPA) is considering a turbidity limit for effluent stormwater on construction and demolition sites and is requesting data to support that limit (EPA, 2011). Laboratory protocols have been developed herein for studying the factors that impact turbidity from construction site soils. Experimental procedures include the use of a rainfall simulator to generate runoff and turbidity values from soils carefully packed in appropriate test boxes. Turbidity characteristics of fourteen different soils in Minnesota were investigated using the laboratory protocols. Trends in turbidity with sediment concentrations were well represented by power functions. The exponent of these power functions was relatively constant between soils and the log-intercept, or scaling parameter varied substantially among the different soils. Multiple soil properties were evaluated for each soil. An extensive regression analysis resulted in a model using percent silt, interrill erodibility, and maximum abstraction that best represented the intercept term. A power value of 7/5 was chosen to represent all soils.

A second laboratory experiment was performed to determine how particle settling affects the coefficients of the turbidity -TSS relationship. The scaling parameter increased with sediment deposition and the power value decreased.

Field studies on two construction sites in the Twin Cities of metropolitan area of Minnesota were performed for this project. Grab samples and continuously monitored turbidity were collected for each site. The grab samples also exhibited a strong power relationship between turbidity and TSS with similar coefficients as the laboratory samples. The laboratory relationships were also applied to the observed field conditions to demonstrate their usefulness in estimating turbidity, concentration, sediment load, and load reduction.

Table of Contents

List of Tables

List of Figures

Chapter One
Introduction

1.1 Background

Stormwater runoff from construction sites is a substantial source of non-point source pollution. This runoff contains eroded sediment from the exposed, barren ground which is often transported to nearby water bodies causing water quality impairment, degrading their biotic communities and filling up the water body with sediment. To mitigate these negative impacts, it is important to determine the mass of eroded sediment (the quantity to which standards are written) in runoff. The quickest and most cost effective method of doing so is to measure the turbidity of the runoff. Turbidity is an optical property of water associated with the light scattering properties of the particles suspended in water. This measurement can be used as a surrogate to determine the actual concentration of sediment in construction site runoff. A significant number of Minnesota water bodies are considered impaired due to high turbidity (EPA, 2013).

Although turbidity can be easily measured it still needs to be related to the actual total suspended sediment concentration (TSS) of sediment in the water. There have been numerous attempts at defining this relationship, but it continues to remain ambiguous. Several studies, most notably Holliday, Rasmussen, & Miller (2003), experimentally derived a power relationship for turbidity and TSS. Others, such as Patil, Barfield, & Wilber (2011) found a near perfect linear relationship. Many studies of this relationship have been done in rivers, causing additional skew due to large particles, organic matter, and microorganisms, or in very controlled bucket tests, much unlike an actual construction site. A suitable relationship between turbidity and TSS for Minnesota construction site runoff has yet to be defined.

The EPA is considering a turbidity limit for construction and demolition sites. Suitable guidelines are needed for contractors to be able to accurately and cost-effectively monitor the turbidity of the runoff from their construction sites. The results of this project will provide a better understanding of the turbidity response for Minnesota soils, which, in turn, will provide a basis for setting a suitable turbidity limit in Minnesota.

1.2 Outline of Thesis

The main objective of this study is to determine a general relationship between turbidity and TSS for Minnesota soils on construction sites that utilize soil properties which can be easily determined on a construction site. This relationship provides an estimation of the turbidity values and sediment loading that can be expected on a construction site. It also provides a simple way to compare the TSS loads on a site and the TSS loads corresponding to a turbidity standard.

A multitude of soils and runoff samples are required to create this relationship. Due to the lack of controlled weather conditions and limited field data, the study was performed in a laboratory, allowing for a controlled environment and a repeatable process. The experiment relied on the acquisition of fourteen soils from different regions of Minnesota. Synthetic runoff was created using a rainfall simulator. The runoff from these soils was thoroughly examined and used to investigate possible relationships between turbidity and TSS using common soil properties.

Further analysis of turbidity data was performed to determine the impact of particle settling on the derived turbidity and TSS relationship. This information is useful when considering how TSS changes on a construction site as it moves to the outlet of the drainage area. Often heavy particles, such as sand, will settle before they make it to the measurement site. Understanding and including the impact of this process improves the accuracy of the turbidity and TSS relationship.

The relationship developed in the laboratory was then applied to actual turbidity and sediment concentration data from local construction sites and data collected in the laboratory as a verification of estimated turbidity. Several useful applications of the relationship are described in detail.

Chapter Two
Literature Review

2.1 Introduction

Although turbidity is a simple measurement of light reflection, there are several complexities that need to be described to fully understand turbidity data. Turbidity meters use several different configurations, causing a disconnect between the turbidity readings of various units. There have been multiple attempts at defining a relationship between turbidity and TSS, but all differ due to variation in experimental set up and environmental variables. Literature was reviewed to better understand how to reduce the variation in turbidity readings for this experiment.

2.2 Turbidity Meters

A turbidity meter is a device that is comprised of at least one light source and one photo-detector. The light source is beamed through a sample, and the light is scattered as it interacts with the particles in the water and the water itself. The photo-detector then reads how much light reaches it and at what angle, thus determining the turbidity of the sample. There are many kinds of turbidity meters that not only vary physically, but also internally.

Maintaining accuracy is an important issue with turbidity readings. Turbidity measurements are more accurate if they do not rely on grab samples alone. If a grab sample is not taken at the right time during a rainstorm or at the right depth, the measured turbidity will not accurately represent the actual turbidity passing that point during the storm. Because of this, there are turbidity meters suited for different purposes such as laboratory work, portability, and field testing. Bench top turbidity meters are laboratory based meters that measure the turbidity of grab samples taken from the site. There are also portable turbidity meters. Portable meters measure the turbidity of grab samples, but are more durable for travelling and on-site weather conditions. There are also turbidity meters designed to continuously monitor and record turbidity on-site. These turbidity meters only measure turbidity at a point, and need to be positioned at optimal places at a

site. However, they capture the changes in turbidity as runoff occurs, creating a better temporal representation of turbidity (Sadar, 2007). For this project, grab samples of laboratory generated runoff from fourteen Minnesota construction site soils will be collected and analyzed with a bench top turbidity meter. Continuous turbidity data will be taken from two local construction sites using permanent field testing turbidity meters.

Beyond the actual uses of the device, a turbidity meter can have many different light/photo-detector set-ups. The U.S. Environmental Protection Agency (EPA) (1999) describes three standard turbidity meters. A standard single beam turbidity meter is comprised of one light source and one photo-detector situated 90° from the light source. This type of turbidity meter uses a tungsten filament light source that can generate a wide range of light wavelengths, measures in nephelometric turbidity units (NTU) directly, and is accurate for samples of colorless water with low turbidity. However, this design has many limitations. This meter has a low range of applicability and needs frequent calibration because of changes in the tungsten filament light source.

A ratio turbidity meter uses one light source and several photo-detectors that detect forward scatter, transmitted light, backscatter, and light scattered at 90°. The light scatter readings are mathematically combined to determine turbidity in NTU's. This limits the effect of water color, allowing for a turbidity reading that better captures the turbidity caused by the suspended particles themselves. This turbidity meter design is more accurate, but it still has a low NTU range. Also, depending on what light source is used, this turbidity meter design may still require frequent calibration (EPA 1999).

A modulated four beam turbidity meter uses two light sources and two photo-detectors all located 90° around the sample volume with each light source directly across from a photo-detector. This design alternates between two light sources, measuring transmitted light and 90° scattered light with each light beam. The light scatter readings are mathematically combined using an algorithm to determine turbidity in NTU's. This algorithm uses an equation such that the effect of water color completely cancels out, allowing for a turbidity reading only based on the effect of suspended particles. This design is accurate from 0-100 NTU's. The NTU range for this type of turbidity meter is

higher, but it is not as high as needed for construction site runoff. Also, depending on the light source, it may need frequent calibration (EPA, 1999).

Because construction site runoff can contain significant amounts of eroded sediment, this project requires a turbidity meter that can read turbidities of 4000 NTU or greater. This range can be accomplished by using multiple light sources and photo-detectors, different types of light sources, and different turbidity meter technologies. As said before, tungsten filament light sources have been widely used because they produce many wavelengths, but this source also has many limitations. Because of this, they are most suitable for water treatment effluent monitoring or monitoring water with low turbidity. Infrared light has been determined to minimize the effect of particle size and water color on turbidity readings (Jastram, 2009; Patil, 2011). However, actually achieving reliable infrared light from a light source can be difficult. Another light source that has been explored is monochromatic light. Monochromatic light uses a small range of light wavelengths. For the best result, these wavelengths can be chosen based on how they react with the suspended particles. Monochromatic light is not greatly affected by water color, but it can often produce inaccurate readings because it is insensitive to small particles. Other turbidity meter technologies have been researched. One such technology is optical fiber sensing. Even though this technology is still being developed, it is already found to have many advantages such as absolute measurement, excellent resolution and range, and modest cost (Omar & MatJafri, 2009). The fiber optic sensing technology currently is not widely available.

2.3 Turbidity TSS Relationship

The relationship between turbidity and TSS is uncertain. Turbidity can be affected by characteristics such as water color, water color, particle concentration, and shape, size and mineral concentration of sediment particles in the water (Packman, Cornings, & Booth,1999). Because turbidity values are so variable, it becomes difficult to relate turbidity to TSS. Holliday et al. (2003) performed laboratory research to find a correlation between turbidity and TSS. From measuring turbidity and settling times of water samples, they found a strong power relationship and a potential for a linear relationship between turbidity and TSS. It was found that turbidity to TSS was 1:1 for

samples comprised of silt plus clay but lower for whole soil samples. Rasmussen et al. (2009) took their turbidity analysis a step further and began to use continuously monitored stream flow data to analyze turbidity and suspended sediment concentration (SSC). Their experiment used site specific regression analysis to develop a linear regression model to compute specific instantaneous values of SSC based on turbidity readings. However, it was determined that their model needed to include samples from every season and over a large range of turbidities. Other problems they experienced were skewed turbidity values because of large particles, black or very dark colored particles, and microorganisms. Jastram et al. (2009) researched how to measure turbidity in rivers more precisely as a means to estimate SSC. Their study included the use of univariate and multivariate estimations to determine the variables on which SSC depends. In the univariate approach, SSC is only a function of turbidity. In the multivariate approach, SSC is a function of several variables such as turbidity, stage, organic matter, and water temperature. In doing this research, they found that a model including turbidity and stage as independent variables was the most accurate.

While much research has been done to relate turbidity to TSS in streams and rivers, research of runoff from construction sites is not as common. Both types of monitoring locations have similarities, but there are still some differences. Turbidity in a stream is likely caused by sediment, dissolved materials, organic matter, and organisms. Runoff on a construction site primarily contains water and sediment. Many of the variables that affect stream turbidity can be disregarded on construction sites; however, turbidity variability is still a concern because of the many soil types and land uses at different sites. Patil et al. (2011) created a linear relationship between turbidity and TSS using a constant variable related to the site characteristics. They did this by measuring the turbidity and TSS of samples and solving for a constant, varying each test by the turbidity factor of different soil types and different particle classes. Patil et al. gave a relationship between turbidity and TSS that requires that the soil type and particle class at a site be known. Their research on a limited number of samples indicated that the turbidity of each soil type can be added together linearly to obtain a total runoff turbidity, thus creating the possibility of predicting turbidity and TSS. However, research on a wider range of soil samples is needed.

2.4 Variables Affecting Turbidity

Rasmussen et al. (2009) reported that the NTU vs. TSS varies because of different meter configurations, measurement methods, and color effects. Careful planning and consideration must therefore be done to determine the best instruments and measurement methods for a specific application. After choosing an instrument, it is also vital that consistent measurement techniques be utilized so that measurements can be comparable. Even with careful planning and consistent measurement, it is generally stated that turbidity can still only be considered a relative value, more useful for revealing trends in information, than an absolute value and should be reported as such (Ankcorn, 2003; Omega Engineering, 2011).

The variables that affect turbidity can be broken down into two groups: variables caused by the sample and variables caused by the measuring device. Sample variability is most often caused by particle size, particle shape, particle color, water color, and organic matter. Variability caused by the measuring device is attributed to the angle of detection, photo detectors, incident light beam wavelength, and color sensitivity of the photocell (Omega Engineering, 2011).

A large contributor to skewed turbidity results is particle size. For particles smaller than the incident light's wavelength, light will be scattered in all directions. For particles larger than the incident light's wavelength, light will be scattered mostly forward (Omar & MatJafri, 2009). This becomes important because light scattered forward may appear to be transmitted and not scattered, skewing the overall turbidity reading. It is also important to note that light is not scattered in all directions equally. Particles larger than incident wavelength, usually 1 micron, will primarily scatter in the forward direction. Particles smaller than 1 micron tend to scatter light in all directions, but in a peanut type shape. Particles smaller than 0.05 microns will scatter light evenly in all directions. Because particles smaller than 0.45 microns are considered dissolved, this shows that even dissolved particles have the capability of scattering light and will affect turbidity measurements (Omega Engineering, 2011). Runoff will mostly suspend small sediment. Most of the mass of sediment will likely be larger than 1 micron; however, dissolved

particles may still be present. Particle size distributions will need to be evaluated to determine what type of soil is affecting turbidity.

When describing the effects of particle size on scattered light, a diameter that assumes a spherical shape is used to describe the particle. However, this is rarely an accurate assumption. Particles that are spherical will produce more predictable light scattering patterns. Irregularly shaped particles, i.e. most soil particles, will produce many light scattering patterns, causing unpredictable effects on turbidity (Omega Engineering, 2011). When working with construction site runoff, it is likely that the particles will be irregularly shaped, adding skew to turbidity readings.

Particles can be a variety of colors. These colors all absorb and scatter light differently. It is important to know the type of soil that is eroded, so the soils can be evaluated for their absorption capabilities. Dark colored sediment has the potential to absorb light causing less light to reach the photo detectors. This will lead to higher turbidity readings (Anderson, 2005). Particle color is also important when choosing incident light wavelengths because different colored particles will absorb different wavelengths of light. The more recent use of near infrared light (λ=860 nm) seems to limit particle color affects (Sadar, n.d.). For naturally occurring soils, color variation is inevitable, and needs to be considered when interpreting turbidity data and choosing measurement devices.

Water color, much like particle color, skews turbidity results because of its ability to absorb light wavelengths. The use of near infrared light will limit these effects as well.

Organic matter and organisms are important when measuring turbidity in lakes and streams. Organic matter has a higher tendency to absorb light, causing skewed turbidity measurements (Ankcorn, 2003). Organic matter can also be dissolved easier into water, causing water color to change. These effects are largely a concern when monitoring lakes and streams. Construction site runoff is expected to have less organic matter and organisms, reducing possible error.

Other sample variables that could affect turbidity readings that have been considered but not thoroughly researched include water pH, water temperature, and particle mineral composition.

Variability in turbidity readings is more easily understood than remedied. A turbidity meter is manufactured with specific specifications, light sources, and photo detectors. Every meter differs. When using a turbidity meter, it is vital to know exactly how to calibrate it, read measurements, what units it is reporting in, and what may affect the measurements.

The wavelength of the incident light source is vital in determining accurate values of turbidity. The size of the wavelength of incident light will determine the light scatter pattern (Ankcorn, 2003; Omega Engineering, 2011). As previously mentioned, particle size and its relation to the size of the light wavelength will cause different scatter patterns. If wavelength is varied between instruments, its reaction to different sized particles will also be different, causing a spectrum of turbidity values. Wavelength is also important because wavelengths in the visible light spectrum are absorbed readily by different colored water and particles. Due to this problem, research has concluded that infrared or near infrared light is less susceptible to absorption. Using such wavelengths will limit variance (Ankcorn, 2003). In general, the nearer the incident light's color spectrum is to being a single wavelength, the more consistent the light scatter patterns (Omega Engineering, 2011). When monitoring construction site runoff, it will be important to use turbidity meters that use the same wavelength light range so that values are comparable.

Other concerns when using multiple instruments is how they are measuring light scatter. This is a problem because an NTU is defined by measuring only light scattered 90° from the light source (Anderson, 2005). The addition of multiple photo detectors and angle measurements cause variance in turbidity readings. Some meters are designed to measure attenuation, backscatter, or a combination of many angles. Each of these instruments defines turbidity using a new unit and it becomes increasingly more difficult to compare measurements to an NTU. Knowing the specifications of the meter being used and how it is set to report turbidity is essential to determining the applicability of turbidity measurements.

Calibration is extremely important to obtain accurate and repeatable turbidity measurements. Calibration is based on a 20.0 NTU formazin solution (Sadar, 2007). For

a turbidity meter to be accurate, it needs to be calibrated with a solution that is expertly prepared. The slightest mistake due to bubbles or dirty glassware can cause significant error in future testing. It is also essential that meters are frequently calibrated in the field. A meter can become inaccurate unless it is calibrated for local testing conditions (Patil et al., 2011). Calibration has been made easier through standard solutions and meter specific procedures.

2.5 Summary

Understanding turbidity measurements and their limitations is essential to understanding how to best utilize turbidity technology for this project. Using turbidity as a surrogate for determining TSS is beneficial. However, it also is limited by the user's understanding of the variables that can affect turbidity readings. Turbidity is dependent on a number of sediment characteristics and is therefore site. Experimentation will be conducted to determine the effect of a multitude of variables on several sites, as well as the settling properties of soil on each site. Once a standard procedure is in place, runoff from each site will be tested to determine how turbidity varies and how it can be predicted.

Chapter Three
Experimental Methods

3.1 Introduction

This study consists of several individual processes that worked together to acquire appropriate data for our analysis of turbidity on construction sites. A description of the soils collected for the study and the apparatus used will be described. A step by step explanation of the experimental methods will be provided, including how the soil was processed and rained on and how samples were collected and analyzed. Finally, all of the soil properties collected for a detailed regression analysis will be defined.

3.2 Soil Acquisition

When determining the impact of soil characteristics on turbidity, it is essential to have a large and diverse group of soil samples. Fourteen soils from eight construction sites around Minnesota were acquired with the help of Dwayne Stenlund from the Minnesota Department of Transportation. Figure 3.1 shows the locations from which the soils were acquired. Of these fourteen soils, eight are considered sub soils and six, top soils.

Soils were classified using the USDA soil triangle (Coduto, Yeung, & Kitch, 2010). The percent of sand, silt, and clay in each soil was determined from a particle size graph created for each soil from standard sieve and hydrometer data. Of these soils, most were classified in the loam family, with the most significant portion being sandy loams. The soil visual descriptions and classifications can be seen in Table 3.1.

3.3 Apparatus

A rainfall simulator was used to create a realistic rainfall event on a soil sample. The soil samples were configured so that the total sediment-laden runoff is collected as well as individual subsamples within the event.

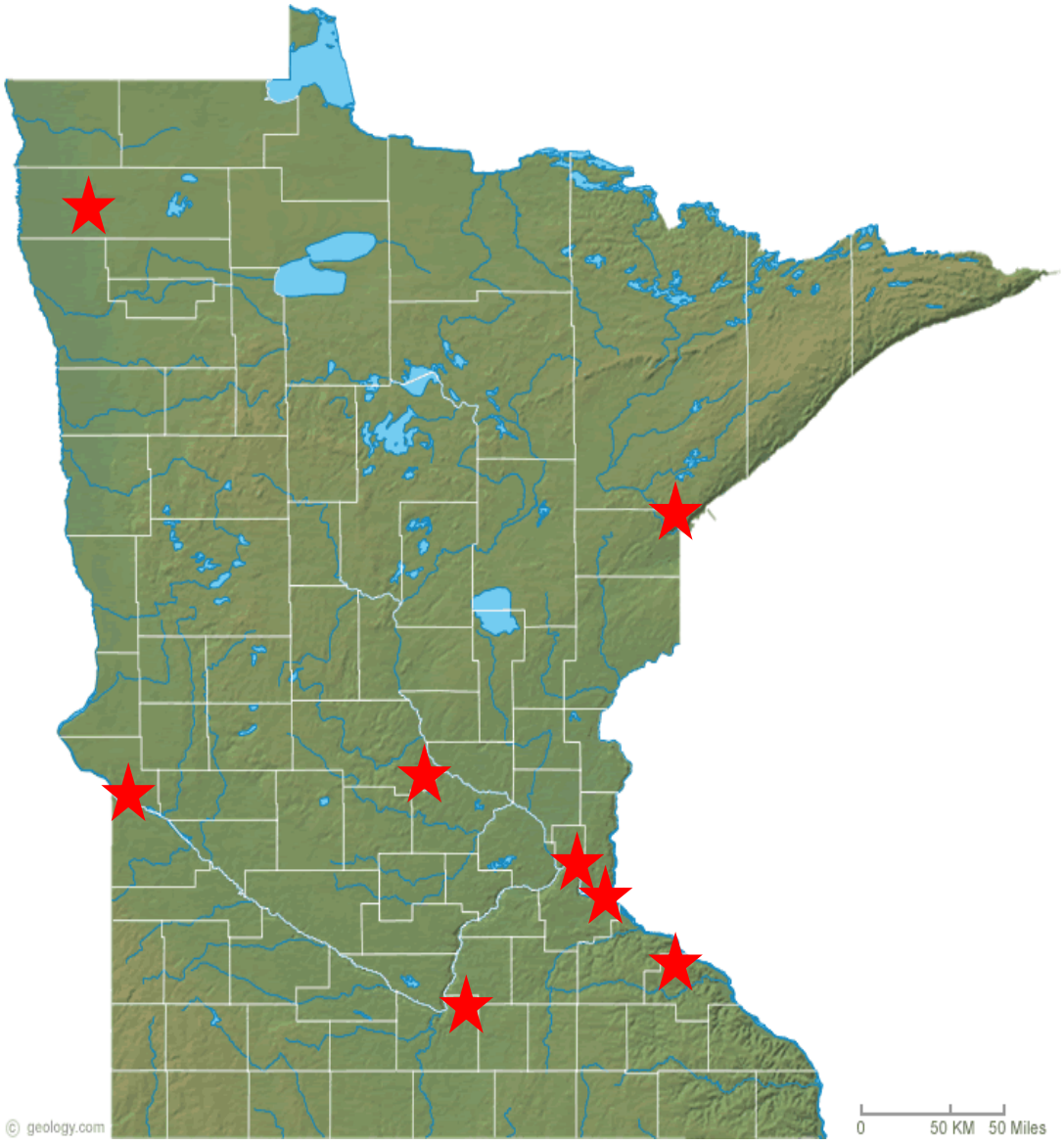

Figure 3.1: Soil site locations marked with red stars on a map of Minnesota.

Table 3.1. Laboratory soil classifications

Name	Type	Location	Description	Classification
AH T	Topsoil	Arden Hills, MN	Silty, dark colored soil	Sandy Loam
AH S	Subsoil	Arden Hills, MN	Silty, yellow colored soil	Sandy Loam
CTY 14 T	Topsoil	Mankato, MN	Silty, dark colored soil	Sandy Loam
CTY 14 S	Subsoil	Mankato, MN	Silty, yellow colored soil	Sandy Loam
Dul T	Topsoil	Duluth, MN	Sandy, dark colored soil	Loamy Sand
Dul S	Subsoil	Duluth, MN	Silty, red colored soil	Silt Loam
Hast T	Topsoil	Hastings, MN	Sandy, dark colored soil	Loamy Sand
Hast S	Subsoil	Hastings, MN	Silty, rust colored soil	Sandy Loam
OV T	Topsoil	Ortonville, MN	Silty, dark colored soil with gravel	Sandy Loam
OV S	Subsoil	Ortonville, MN	Silty, dark colored soil with gravel	Silt Loam
TH-23 T	Topsoil	St. Cloud, MN	Silty, grey colored soil	Loam
TH-23 S	Subsoil	St. Cloud, MN	Silty, red colored soil	Sandy Loam
Soil A	Subsoil	Redwing, MN	Silty, tan colored soil	Silt
Soil B	Subsoil	Red Lake Falls, MN	Very fine, tan/grey soil	Silty Clay Loam

3.3.1 Rainfall Simulator

A rainfall simulator from a previous project was calibrated and used for this experiment (Figure 3.2). The rainfall simulator is a box constructed from aluminum. It has a rectangular surface are with dimensions 0.61 m by 0.91 m. The bottom of the box contains 96 hypodermic needles designed to utilize water pressure to push water droplets out through the needles (Figure 3.3). The rain then falls from the tip of needle and accelerates with gravity. Onstad, Radke, and Young (1981) describe this type of rainfall simulator in greater detail. The rain falls a total distance of 2.6 m from the tip of the needle to the box of soil underneath.

The rainfall simulator was calibrated to replicate the peak hour of a 2 year, 24 hour storm. For Minnesota, that rainfall intensity is interpolated as 1.27 in/hr (United States Weather Bureau, 1961). The volume and collection area were measured and rainfall rate was calculated with the following equation:

$$I = \frac{V_f}{A_f \ t} \tag{3.1}$$

where I is the rainfall intensity, V_f is the rainfall volume collected, A_f is the surface area, and t is the amount of time rainfall was collected.

The simulator was also calibrated to replicate natural raindrop size. Sheppard (1990) and Marshall and Palmer (1948) both note that natural raindrop diameters are less than 4 mm. To measure the raindrop size for this experiment, rain volumes were collected for each needle over 10 minutes of rain. Then a raindrop rate in drops/min was measured for each needle. The raindrop diameter was calculated assuming spherical raindrops with the following equations:

$$V_n = t \, V_d \, n_d \tag{3.2}$$

$$V_d = \frac{1}{6} \pi \, {D_d}^3 \tag{3.3}$$

where V_n is the total rain volume associated with a single needle of the rainfall simulator, t is the rainfall time, n_d is the number of drops rained from that needle in a unit of time, V_d is the volume of an individual raindrop, and D_d is the equivalent raindrop diameter.

Tables A.1, A.3, A.4 in the appendix show the total rain volumes, raindrop rates, and raindrop diameters for each needle respectively. An X indicates that rainfall data could not be collected for that needle. The average raindrop diameter from Table A.4 is 3.53 mm which falls within the reported raindrop diameter range in the literature.

To ensure that the simulator was raining evenly over the surface of the soil, oscillating fans were installed around the simulator to push the raindrops in random directions. In Table A.1, there are columns of zeroes representing the 1.2 cm space between needles. Rain volumes for each needle were collected in a similar manner as in Table A.1 but with the fans on. Table A.2 shows the rain distribution under and between needles. Based on the values reported in Table A.2 and A.4, there is an adequate distribution of rainfall below the simulator and the raindrop diameters are of reasonable size.

3.3.2 Soil Box and Runoff Collection

A platform was constructed underneath the rainfall simulator that holds the soil sample during rain events. This platform is placed at a 9% slope, which is the slope of a standard plot used in Universal Soil Loss Equation (United States Department of Agriculture, 1978). Although there are many slopes and conditions on a construction site, a single, standard slope is needed for our protocols.

The soil is contained in a long plywood box that was constructed for this experiment. The soil box can be seen in Figure 3.2. The box is 91.4 cm x 25.4 cm x 15.2 cm and can hold approximately 19 liters of soil. Soil was weighed, placed into the box, and was compacted evenly over the area of the box using a standard packing method developed for this study. The box had 12 holes drilled into the bottom and perforated fabric was placed over the holes. This allowed the soil to soak in water and drained, bringing the soil to field capacity prior to rainfall.

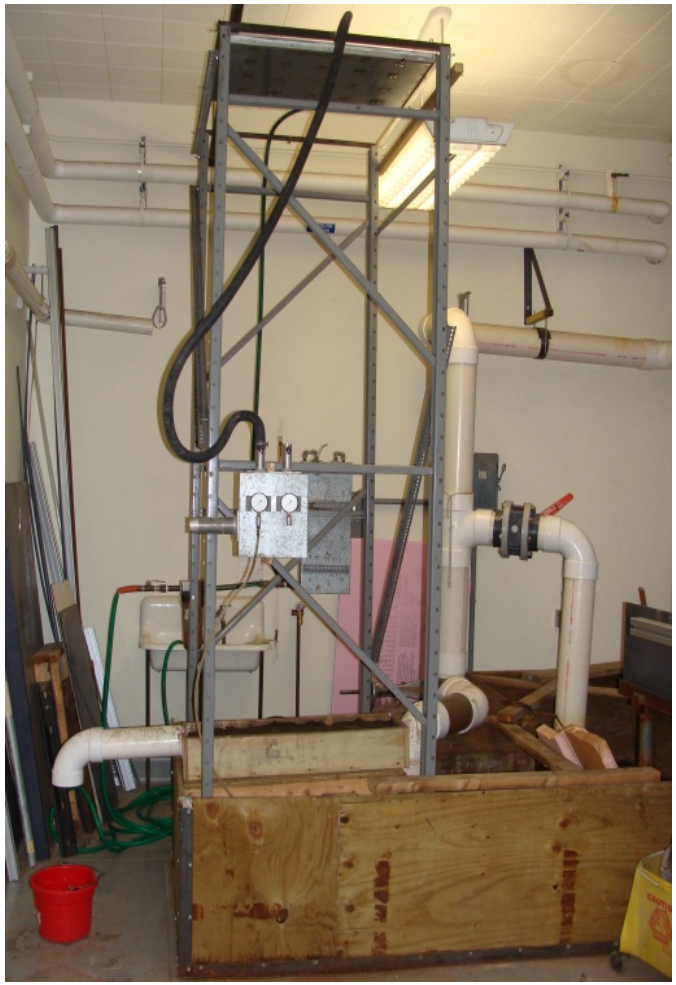

Figure 3.2. Rainfall simulator.

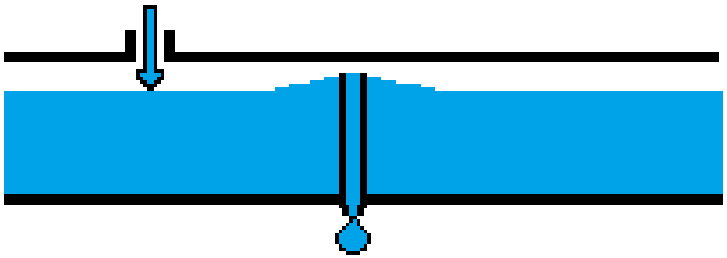

Figure 3.3. Illustration of raindrop created by rainfall simulator needle.

A 15.2 cm PVC pipe with an elbow joint was connected to a circular drain on the box to collect runoff. This can be seen in Figure 3.5.

3.4 Soil Processing

The soil collected from the construction sites needed to be processed to remove organic matter and large rocks. An assumption made prior to processing the soil was that large rocks would have little to no effect on turbidity readings. This assumption is justified because large rocks are unlikely to be transported with runoff and would settle out quickly if transported. Therefore, the soil was broken down and run through a 6.35 mm sieve to remove large rocks, clumps of dirt, and sticks. Each soil was processed with the following procedure:

1) If soils are moist, let air dry
2) Separate soil into 5 gallon buckets
3) Remove large chunks (larger than a fist) and break down with a sledge hammer
4) Add 2 buckets (of the same soil) at a time to a cement mixer
5) Mix soil for 30 minutes
6) Place ¼ in. sieve on top of a 5 gallon bucket and place bucket inside a tub or larger container to collect excess soil
7) Pour a little soil at a time through sieve and separate chunks larger than ¼ in.
8) Break down large chunks using sledge hammer
9) Re-sieve broken down chunks
10) Repeat steps 7 and 8 if needed
11) Discard rocks > ¼ in.

3.5 Rainfall Procedure

3.5.1 Soil Box Preparation

The soils were compacted into a soil box. Although many different soil conditions can be found on a constructions site, a standard soil packing method is needed for our test. One option is to attain a highly compacted soil by compacting a wet soil. A medium compacted soil can be obtained by compacting a dry soil. A third option is to use a loose

soil with no compaction. A medium compaction was chosen as an average of these three conditions. The soils were then allowed to soak up water for a day and drain for a day while in the box. The soils were prepared with the following procedure:

1) Use dry, processed soil (see soil processing procedure) and a plywood box
2) Weigh out enough soil to fill box to top and fill box
3) Compact soil into box using a metal plate that spans the entire width of the box and a proctor hammer
4) Place plate at one end of box and strike it with 25 blows from a proctor hammer
5) Move plate to the next uncompact section and repeat steps 3 and 4 until the entire length of the box has been compacted
6) Using a shallow pool, place box inside and fill with enough water to saturate soil in box
7) Leave box in pool for 24 hours to allow water to soak into soil profile
8) Remove box from pool and place on blocks
9) Leave box on blocks for 24 hours, letting excess moisture drain from soil

3.5.2 Pre-rainfall

Although the rainfall simulator was calibrated to rain at specific rainfall intensity, the subtle fluctuations in flow rate from the faucet supplying the water caused discrepancies in the actual rainfall intensity. Before starting the experiment and placing the soil box under the rainfall simulator, rainfall intensity was measured to assure the rainfall was within range of the desired rainfall intensity. This procedure is outlined below:

1) Set rainfall simulator to rain at desired rainfall intensity
2) Place rainfall gauges under simulator and rain for 30 minutes
3) Measure volume of water
4) Convert to rainfall intensity

3.5.3 Rainfall

The following procedure describes the steps done immediately before and during rainfall on each soil:

1) Turn fans on
2) Place soil box under rainfall simulator
3) Place plate in front of runoff opening and remove when sample is ready to runoff (can take 1-15 minutes depending on the drainage capability of the soil)
4) Place 5 gallon bucket under opening to collect runoff
5) Attach PVC pipe to runoff opening to guide runoff to 5 gallon bucket (Figure 3.5)
6) Once sample begins to runoff, begin taking 5 minute runoff samples of 50 mL (Figure 3.4)
7) After 30 minutes of rainfall, remove box
8) Repeat for next soil box

3.6 Aliquot Sample Analysis

During the rainfall on each soil, six 50 mL samples of runoff were collected. These samples were used to determine the relationship between turbidity and concentration for each soil. The procedure used to analyze these samples is described below:

1) Dilute 50 mL runoff samples (see rainfall procedure) to 4000 NTU, recording the amount of water used
2) Slowly dilute sample to 280 NTU (using 4-6 dilutions), recording turbidity and water added every time sample is diluted. Dilute as far as the beaker will allow.
3) To take turbidity measurements using a Hach 2100N bench top turbidimeter:
    a. Put sample in 500 mL beaker
    b. Place beaker on magnetic stirrer and mix completely
    c. Fill 30 mL vial with sample
    d. Use bench top turbidity meter to measure turbidity
    e. Take 3 turbidity measurements to get an understanding of the range of turbidity of the sample
    f. Empty vial back into beaker and rinse with dilution water for next dilution
4) Dry out sample in oven at 110°
5) Remove sample and allow to cool. Weigh sample determine total sediment mass.
6) Plot turbidity vs. concentration curve

Figure 3.4. Undergraduate collecting 5 mL samples

Figure 3.5. Total runoff collection in 5 gal bucket

3.7 Total Runoff Sample Analysis

Aside from the 50 mL samples that were collected for each soil, a 5 gallon bucket of remaining runoff was collected. This sample contained a majority of the runoff from the soil and was analyzed to determine the effect of particle settling on the turbidity and TSS relationship. The analysis procedure is described below:

1) Measure volume of runoff in 5 gallon bucket used in Rainfall Procedure
2) Dilute sample to less than 4000 NTU by adding water to the runoff sample. Determine the amount of water needed from the dilution curve created in Dilution Procedure.
3) Prepare 4 sets of 6, 30 mL vials by adding 0, 5, 10, 15, 20, 25 mL of water to the 6 vials
4) Pipette out enough runoff to fill one set of diluted vials while mixing sample with paint stirrer. Pipette at a consistent depth for all samples.
5) Stop mixing, start stop watch or other timing device, and allow sample to settle
6) Pipette out enough runoff at 3 minutes, 6 hours and 52 minutes, and 24 hours and fill the other 3 sets of vials. These samples represent the breaks between sand, silt, clay, and colloidal particles.
7) Pipette out enough runoff to fill a single, empty vial at 0.25, 0.5, 1, 2, 3, 4, 5, and 6 hours. These samples represent different sizes of silts.
8) Measure turbidity of the vials using bench top turbidity meter and record values
9) Using a standard procedure for determining total suspended solids in water (ASTM, 2010), measure the weight of soil in the 0 mL vials for the 0 min, 3min, 6:52 hour, and 24 hour samples and for each silt sample. Use these weights to determine the soil concentration in the sample.

3.8 Determination of Rainfall Duration

The duration of rainfall should be long enough to achieve steady state conditions but short enough to be time and cost efficient. To determine this duration, a trial run was done with one of the soils. Using the 50 mL sample analysis, a set of time dependent,

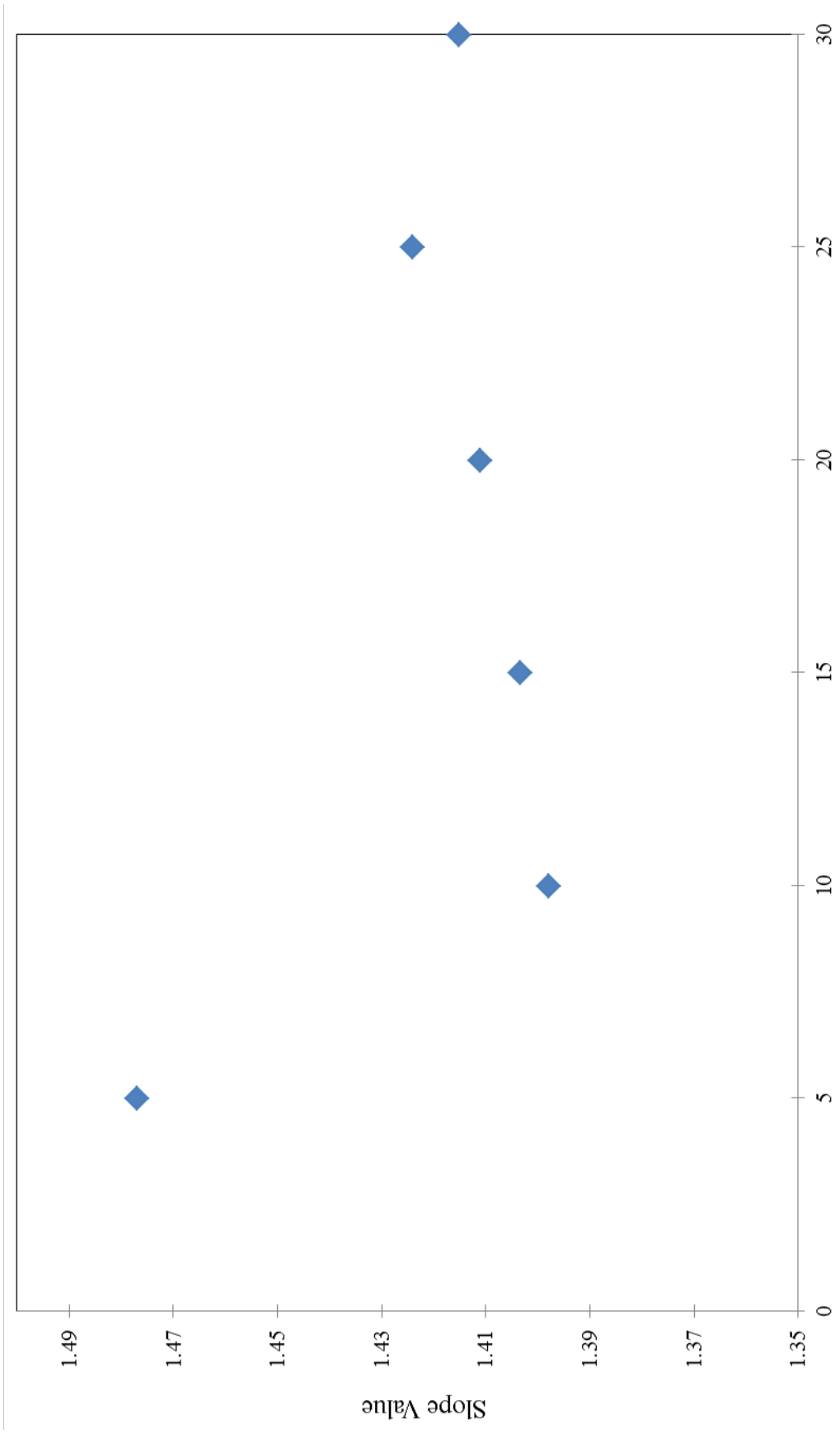

Figure 3.6. Same slope regression for trial run.

turbidity vs. concentration curves was acquired for 5, 10, 15, 20, 25, and 30 minutes after the start of runoff. Conditions corresponding to steady state were assessed by examining changes in the power coefficient with the successive combination of collected data with cumulative time. The power coefficient was determined using the log slopes (Nater et al., 1996). The result of the regression is a common slope value for the 5 minute data, the combined data corresponding to sampling times of 5-and-10 minute data, to sampling times of 5-10-and-15 minutes and so forth for each subsequent sampling time. The common slope for different cumulative sampling time is shown in Figure 3.6. The scatter significantly decreased between the 5 minute intervals over the 30 minute time period. The slope collapsed to a robust value of approximately 1.41 after 15 minutes. It was decided that 30 minutes is a satisfactory duration of rainfall.

3.9 Soil Properties

To determine how the turbidity and TSS relationship varies between soils, soil parameters were determined for each soil. For ease of analysis and application, the selection of soil properties was limited to those that can be gathered or estimated directly from soil samples from raw construction sites. These soil properties are described below.

Percent Sand, Silt, Clay

A standard sieve and hydrometer procedure using a dispersing agent was performed to determine the particle-size distribution for each soil prior to packing the soil in the test apparatus (ASTM 2007). Using the USDA particle size scale, percent sand is defined as the percent of the sample that is 0.05-10 mm in diameter. Percent silt is the percent of the sample that is 0.002-0.05 mm in diameter. Percent clay is the percent of the sample that is < 0.002 mm in diameter (Coduto et al., 2010).

Information on particle sizes was also collected from the runoff samples using the pipette method (Klute [Ed.], 1986). In contrast to the primary particle size distributions obtained with the sieve/hydrometer method, data collected from the runoff samples are used to determine the particle sizes of the eroded sediment that contains aggregates. The percentages of clay, silt, and sand particles for the aggregates are given in Appendix F. These percentages are considerably different than those obtained for the primary

particles. For example, the largest percent clay of primary particles was 26%. The percent clay of the eroded sediment for this soil was only 7.3%.

Percent Silt plus Clay

Because sand can easily settle out of suspension, the percent sand in the runoff treated by an effective sediment control plan is likely quite small. It was decided to use a statistical analysis with a variable that is not nearly equal to zero. Therefore, the role of percent sand was represented by the summation of percent silt and percent clay. The term percent silt plus clay is the mathematical equal to one minus percent sand. Nonetheless, problems with relationships using the inverse of percent sand can be avoided.

Rainfall Intensity, I

For each rainfall trial of each soil, rainfall intensity was measured by placing a catch basin below the rainfall simulator. This basin collected the rainfall over ½ hour. The volume of water collected in the catch basin was measured in milliliters using a large graduated cylinder. The surface area of the catch basin was measured and the rainfall intensity was evaluated using Equation 3.1.

Dry Bulk Density, BD

Dry bulk density was determined after the previously described soil preparation procedure was completed. Dry bulk density is measured in g/cm^3. The mass of soil placed into the soil box was first determined. The soil was then evenly compacted into the soil box. The volume of compacted soil was measured using the box dimensions and subtracting the empty space above the soil from the depth of the box. The equation used to evaluate dry bulk density is as follows:

$$BD = \frac{M_B}{A_B H} \tag{3.5}$$

where BD is the dry bulk density, M_B is the mass of soil in the box, A_B is the surface area of the soil box, and H is the depth of soil in the box.

Volume of Runoff, V_t

The volume of runoff was measured directly by collecting the total runoff from the boxes in a bucket and measuring the total runoff volume in the bucket using a graduated cylinder. A volume of 300 mL was added to this volume to account for the six 50 mL samples that were collected over the rainfall period.

Runoff Flow Rate, Q

The runoff flow rate was calculated using the volume of runoff and the duration runoff. The average runoff flow rate was calculated using the following equation:

$$Q = \frac{V_t}{t_t} \tag{3.6}$$

where Q is the flow rate of runoff, V_t is the total volume of runoff, and t_t is the duration of runoff.

Curve Number, CN

The NRCS Curve Number Method uses following equations:

$$Z = \frac{(P-I_a)^2}{P+I_a+S}, P \geq I_a = 0.2S \tag{3.7}$$

$$Z = 0\,, P \leq I_a = 0.2S \tag{3.8}$$

$$S = \frac{1000}{CN} - 10 \tag{3.9}$$

where Z, P, S, and I_a are in inches and CN is dimensionless. Z is the depth of runoff. P is the total depth of precipitation. S is the maximum abstraction during runoff. I_a is the initial abstraction prior to runoff (Wurbs and James, 2001). P and Z were solved for using data collected prior and during rainfall. S was found using solver software. The equations used for P and Z are as follows:

$$P = I\,t \tag{3.10}$$

$$Z = \frac{V_t}{A_B} \tag{3.11}$$

where V_r is the total runoff volume and A_B is the surface area of the box.

Moisture Content, w

Moisture content was determined for each sample after the samples were soaked in water and drained, as described in the previous Soil Preparation section. A sample of soil from the middle of the soil box was extracted, quickly weighed, and then dried overnight in an oven and weighed again. Moisture content was determined with the following equation:

$$w = 100\ \frac{M_w}{M_d} \tag{3.12}$$

where w is the soil moisture content as a percent, M_w is the mass water in a soil in grams, and M_d is the mass, in grams, of soil after it was dried (Coduto et al., 2011).

Optimum Moisture Content, OMC

The optimum moisture content was found for each soil using a standard proctor test (Coduto et al., 2011).

Total Eroded Sediment, TES

The total amount of eroded sediment was determined from the total runoff sample that was collected in a bucket. The majority of the water in the bucket was decanted and the the excess water and sediment was transferred into pre-weighed containers to be dried at 45º C in an oven over night. The container and sediment was then weighed and the total eroded sediment (TES) was determined The same procedure was used for the 50 mL samples, and the mass of soil in the six samples was added to the mass of soil in bucket to determine the TES for each soil.

Soil Shear Strength, τ

Three replicate cohesive strength meter (CSM) tests were performed on each soil. Using the data collected with this test, a soil shear stress in Pascals was determined (Tolhurst et al., 1999).

Interrill Erodibility Constant, K_i

Interrill erodibility is a measurement of the erosion caused by raindrop impact (Elliot, Liebenow, Laflen, & Kohl, 1989). To determine interrill erodibility, the interrill detachment and the dimensionless slope factor, S_f, were calculated with known values:

$$D_i = \frac{TES}{A_B\, t} \tag{3.13}$$

$$S_f = 1.05 - 0.85e^{(-4\,sin(\%\,Slope))} \tag{3.14}$$

where A_B is the surface area of the soil box and t is the duration of runoff..

The interrill erodibility constant, K_i, could then be determined using the following equation:

$$K_i = \frac{D_i}{I^2\, S_f} \tag{3.13}$$

Maximum Abstraction, S

Maximum abstraction, S, was previously described in the curve number section. Equation 3.9 shows the relationship between curve number and maximum abstraction. Based on laboratory results, the assumption that initial abstractions are equal to 20% of the maximum abstraction is valid.

Chapter Four
Evaluation of Turbidity-Concentration Relationships

4.1 Introduction

The experimental methods of Chapter 3 were used to investigate the relationship between turbidity and concentration. The analysis is based largely on the six 50 mL aliquot samples. The first section of the chapter will evaluate the samples using a general power relationship. This evaluation will be done for all of the soils. Trends in the coefficients of this power relationship will be further explored. Predictive relationships are proposed and their usefulness is evaluated.

4.2 General Power Relationship

Insight into the relationship was obtained by plotting the turbidity data as a function of sediment concentration. An example of turbidity-concentration trends is shown in Figure 4.1. Each soil had six sets of data and six separate relationships to describe the data. Several regressions were performed on the data to determine the correct form of the turbidity and TSS relationship. A power relationship for turbidity and sediment concentration was clearly suggested from these plots.

All of the soils in the study were well represented by a power function. The general relationship used to describe turbidity as a function of TSS is as follows:

$$T = \alpha\, TSS^{\beta} \tag{4.1}$$

where α and β are scaling and power coefficents, respectively. They are considered to be soil dependent. In the above equation, turbidity and TSS are measured in NTUs and mg/L respectively. Equation 4.1 was evaluated for each of the six samples collected at different times during the runoff event. The power coefficent, β, remained relatively stable while the scaling coefficient, α, varied among samples.

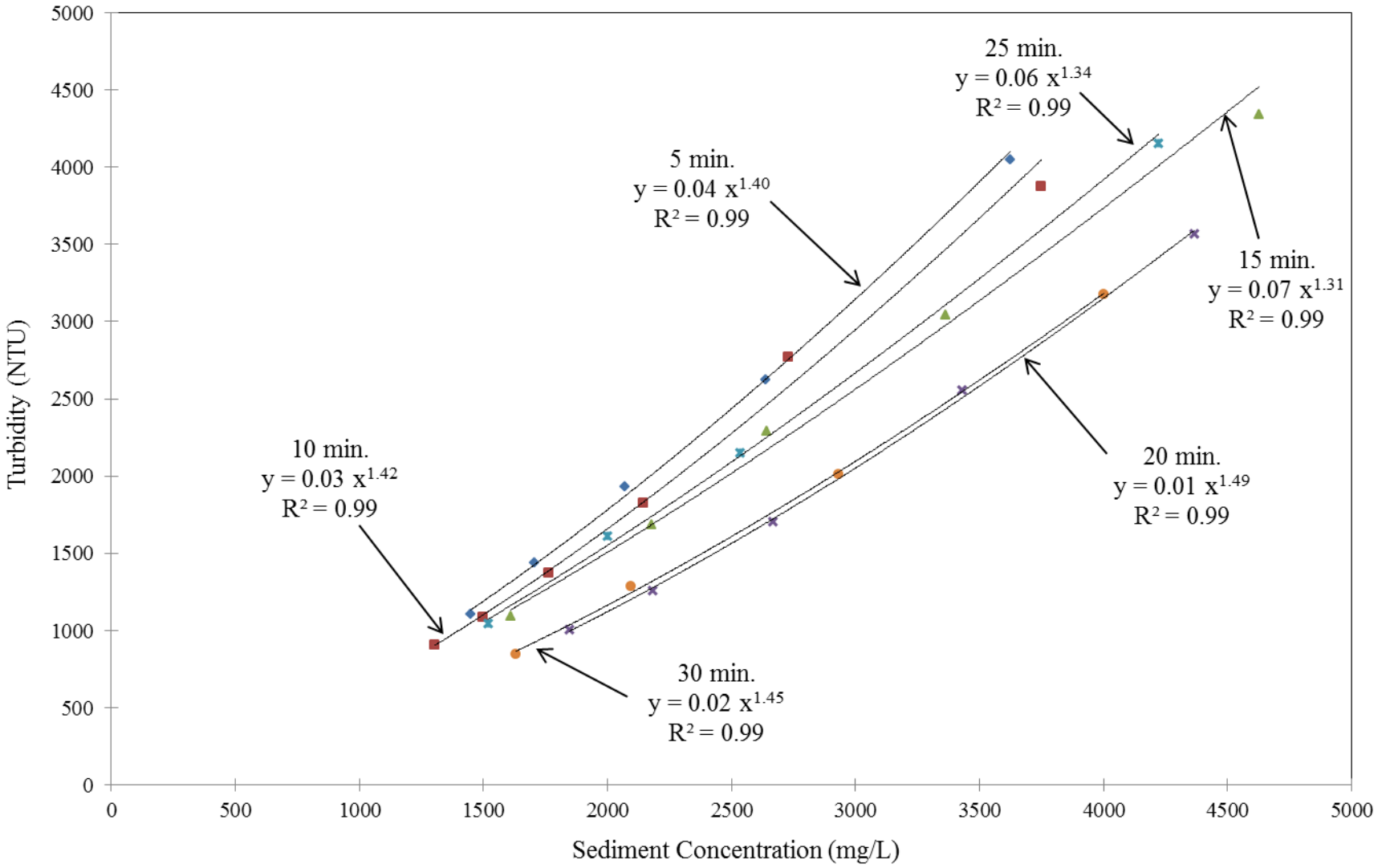

Figure 4.1. Time Dependent 50 mL sample dilution curves for one soil.

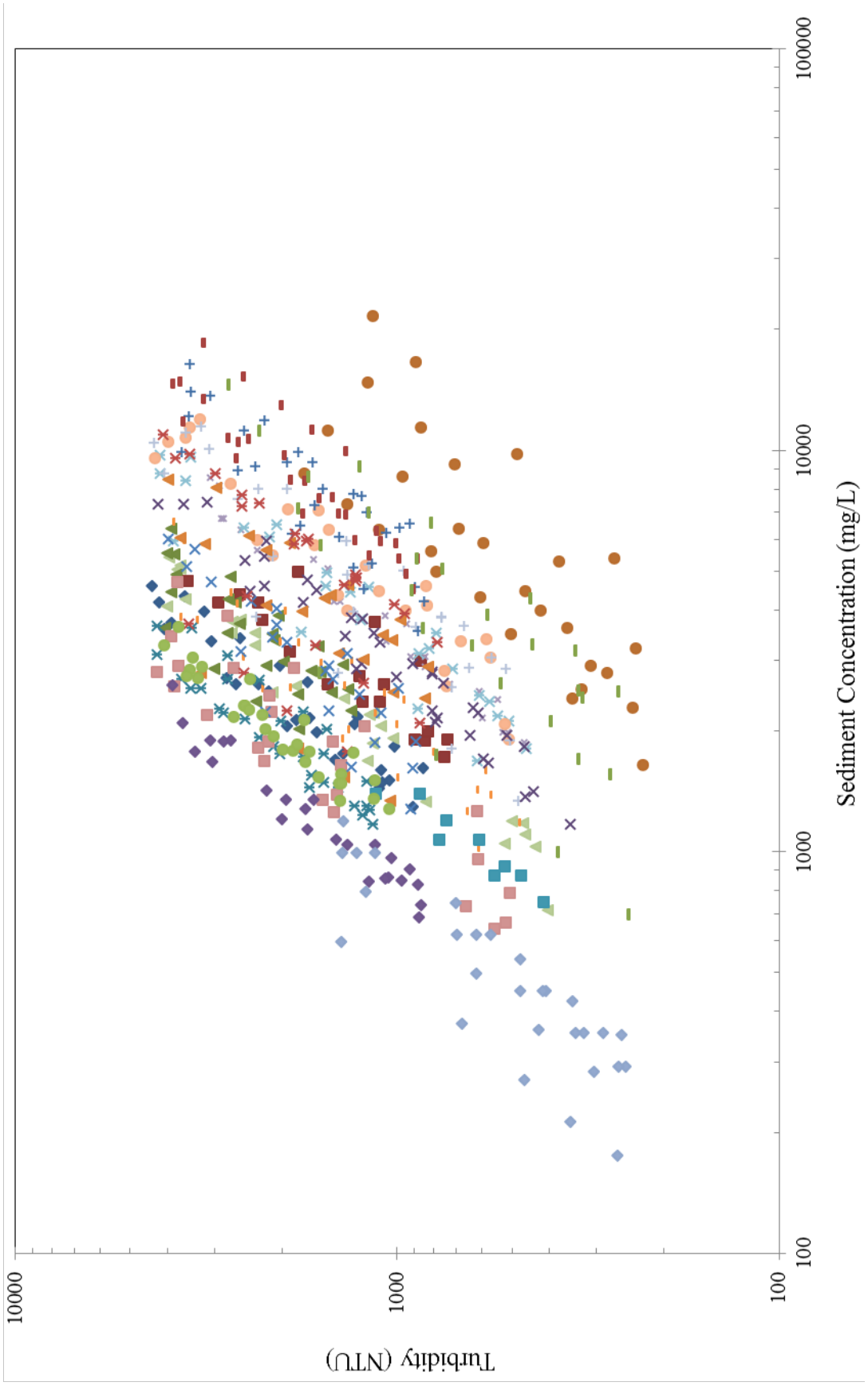

Figure 4.2. Dilution curves for all soils.

In addition to variation of α and β with samples of a particular soil, possible trends for α and β were further investigated by comparing values between soils. Turbidity and concentration data for all fourteen soils are plotted on a single graph in Figure 4.2. The data for all of the soils are well represented by the general power relationship of Equation 4.1. Between all of the soils, the β value varied between 1.3 and 1.5 and the α values varied between 0.001 and 0.1. The time dependent variation in α in Figure 4.1 is small in comparison to its variation between soils. Investigation into possible trends of α will be limited to measurable soil properties. This investigation is given later in this section.

4.2.1 Estimation of β

Investigations were done to estimate β when observed turbidity and concentration data are unavailable for a construction site. The first step was to select a single value β for each of the soils. This value was obtained using the regression analysis for common slope described in Section 3.8. The result of this analysis is a β value for each soil which varied between 1.3 and 1.5. The mean and median of the β values are 1.38 and 1.39, respectively.

Since the range in β is relatively small between soils, the possibility of a single power value that can represent the range of soils was tested. The mean and median values of β are well represented by a power value of 1.4 or 7/5. This fraction is also simple to use and communicate to others. A standard hypothesis test was performed using a null hypothesis of $b_1 = 1.4$, and an alternate hypothesis of $b_1 \neq 1.4$. Using a standard normal distribution, 9 of 19 soils were found to have a β value significantly different from 1.4 at a 95% confidence level.

The effect of setting β to a constant value was also evaluated using standard hypothesis tests on changes in α. Hypothesis tests were performed for each soil where the null hypothesis was that the median α using β = 7/5 equals the median α using the least-square estimate of β. This test was repeated using the mean instead of median values. The results of these hypothesis tests show that there is no statistically significant difference between using β =7 /5 and the least-square estimate.

Because there were nine β values significantly different from 7/5, a multiple linear regression was done on the β using the soil properties described in Section 3.9. No discernible trend was found for β between soils. Because of this, β was set at a constant value of 7/5.

4.2.2 Estimation of α

The determination of α for construction sites without observed turbidity-concentration data was also investigated. Since the value of α varied by nearly two orders of magnitude for our experimental methods, a predictive relationship for this factor as a function of measurable soil properties is needed.

The soil properties previously described in Section 3.9 were used in a multiple linear regression (Neter et al., 1996) to determine a relationship for α. The log transformed multiple linear regression was performed using the median α values when β was set at 7/5. Nearly 40 regression models were evaluated, and the most useful regression models are given in this section. The correlation matrix and details of the best regression models are given in Appendix E. The most significant variables in the model are percent silt plus clay, percent silt, interrill erodibility, and curve number.

Multiple regression models are used to determine a relationship between significant independent variables that describe the dependent variable. The independent variables are the soil properties in Table 2, and the dependent variable is the median α values for each soil. The three independent variables of percent silt, curve number, and interrill erodibility were identified as important indicators of physical processes of particle detachment and transport and well represented the observed α values having a $R^2 = 0.69$. Percent silt represents the available particles on a site that can be easily eroded and transported in stormwater, curve number is a measurement of runoff potential on a site, and interrill erodibility is a value that quantifies the detachment and transport of soil by raindrops and overland flow. Both the percent silt and interrill erodibility were significant at the 10% level. However, the curve number was not significant at a 10% level. It was significant at the 30% level. Because of its importance in the erosion process, it was decided to still include it in the regression model. The regression model using these three

parameters explained 70% of the variability in α. The equation for this model is as follows:

$$\alpha = 1.68\text{E-}16\ \text{Silt}^{1.20}\ \text{CN}^{8.15}\ K_i^{-0.66} \quad (4.2)$$

This model is highly nonlinear with respect to the curve number. Although curve number is a variable that can be easily determined with simple calculations and table values, it is still a dimensionless index of runoff. Because of this, maximum abstraction depth, a physical property of the site that is used in curve number calculations, was substituted for curve number in the regression models. This substitution had little effect on the overall fit of the regression model, but it did decrease the nonlinearity of the regression model. The equation for this model is as follows:

$$\alpha = 0.43\ \text{Silt}^{1.19}\ S^{-0.31}\ K_i^{-0.56} \quad (4.3)$$

Although Equation 4.3 is the preferred prediction model for α, the interrill erodibility and maximum abstraction may not be readily available for soils at construction sites. An alternative and simpler predictive model was obtained using only percent silt. This regression model explained 55% of the variability of α. The equation for this model is as follows:

$$\alpha = 1.94\text{E-}4\ \text{Silt}^{1.22} \quad (4.4)$$

Equation 4.4 provides a simple estimate of α if only particle size distribution is available for the site. The fit of these two models will be described later in this chapter.

Clay particles are often considered a significant factor to turbidity because when suspended, they stay suspended for long periods of time and are difficult to remove from water with traditional BMPs. On average, 4% of the sediment in the runoff samples collected was clay. Because of the insignificant amount of clay present in the analysis, it is unlikely that our experimental design was adequate to identify a statistical significant trend between percent clay and α.

4.2.3 Evaluation of Regression Models

The usefulness of the regression models of Equation 4.3 (Model 1) and Equation 4.4 (Model 2) was evaluated by comparing the predicted α to those observed. For all soils, the observed α values correspond to the minimum, maximum, and median obtained using a β of 7/5. The results of this comparison are shown in Figure 4.3 for the predicted α using Equation 4.3 and in Figure 4.4 for the predicted α using Equation 4.4.

Model 1 and Model 2 are evaluated using the normalized mean square error (NMSE) and the relative mean error (RME). When NMSE = 0, the model has a perfect fit, but when NMSE ≥ 1, the mean describes α as good as or better than the regression model. The RME shows the bias in the models. A model with a positive RME over estimates α and a model with a negative RME underestimates α. NMSE and RME were calculated with the following equations:

$$NMSE = \frac{\sum(P_i - O_i)^2}{\sum(O_i - \bar{O})^2} \tag{4.5}$$

$$RME = \frac{\sum(P_i - O_i)}{n\,\bar{O}} \tag{4.6}$$

where P_i and O_i are the predicted and median of observed α values for each soil, i. $\overline{O}$ is the mean of the observed α values and n is the number of soils used in the analysis. The error of each model is summarized in Table 4.1.

Table 4.1. Model error values.

Error	Model 1	Model 2
NMSE	0.19	0.72
RME	-0.02	-0.15

The NMSE of Model 1 is smaller than Model 2, indicating a better fit. Both models have NMSE values <1 indicating that the Models better represent α then the mean of observed α values. The negative RME values indicate that both models are slightly under-predicting α.

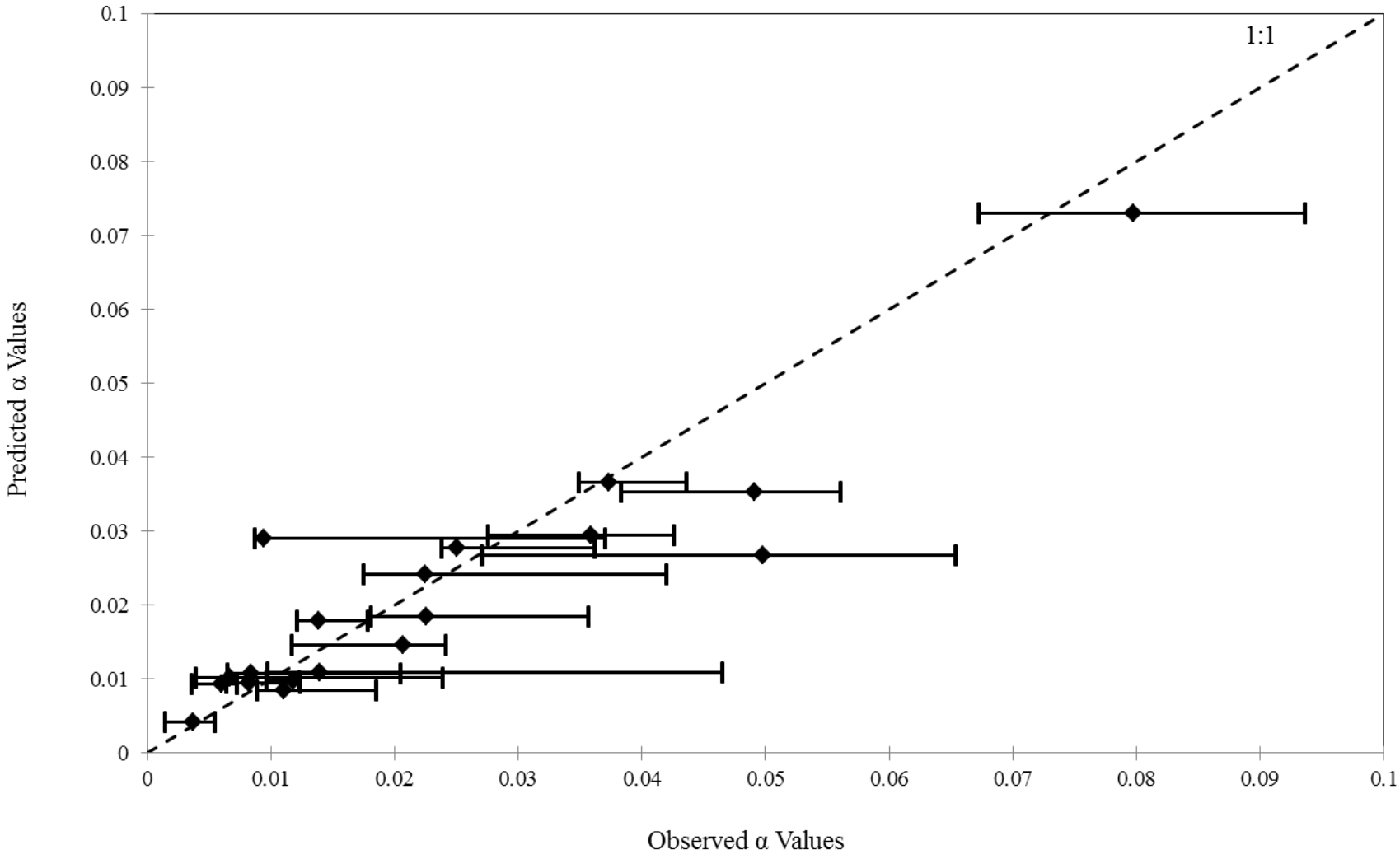

Figure 4.3. Observed α values plotted against predicted α values for Model 1.

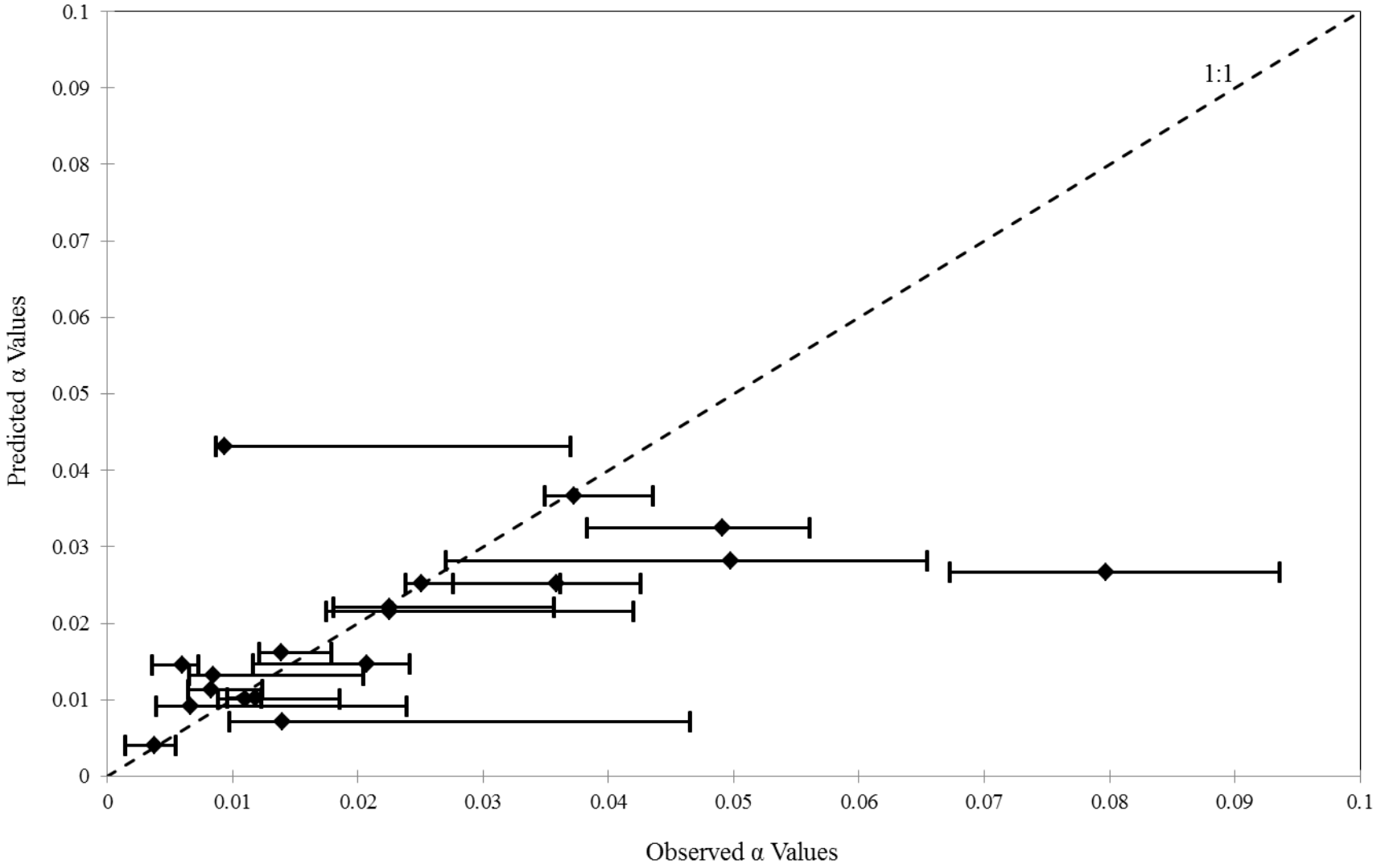

Figure 4.4. Observed α values plotted against predicted α values for Model 2.

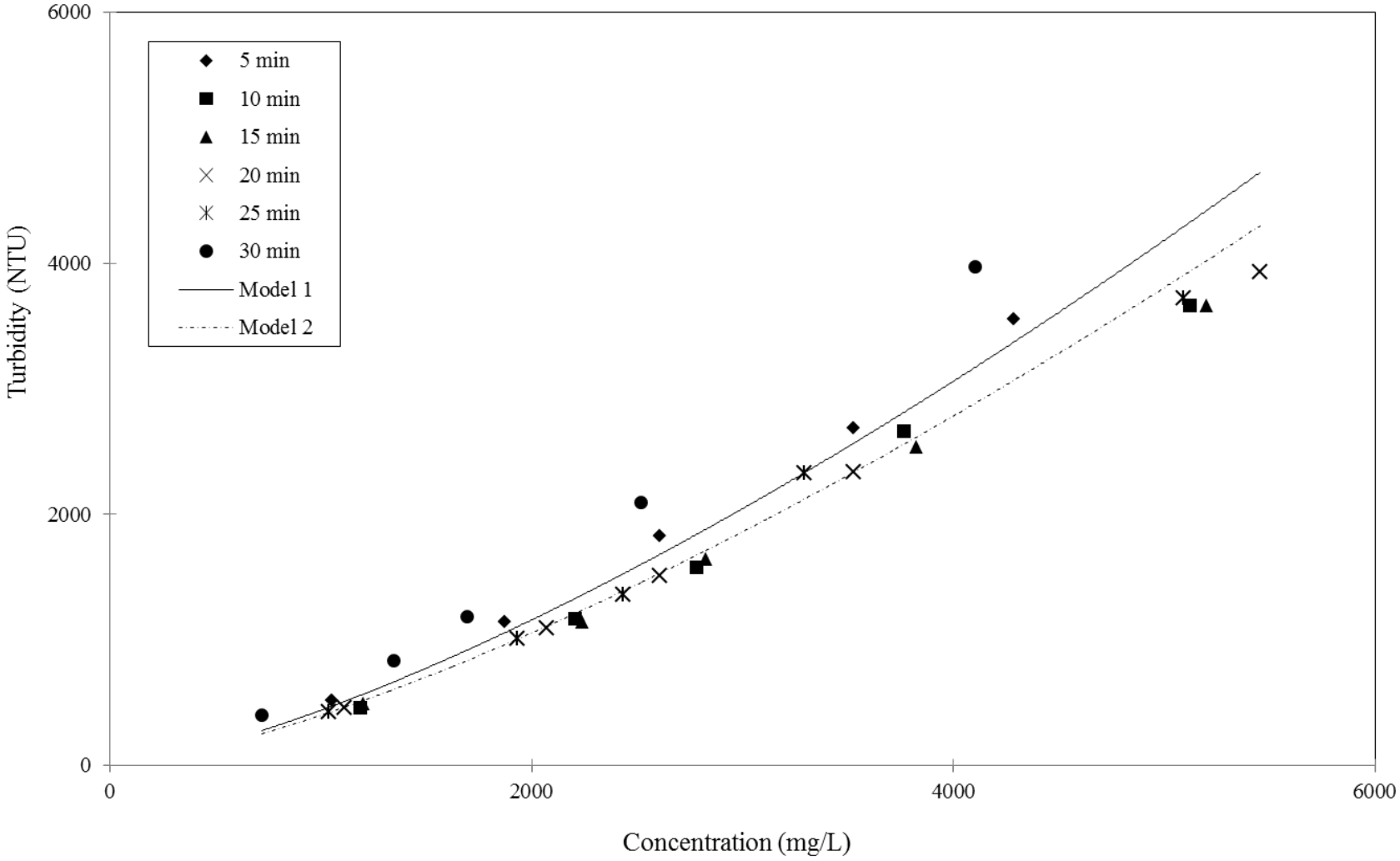

Figure 4.5. Estimated α functions for an example soil.

The α regression-based predictions were then applied to each soil to demonstrate how turbidity would be predicted based on collected TSS data. This analysis shows the impact of potential errors in α on predicted turbidity. Further application will be discussed in Chapter 6. Figure 4.5 shows the turbidity-TSS relationships for a soil with α estimated using both Equation 4.3 and 4.4. Turbidity was then determined by using the estimated α value in Equation 4.1 with a β value of 7/5.

4.3 Data Normalization

A single dimensionless curve is useful in representing the turbidity-concentration data. The power functions for the different soils can be collapsed into a single curve using a turbidity defined for an index concentration. The index concentration can be set by a turbidity standard or it can be a known value collected from a site.

4.3.1 Normalization by a Standard

Turbidity-concentration data can be normalized with a chosen turbidity standard, T_{std}. Using Equation 4.1, T_{std} can be used to determine the corresponding standard concentration, C_{std}, with an appropriate estimate or known α. Equation 4.1 can then be normalized with these standard values as seen in Equation 4.7.

$$\frac{T_{site}}{T_{std}} = \frac{\alpha_{site}}{\alpha_{std}}\left(\frac{C_{site}}{C_{std}}\right)^{7/5} = \left(\frac{C_{site}}{C_{std}}\right)^{7/5} \tag{4.7}$$

Because α_{site} and α_{std} are both determined using the same site data, they are the same value and would cancel out in Equation 4.7. With the removal of α, the data collapses nicely on a single curve. A dimensionless plot of all of the laboratory data is shown in Figure 4.5. A single dimensionless curve was able to accurately represent the observed data.

4.3.2. Normalization with a Single Known Data Value

A single measured pair of turbidity and concentration values for a storm event can be used to establish the relationship between turbidity and concentration. This approach is

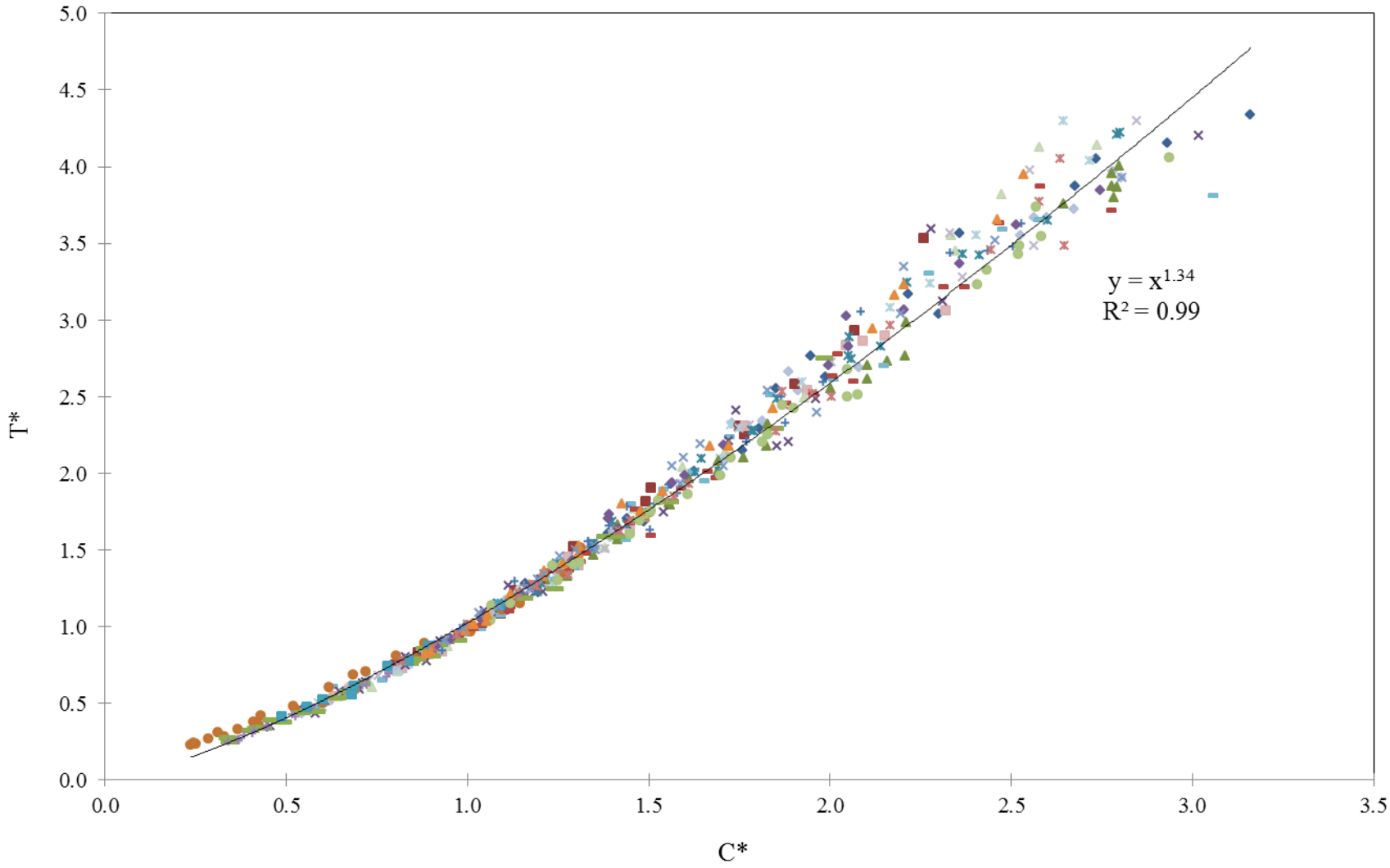

Figure 4.6. Laboratory turbidity and concentration data normalized by a 1000 NTU turbidity standard.

preferred if resources allow the collection of a single sample but are insufficient to allow multiple sampling during a storm event. The use of this known data avoids the uncertainty in estimating α from regression equations. In addition, as discussed in Chapter 5, α values change with deposition along the flow path, which further complicates the determination of α from regression equations.

Let's define a single sample from the site from which a known turbidity, T_{known}, and corresponding concentration sample, C_{known}, are obtained. Using Equation 4.1, T_{known} and C_{known} can be used to determine α_{known}. Equation 4.1 can then be normalized with these values as seen in Equation 4.8.

$$\frac{T_{site}}{T_{known}} = \frac{\alpha_{site}}{\alpha_{known}}\left(\frac{C_{site}}{C_{known}}\right)^{7/5} = \left(\frac{C_{site}}{C_{known}}\right)^{7/5} \tag{4.8}$$

Again, α_{site} and α_{known} are equal. For measured or predicted concentrations, the turbidity can then be computed by Equation 4.8. The α value is inherently embedded in the known turbidity and concentration values.

4.4 Summary

Through laboratory procedures, each soil was rained on for thirty minutes and runoff was collected every five minutes in 50 mL vials. These samples were then analyzed to determine time dependent relationships between turbidity and TSS. Each soil exhibited a strong power relationship with varying coefficients, α and β. These coefficients were then evaluated to determine suitable relationships for each coefficient. Using soil properties, a regression analysis determined a relationship to define the widely variable α coefficient. Due to the complicated process to attain the proper soil properties to use the regression model for α, a second, simpler, model was given that gives a suitable, yet less accurate approximation of α. Because β varied significantly less than α and had no visible trends with soil properties, it was set to a constant value of 7/5.

This relationship gives the ability to predict turbidity based on known soil concentration. Turbidity-concentration data can also be normalized into a single curve with a turbidity

standard and corresponding standard concentration or a known turbidity and corresponding concentration value from the site being monitored.

Chapter 5
Representation of Particle Settling in Turbidity Relationships

5.1 Introduction

Most sediment control practices remove eroded particles by gravitational settling. The larger sediment particles are then deposited and finer sizes are more likely discharged from the construction sites. Sediment control practices not only change the mass of sediment but also the particle size distribution. The analysis given in Chapter 4 can be used to evaluate changes in sediment mass on turbidity. The focus of this chapter is to investigate the impact of changes in the size of particles in the sample on turbidity.

A theoretical framework for changes in turbidities with sediment deposition will first be given. Data collection methods for this part of the study will then be explained. The collected data will be analyzed to determine parameters established by the theoretical framework. The chapter will conclude with recommendations on methods for changing turbidity with sediment deposition.

5.2 Theoretical Framework

5.2.1 Turbidity-Fraction-Finer Relationship

The distribution of mass with particle sizes is widely represented using the fraction finer. The fraction finer can be defined as

$$F_d = \frac{M_d}{M_T} = \frac{M_d/V}{M_T/V} = \frac{C_d}{C_i} \tag{5.1}$$

where M_d and C_d is the cumulative mass and corresponding concentration for a particle diameter of d, M_T is the total mass of a sample volume V without any deposition, and C_i is the initial concentration of the sample without any deposition.

The turbidity relationships developed in Chapter 4 are applicable to the initial concentration. For this chapter, the relationship is written as

$$T_i = \alpha_0 C_I^{\beta_0} \tag{5.2}$$

where T_I is the turbidity without deposition and α_0 and β_0 can be determined using the methods given in Chapter 4.

To allow for changes with sediment deposition, the turbidity relationship will be written in a more general form as

$$T_d = \alpha_d C_d^{\beta_d} = \alpha_d (F_d C_I)^{\beta_d} \tag{5.3}$$

where T_d is the turbidity with deposition corresponding to a diameter for F_d. In the above relationship, α_d and β_d vary with sediment deposition. Equation 5.1 was used for C_d.

A normalized turbidity can be obtained by using Equation 5.2 to obtain

$$T_d^* = \frac{T_d}{T_I} = \frac{\alpha_d (F_d C_I)^{\beta_d}}{\alpha_0 C_I^{\beta_0}} = \nu_d F_d^{\beta_d} C_I^{\beta_d - \beta_0} = \nu_d F_d^{\omega_d \beta_0} C_I^{\beta_0(\omega_d - 1)} \tag{5.4}$$

Where dimensionless parameters of ν and ω are defined as

$$\nu_d = \frac{\alpha_d}{\alpha_0} \tag{5.5}$$

$$\omega_d = \frac{\beta_d}{\beta_0} \tag{5.6}$$

As an alternative formulation, the relationship for T_d can be determined directly as

$$T_d = \nu_d F_d^{\omega_d \beta_0} C_I^{\beta_0(\omega_d - 1)} \left(\alpha_0 C_I^{\beta_0}\right) = \nu_d \alpha_0 F_d^{\omega_d \beta_0} C_I^{\omega_d \beta_0} \tag{5.7}$$

The experimental analysis in this chapter is done using the fractions of sand, silt, and clay in the initially eroded sediment. The upper limit of sand-sized particles corresponds to $F_d = 1$, and the lower limit of clay-sized particles corresponds to $F_d = 0$. The subscript "c" will be used to identify the breakpoint between clay-sized particles, that is, F_c corresponds to the finer fraction for the upper limit of clay-sized particles (and the lower limit of the silt-sized particles). Similarly the subscript "s" will be used for the breakpoint between silt and sand, and therefore F_s is the fraction finer corresponding to the upper limit of silt-sized particles. By using this notation, the initial turbidity can then be divided into clay, silt, and sand components as

$$T_I = \Delta T_{Clay} + \Delta T_{silt} + \Delta T_{Sand} \tag{5.8}$$

where each component is defined by Equation 5.7 as

$$\Delta T_{clay} = \nu_c \alpha_0 F_c^{\omega_c \beta_0} C_I^{\omega_c \beta_0} \tag{5.9}$$

$$\Delta T_{silt} = \nu_s \alpha_0 F_s^{\omega_s \beta_0} C_I^{\omega_s \beta_0} - \nu_c \alpha_0 F_c^{\omega_c \beta_0} C_I^{\omega_c \beta_0} \tag{5.10}$$

$$\Delta T_{sand} = \alpha_0 C_I^{\beta_0} - \nu_s \alpha_0 F_s^{\omega_s \beta_0} C_I^{\omega_s \beta_0} \tag{5.11}$$

For the upper limit of sand-sized particles, $\omega_d = \nu_d = 1$. The use of these relationships requires particle size distribution information to define F_s and F_c. Experimental data were collected and are analyzed in this chapter to obtain insight into ν_d and ω_d.

5.2.2 Simplified Forms

Insight into the role of deposition can be obtained by simplifying Equation 5.7. Let's first consider the special case where $\omega_d = \nu_d = 1$. The parameters of the turbidity relationship are then independent of the deposition processes. Equation 5.7 can be written as

$$T_d = \alpha_0 F_d^{\beta_0} C_I^{\beta_0} = \alpha_0 C_d^{\beta_0} \tag{5.12}$$

The turbidity is now defined using the relationships of Chapter 4. The turbidity is only a function of changes in the sediment mass. Mathematically, change in turbidity with size of sediment can now be directly written as

$$\frac{dT_d}{dF_d} = \alpha_0(\beta_0 - 1) F_d^{\beta_0 - 1} C_I^{\beta_0} \tag{5.11}$$

Relationships are further simplified if the turbidity varies linearly with concentration, which corresponds to $\beta_0 = 1$. With this condition, and again using $\omega_d = \nu_d = 1$, the clay silt and sand components of turbidity can be evaluated as

$$\Delta T_{clay} = T_{clay} = \alpha_0 F_c C_I = \alpha_0 C_{clay} \tag{5.12}$$

$$\Delta T_{Silt} = T_{silt} = \alpha_0 F_s C_I - \alpha_0 F_c C_I = \alpha_0 (F_s - F_c) C_I = \alpha_0 C_{silt} \tag{5.13}$$

$$\Delta T_{Sand} = T_{sand} = \alpha_0 C_I - \alpha_0 F_s C_I = \alpha_0 (1 - F_c) C_I = \alpha_0 C_{sand} \tag{5.14}$$

where the turbidity for each component varies linearly with its concentration. The initial turbidity can be written as

$$T_I = T_{clay} + T_{silt} + T_{sand} \tag{5.15}$$

that is, it is a linear combination of the turbidities of each of its component. This relationship corresponds to the results obtained by Patil et al. (2011). It is limited to a linear relationship between turbidity and concentration and to a scaling factor, α, that remains constant for all particle sizes.

5.3 Data Collection

Data were collected to further investigate the effect of particle settling on the relationships developed in Section 5.2. The initial sediment concentration and turbidity data were obtained using the same experimental design given in Chapter 3. Each soil was allowed to run off for 30 minutes. However, in addition to collecting the 50 mL samples used in Chapter 4, the runoff was collected in a bucket. This relatively large sample of runoff was used to investigate the effect of particle settling on the ν_d and ω_d coefficients.

To analyze particle settling, a pipette experiment (Klute [Ed.], 1986) was performed on each runoff sample. To do this, each sample was mixed thoroughly with a paint stirrer to adequately suspend all of the sediment in the sample. As the sample was being mixed, an initial 120 mL sample was extracted at a depth of 10 cm from the water surface level. This sample represented the total turbidity of the bucket sample. The sample was then allowed to settle and samples were extracted according to the settling rate of the primary sediment particles sand (> 50 μm), silt (2-50 μm), and clay (< 2 μm). The universal grain settling equation developed by Ferguson and Church (2004) was used to determine the equivalent spherical diameters of the extracted particles based on settling time and extraction depth.

Each 120 mL sample was mixed and divided into six 30 mL vials containing 0, 5, 10, 15, 20, and 25 mL of water. Each vial was then mixed and the turbidity of the sample was taken. The TSS concentration was determined for each sample, and the values were plotted on a TSS vs. Turbidity plot. Figure 5.1 shows an example plot of this information.

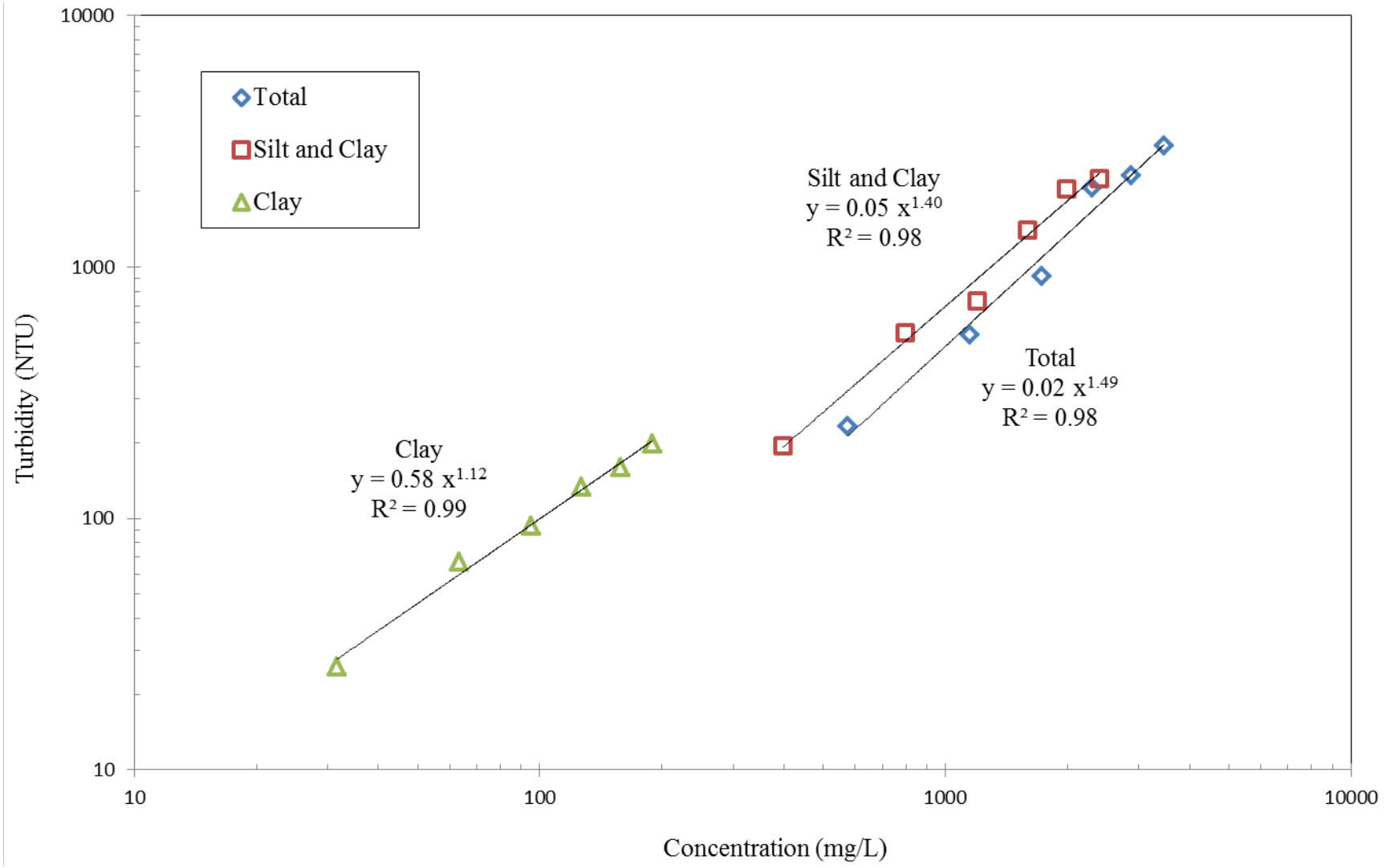

Figure 5.1. Example of turbidity and concentration data corresponding to a total runoff sample.

5.4 Data Analysis

For the total runoff sample, three turbidity relationships were developed using Equation 5.2 corresponding to sand-silt-clay, silt-clay, and clay sized particles. A typical set of curves is shown in Figure 5.1. As shown by this figure, both power and scaling coeffiecients vary with changes in the size of particles in the sample. Using the theoretical framework described in Section 5.2, each soil was evaluated to quantify these changes with the adjustment parameters, ν and ω.

5.4.1. Estimation of ω_d

To start the analysis, a relationship for ω with fraction finer, F_d, was sought, where, as given by Equation 5.1, F_d represents the fraction of the total mass smaller then diameter, d. A relationship between these two variables then represents changes in ω_d as particles are removed from suspension. To determine this relationship, ω_d was determined for the each soil using Equation 5.6. The upper limit for ω is $\omega_d = F_d = 1$.

Each individual soil showed a strong logarithmic trend between the ω_d and F_d values of the following form

$$\omega_d = \gamma \ln(F_d) + 1 \tag{5.16}$$

where the coefficient γ varied between 0.05 and 0.16.

Further analysis was performed to determine if the coefficient γ could be estimated using the soil properties described in Chapter 3. A multiple linear regression, similar to the regression performed on α in Chapter 4, was used to analyze the coefficient γ. This analysis showed a slight trend in γ with dry bulk density. A regression on all of the soil's ω_d and F_d values to develop a constant relationship that uses a constant γ. This regression can be seen in Figure 5.2. The two regression models are

$$\omega_d = \left(0.23 - 9.20E\text{-}2\ BD\right) Ln(F_d) + 1 \tag{5.17}$$

$$\omega_d = 0.09\ Ln(F_d) + 1 \tag{5.18}$$

where F_d is the fraction finer and BD is the dry bulk density of the soil in g/cm^3.

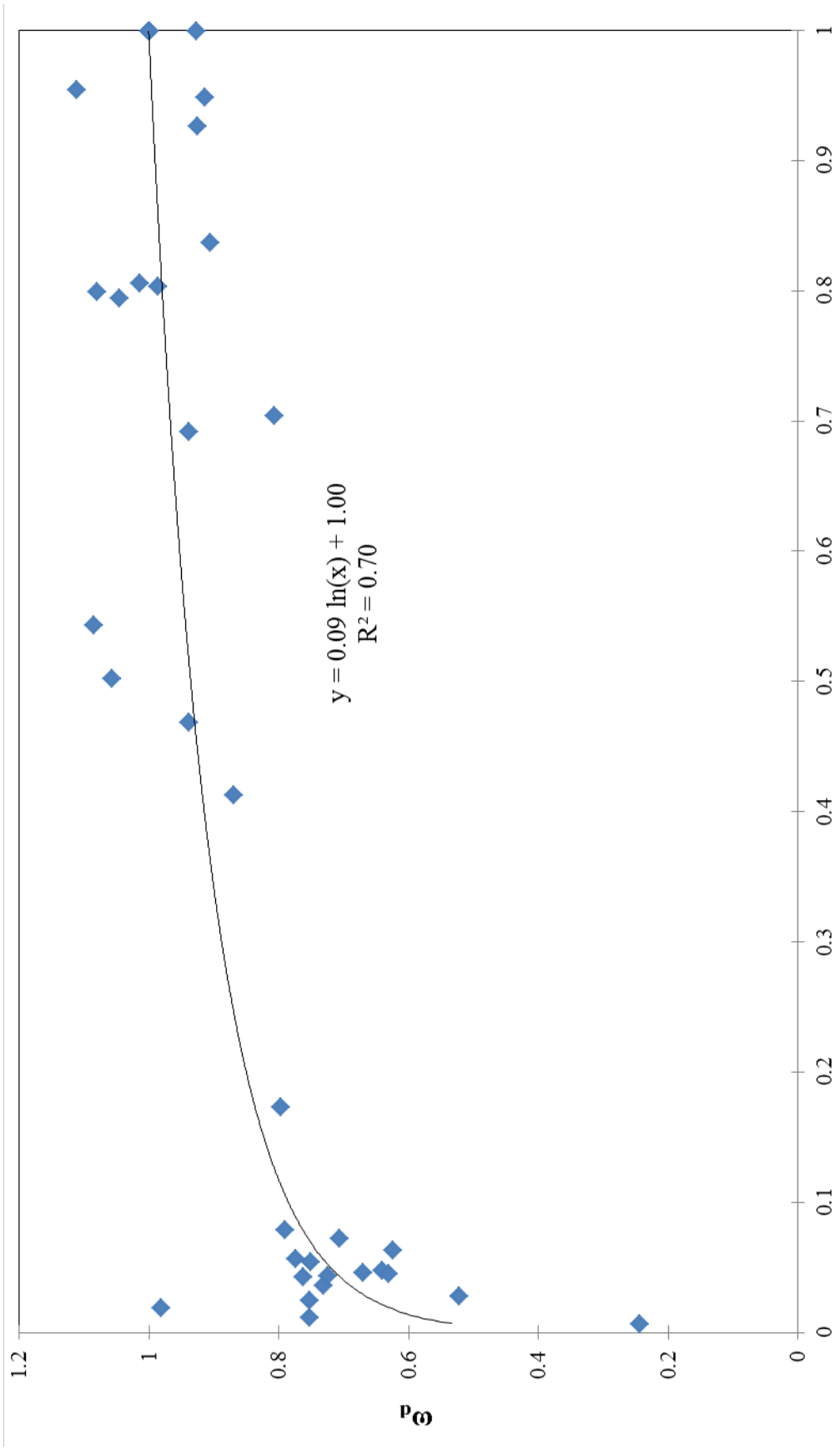

Figure 5.2. Overall logarithmic regression between ω_d and F_d for all soils.

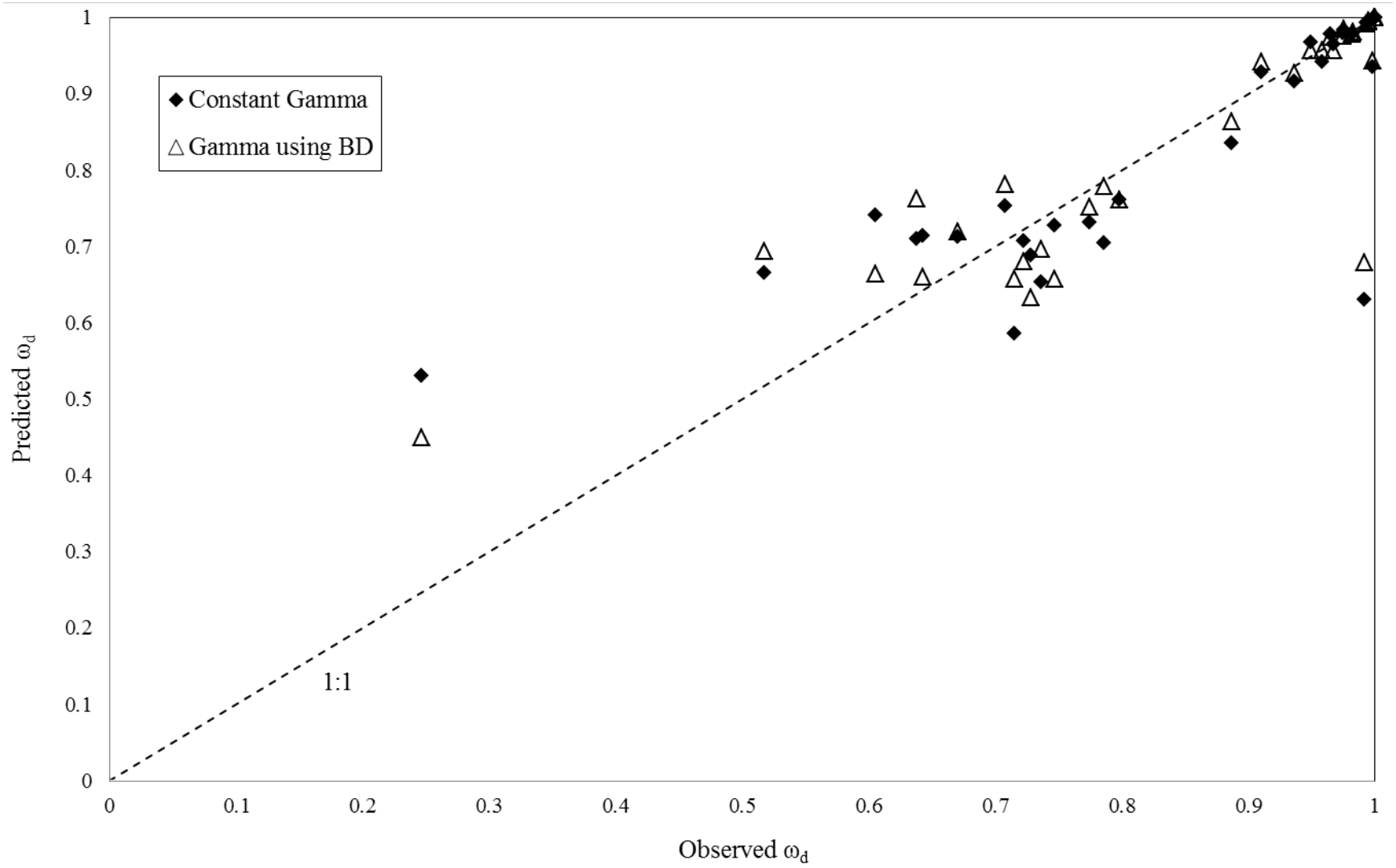

Figure 5.3. Observed vs. Predicted ω_d using Equation 5.17 and Equation 5.18.

Figure 5.3 shows the observed ω_d values plotted against ω_d predicted with Equations 5.17 and 5.18. This figure has a 1:1 line that represents a model that perfectly predicts ω_d. The normalized mean square error (NMSE) of each model was determined with Equation 4.5 for just the ω_s and ω_c values. Predictions of ω_t contain no error because $\omega_t = 1$ at all times. Using dry bulk density to estimate γ and using a constant γ had an NMSE of 0.23 and 0.31, respectively.

Predicting ω_d using bulk density (Equation 5.17) has less error then an overall regression with a constant γ; however, the error is not considerably smaller than using a constant relationship for ω_d. The next section will use Equation 5.18 to predict ω_d and determine a relationship for ν_d.

5.4.2 Estimation of ν_d

The scaling factor is adjusted for the size of particles using the ν_d parameter. This adjustment parameter was determined for each soil using Equation 5.7. The ω_d parameter in this equation was estimated using Equation 5.18 developed in the previous section. Once again, three ν_d values were obtained for the sand-silt-clay, silt-clay, and clay sized particles. Results for all soils were plotted together to determine how the parameter varied with particle settling (see Figure 5.4). The best least square fit to the ν_d data is

$$\nu_d = F_d^{-0.85} \tag{5.19}$$

The ν_d parameter varied between 1 and 45 for our soils. This range is consistent with that obtained for the observed variability in α for our analysis given in Chapter 4. This analysis showed that the range in the x-intercept values was approximately 50, with the soil containing the least amount of clay on the far right of Figure 4.2. Likewise, Figure 5.2 shows that the α value and x-intercept can vary significantly as large particles are removed from suspension. The range in ν_d is consistent with the variability found in α in the other components of our study.

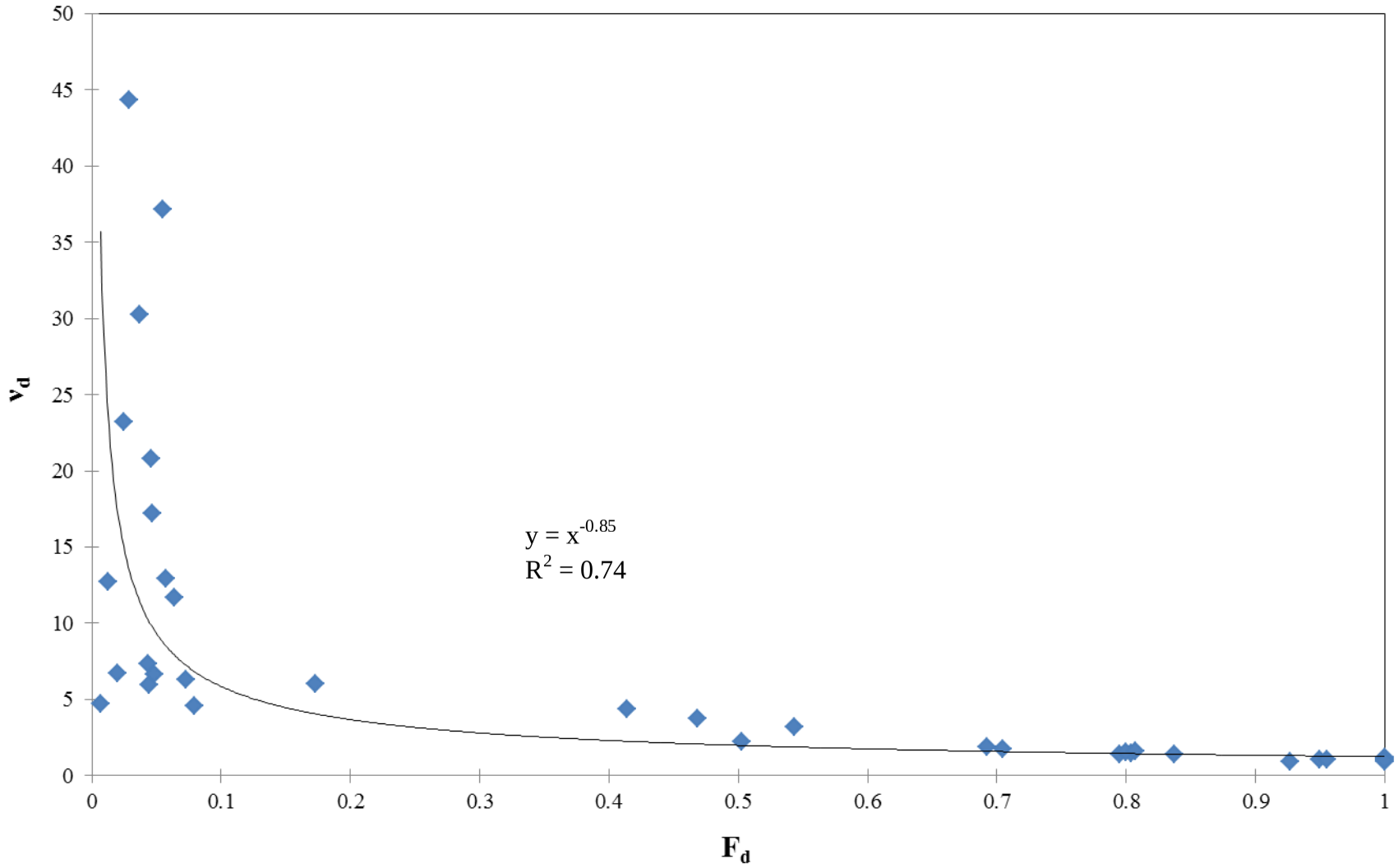

Figure 5.4. Overall power relationship between v_d and F_d for all soils.

5.5 Dimensionless Turbidity

Equation 5.4 defines dimensionless turbidity, T_d^*, as the ratio of the turbidity corresponding to particle size d to the initial turbidity corresponding to the sample. It is a function of the initial power value, β_0, and concentration, C_I, of a soil, the dimensionless parameters, ω_d and ν_d, and the fraction finer, F_d, corresponding to the diameter d. If the initial concentration of the sample does not significantly impact the dimensionless turbidity, then dimensionless turbidity is defined as

$$T_d^* = \frac{T_d}{T_I} = \nu_d F_d^{\omega_d \beta_0} \tag{5.20}$$

The removal of concentration simplifies the determination of the turbidity with sediment deposition. Equation 5.19 is only a function of fraction finer and fitted coefficients. It provides a simple way to estimate what size particles need to be removed from runoff to meet a specific turbidity, greatly aiding the development of erosion control plans.

The dimensionless turbidities for the sand, silt, and clay particles in each of the laboratory soils were found using both Equation 5.4 and Equation 5.19. ω_d and ν_d were estimated using the relationships shown in Figure 5.3 and Figure 5.4. The minimum, maximum, and median values for fraction finer and both dimensionless turbidities are given in Table 5.1.

Table 5.1. Dimensionless turbidity calculated with and without concentration.

	Sand				Silt		
		min	max	median	min	max	median
F_d	1	0.1733	0.9998	0.7974	0.0067	0.0795	0.0451
T* w/ conc.	1	0.2401	0.0998	0.7651	0.7416	0.0999	0.0935
T* w/o conc.	1	0.0207	0.1257	0.0465	0.4881	3.896	0.8547

Unfortunately, the simplified equation does not accurately predict the dimensionless turbidity of clay. For most applications, it should not be used to evaluate the impact of deposition on turbidity.

5.6 Summary

The effect of particle settling on the turbidity-concentration relationship developed in Chapter 4 was evaluated. A theoretical framework was developed to explain how turbidity can be divided into primary particle classes. Dimensionless adjustment parameters ν and ω were developed to represent the change in α and β as sediment is removed from suspension. Relationships for the change in ν and ω with fraction finer were developed. These relationships were used to determine the turbidities of each particle size for each soil evaluated.

Chapter 6
Field Application

6.1 Introduction

A field study was conducted on two construction sites as a companion project to the laboratory work. With the aid of several Minnesota Department of Transportation (MN DOT) employees, monitoring plans were developed and implemented to evaluate sediment control practices at these sites. Both continuously monitored turbidity data and grab samples at various locations on the two sites were collected for comparison to our laboratory study.

A complete description and analysis of data for the field study are beyond the scope of this thesis. Nonetheless, dilution curves for a single storm are compared to those results obtained from the laboratory study. The field study will also be used to illustrate on how our turbidity relationships can be applied to construction sites. A brief overview of the construction site will first be given. Our relationships will then be used (1) to determine the turbidity from observed concentrations and (2) to determine total suspended solids and the total sediment yield from observed turbidities.

6.2. Description of Field Sites

Two construction sites were monitored as part of the field study. At one site, in Arden Hills, MN, the monitoring efforts were largely focused on an overpass constructed for Interstate-694. The initial discharge point of the runoff from the site was located near a small lake bordering a residential area. Monitoring and sample collection was done at the culvert directly upstream of the lake. This information was used for comparison to the laboratory data.

The second site was located west of Bloomington, MN for a constructed interchange at the intersection of Interstate-494 and Highway-169. Several large detention ponds were constructed that were able to contain most of the stormwater from the site. Because significant discharge was rare from these ponds, monitoring efforts were shifted to a ditch

upstream of the interchange. This new site was used to evaluate turbidity monitoring capability and installation issues associated with construction sites.

6.3 Comparison of Field and Laboratory Dilution Curves

Grab samples from both sites were brought to the lab and were analyzed using the same process described in Chapter 4 to create dilution curves. An ISCO model 3700 water sampler was installed at the Arden Hills site. This sampler collected 1000 mL every five minutes during a rainfall event on August 3, 2012. A total of 24 samples were brought into the lab to be analyzed. A turbidity reading was taken for every sample, but all of the readings were greater than the maximum possible turbidity reading of our instruments of 4000 NTUs. Three temporally representative samples were chosen to develop observed dilution curves. An ISCO model 3700 water sampler was also placed on the Bloomington site for the same storm, but there was not enough runoff to trigger the sampler. A single grab sample was collected and brought into the lab for analysis with the Arden Hills samples.

One of the soils used in the laboratory experiments was from the Arden Hills site, allowing for a comparison of the field and laboratory turbidity data. The field samples collected on August 3 are best represented by the subsoil collected from that site. Figure 6.1 shows the dilution curves for the laboratory and field samples. There were two replicates done on the Arden Hills subsoil in the laboratory. Since the laboratory methods collected samples at six different times, there are a total of twelve time-dependent dilution curves. For the six dilution curves from the first replicate, the average power value, shown as β_1 in Figure 6.1, was 1.40. For the second replicate, the average power value, β_2, was 1.38. The field data had an average power value of 1.37. The scaling factor α for the laboratory and field samples ranged from 0.01 to 0.07 and 0.08 to 0.1, respectively.

The β values found in the field are similar to those found in the laboratory. This result suggests that the power values obtained in the laboratory study are representative of field conditions. The α values of the field samples are noticeably larger than values reported for the laboratory data. This result is not surprising. Deposition of larger sized particles is

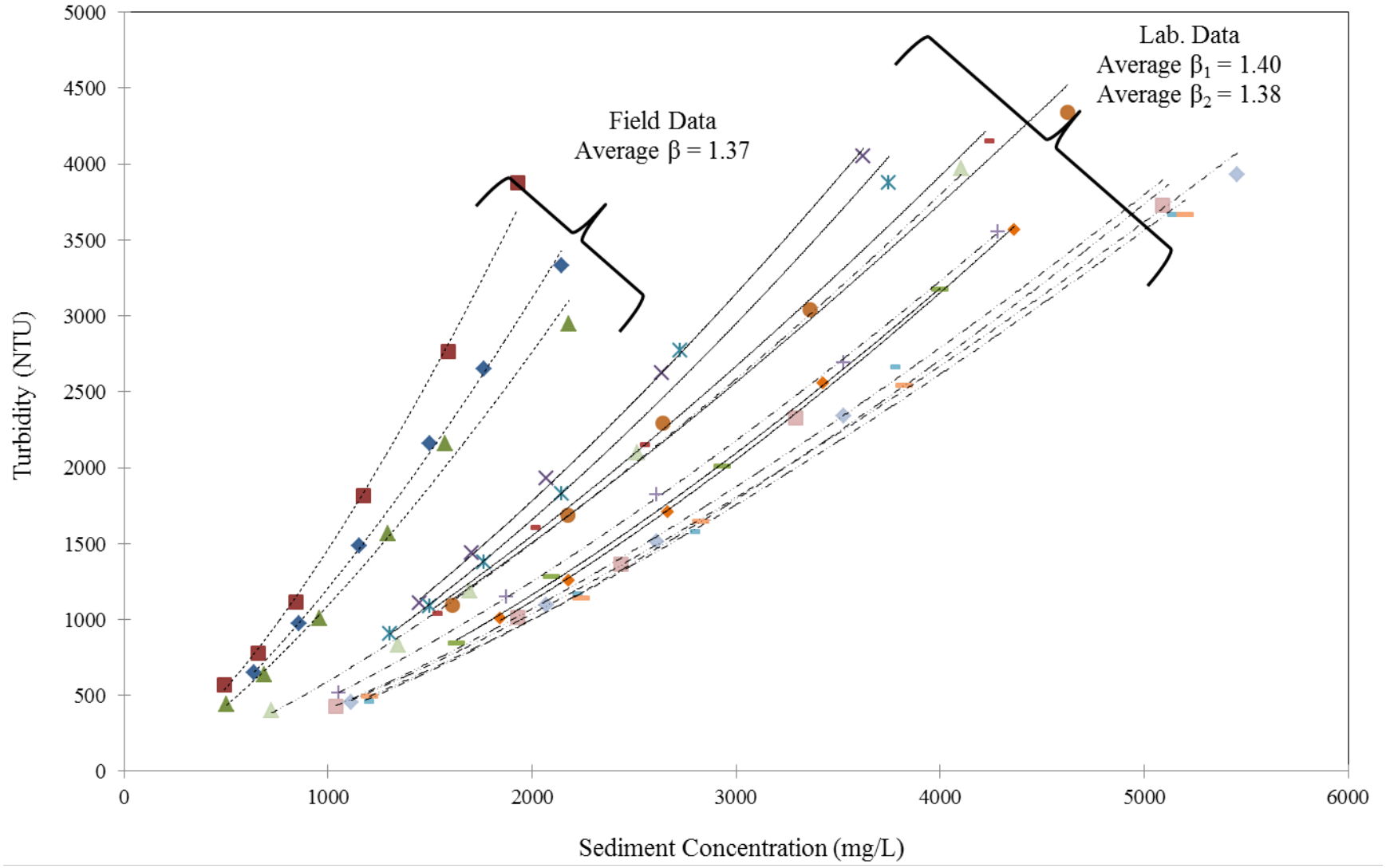

Figure 6.1. Arden Hills dilution curves for laboratory and field samples.

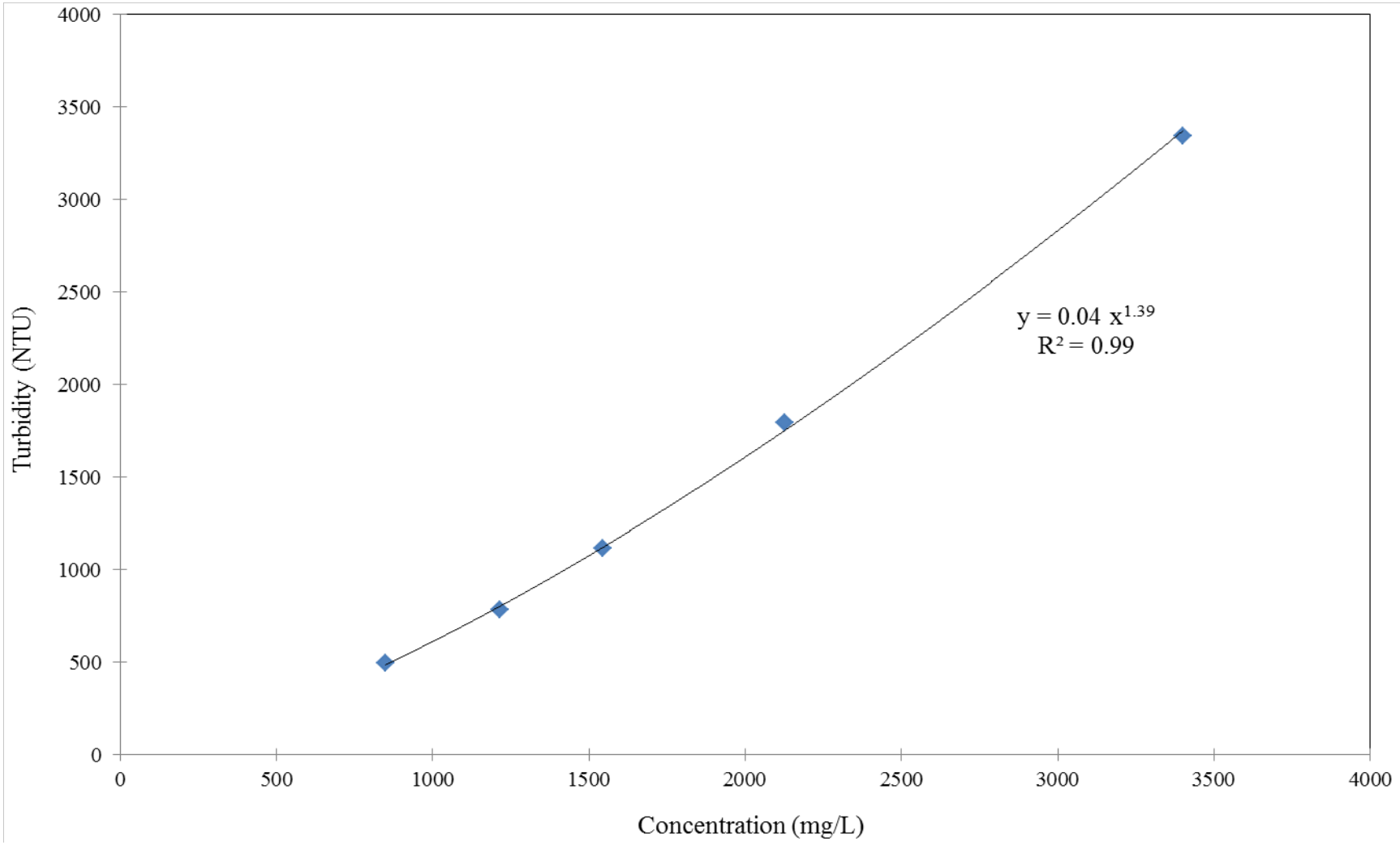

Figure 6.2. Dilution curve for Bloomington construction site.

likely at the construction site. Changes in particle-size distributions were shown in Chapter 5 to decrease the power coefficient and increase the scaling factor. Differences between field and laboratory dilution curves are consistent with both of these trends. Observed differences in laboratory and field α values are within the range of expected shifts in α with finer sediment for the Arden Hills subsoil given in Chapter 5.

A dilution curve was created for the single sample from the Bloomington site (Figure 6.2). There is no laboratory data to compare to this dilution curve, but it does show the same strong power relationship between turbidity and concentration and a β value of nearly 7/5.

6.4 Example Applications

Turbidity-TSS relationships developed with this study are useful to (1) estimate turbidities from measured sediment concentrations and (2) estimate sediment concentrations from measured turbidities. The first type of application will be illustrated using the data collected at the Arden Hills site. This application is particularly useful for the assessment of turbidity water quality standards from measured or predicted TSS.

Determination of concentrations from measured turbidities will be illustrated using data collected at the Bloomington site. This application is of interest in the assessment of a TSS water quality standard from turbidity data. With the additional use of an observed or predicted hydrograph, sediment load can be obtained from the estimated concentrations. The impact of a turbidity standard on the reduction in sediment loads to lake and streams can then be assessed.

6.4.1. Estimating Turbidity from Observed Concentrations

The simplest application of Equation 4.1 is to predict turbidity from a known concentration. On a construction site, turbidity is more likely measured then concentration data. However, process-based simulation models, such as SEDIMOT II (Wilson et al., 1984) and WATER (Wilson et al., 2008) can predict concentrations. These models can be used to assess the effectiveness of different sediment control

measures. Equation 4.1 can then be used to determine the impact of these measures on turbidity and their effectiveness in meeting potential turbidity standards.

The estimation of turbidity from concentrations will be done using the 24 samples collected on August 3rd at the Arden Hills site. The observed concentrations are plotted with time in Figure 6.3. To use Equation 4.1, the α and β coefficients need to be determined. As previously discussed in Section 4.2, setting $\beta = 7/5$ is a reasonable assumption for Minnesota construction site soils. Three approaches are available to estimate α. They are (1) estimate α using Equation 4.3 (Model 1), which requires soil properties of percent silt, interrill soil erodibility, and the NRCS maximum abstraction depth, (2) estimate α using Equation 4.4 (Model 2) using only percent silt, and (3) solve for α directly from an observed pair of concentration and turbidity values using a $\beta = 7/5$. The third approach is preferred, but often data from individual storm events are unavailable. Equation 4.3 is the more accurate regression model for determining α, but it requires information that may not be readily available for construction sites. If a simple approximation is adequate, Model 2 can then be used to determine α.

Differences between the two methods can be assessed using all of the soil property information for the Arden Hills site determined in the laboratory experiment. Both Model 1 and Model 2 were evaluated for Arden Hills subsoil to obtain α of 0.027 and 0.025, respectively. The α values for the field samples were higher than these values, ranging from 0.08 to 0.1. Based on a particle size analysis, the soil is comprised of 46% sand and 54% silt. Using the relationships for ν_d and ω_d from Chapter 5 and assuming sand was removed from the runoff prior to sampling, the scaling factor α increased to 0.046 and the power β decreased to 1.32. This shows that deposition plays an important role in estimating turbidity.

Figure 6.3 shows the estimated turbidity using Model 1 and Model 2 and estimated turbidity if sand were removed from suspension for the grab samples collected at Arden Hills. The predicted turbidity values are larger than the range of turbidities obtained in the laboratory study. All samples would likely violate any turbidity standard established by the State of Minnesota. Percent differences in predicted turbidities obtained for the two different estimates of α are reasonable; however, absolute difference are substantial.

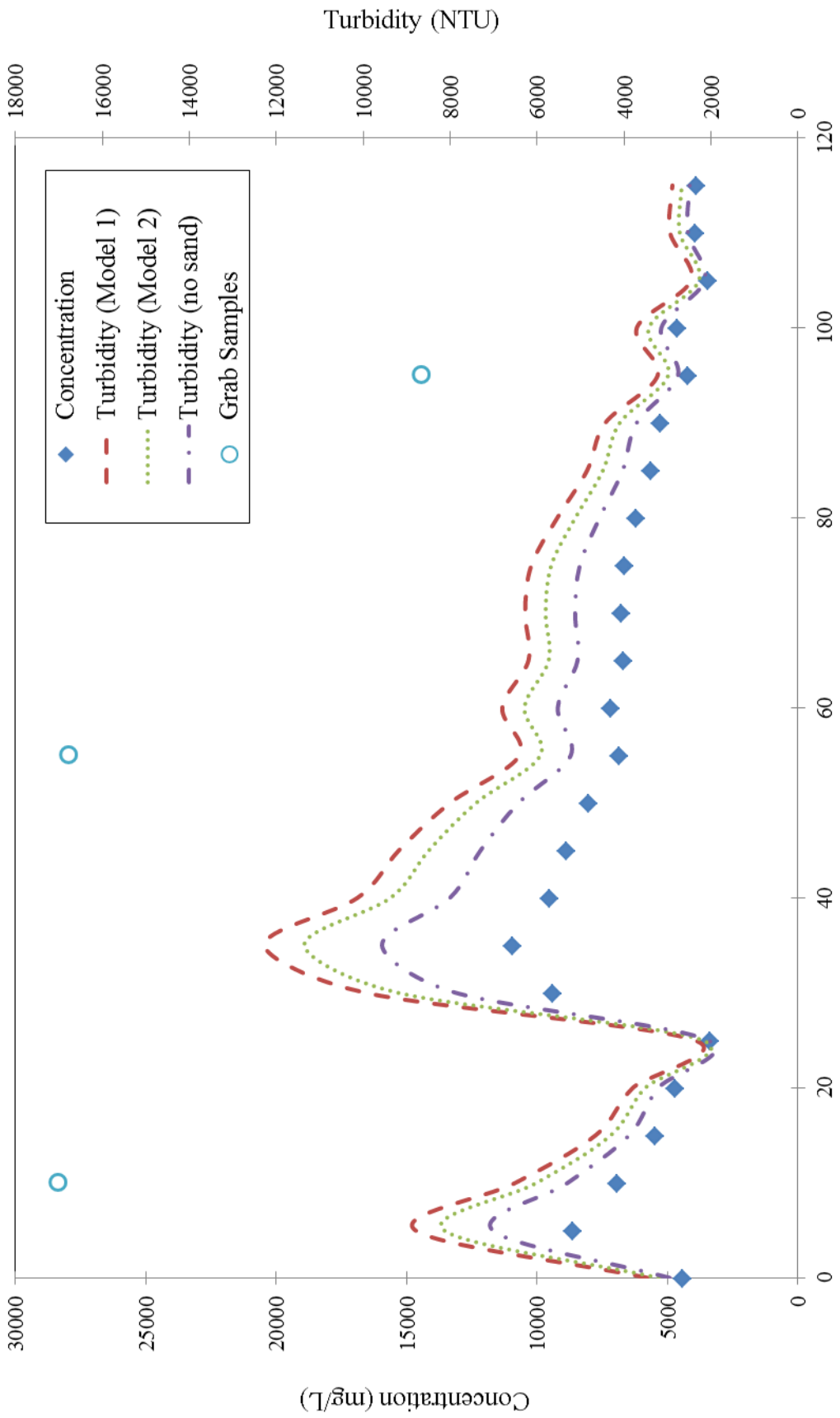

Figure 6.3. Predicted turbidity values for the August 3rd storm on the Arden Hills construction site.

Dilution curves were created for three grab samples for this storm. Those curves were used to estimate the turbidity based on the concentration of sediment in the sample. These values were also plotted on Figure 6.3 to compare the predicted turbidities with the actual turbidities. The predicted turbidities are significantly lower. This discrepancy may be attributed to the August 3rd storm being larger than the control storm used in the laboratory experiment or changes in the soil's particle-size distribution.

6.4.2 Estimating Sediment Loads

On a construction site, it is more likely that turbidity is being monitored and not TSS concentration. By using relationships developed as part of this study, continuously monitored turbidity data can be converted into concentrations and used to determine sediment loads from a site. Similar to Section 6.3, this conversion requires values for α and β for the storm event. Rearranging Equation 4.1, concentration is related to turbidity in the following format:

$$C = \left(\frac{T}{\alpha}\right)^{5/7} \tag{6.1}$$

Continuously monitored turbidity data and rainfall data were collected in a ditch on the Bloomington site during a 19 hour rainstorm on May 23, 2012. The observed turbidity-concentration data shown in Figure 6.2 were used to estimate α for this storm. The estimated concentration using Equation 6.1 is shown with the corresponding turbidity data in Figure 6.4.

A hydrograph was created for the May 23 rainstorm using an estimated time of concentration and rainfall excess determined with the SCS curve number method (Wurbs & James, 2001). Because the time of concentration was less than ten minutes, the runoff hydrograph was estimated assuming that the runoff rate equaled the excess rate at the end of each time interval. The calculations used to create the hydrograph can be seen in Appendix G. Figure 6.5 shows the estimated concentration data and hydrograph for the May 23rd rainstorm. With the estimated concentration and hydrograph, sediment load at each time step can be calculated with the following equation:

$$Sediment\ Load = Q\ C \tag{6.2}$$

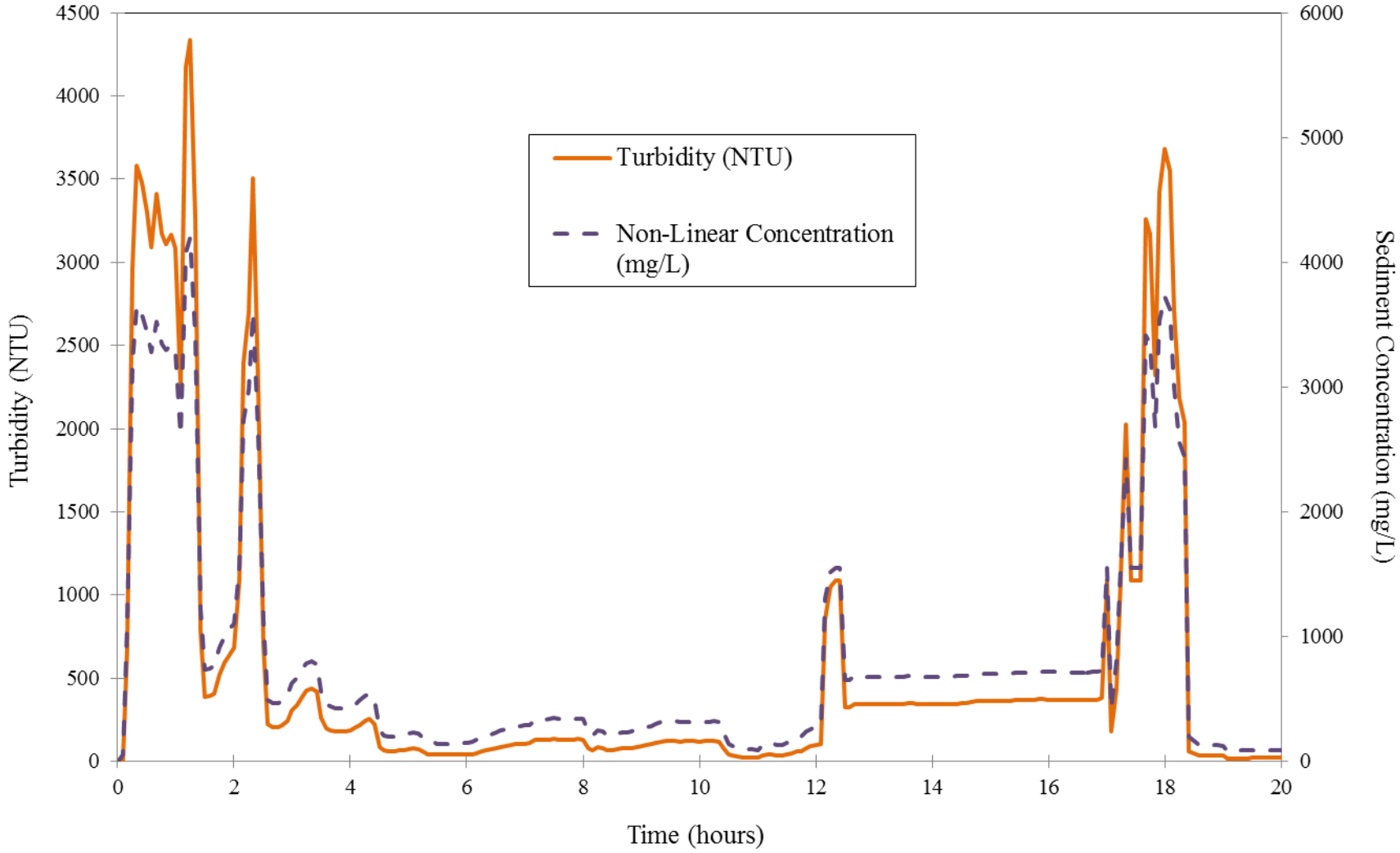

Figure 6.4. Estimated concentration values corresponding to the turbidity data collected on the Bloomington site for the rain storm on May 23, 2012.

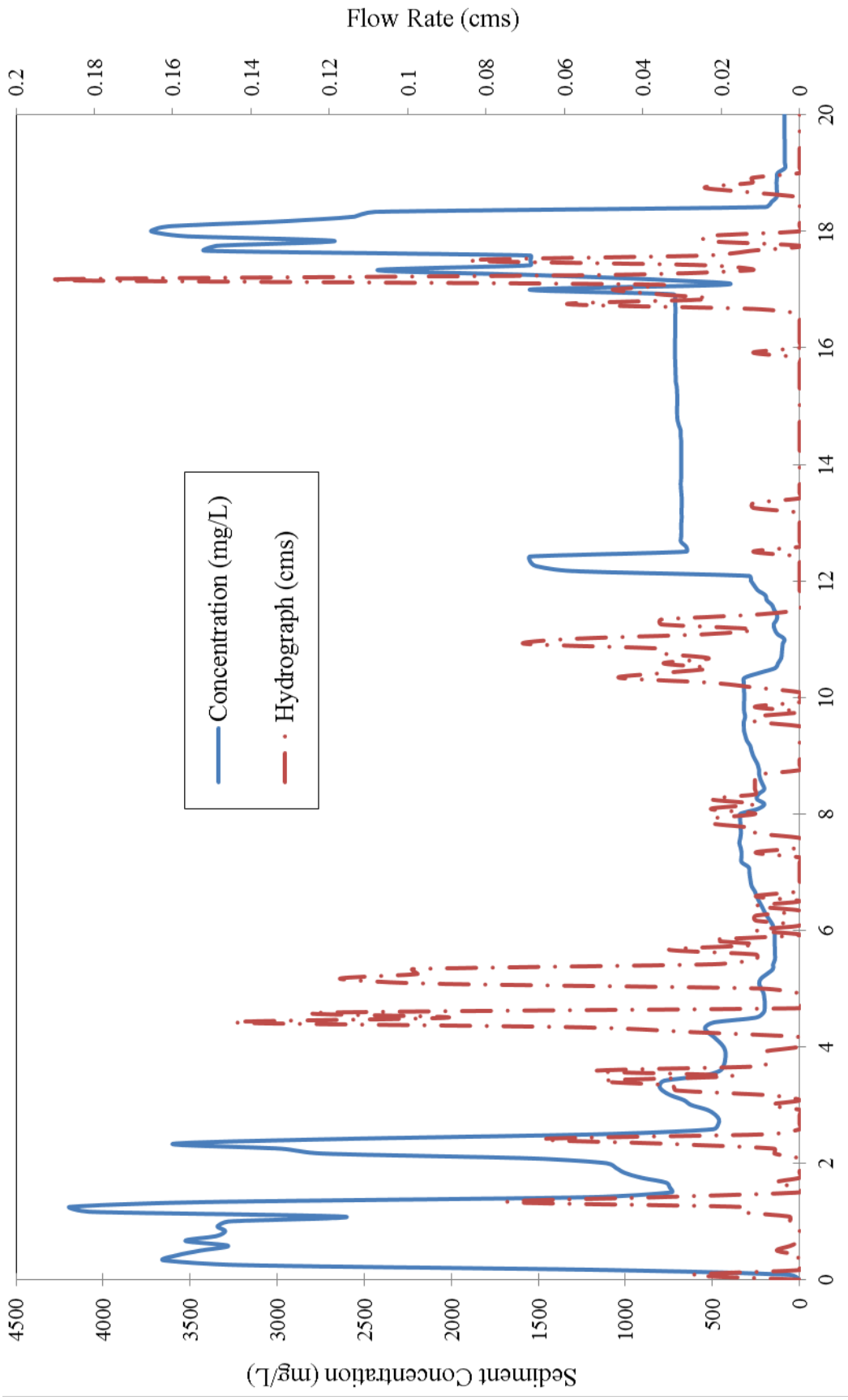

Figure 6.5. Estimated concentration data and hydrograph for May 23 storm on Bloomington site.

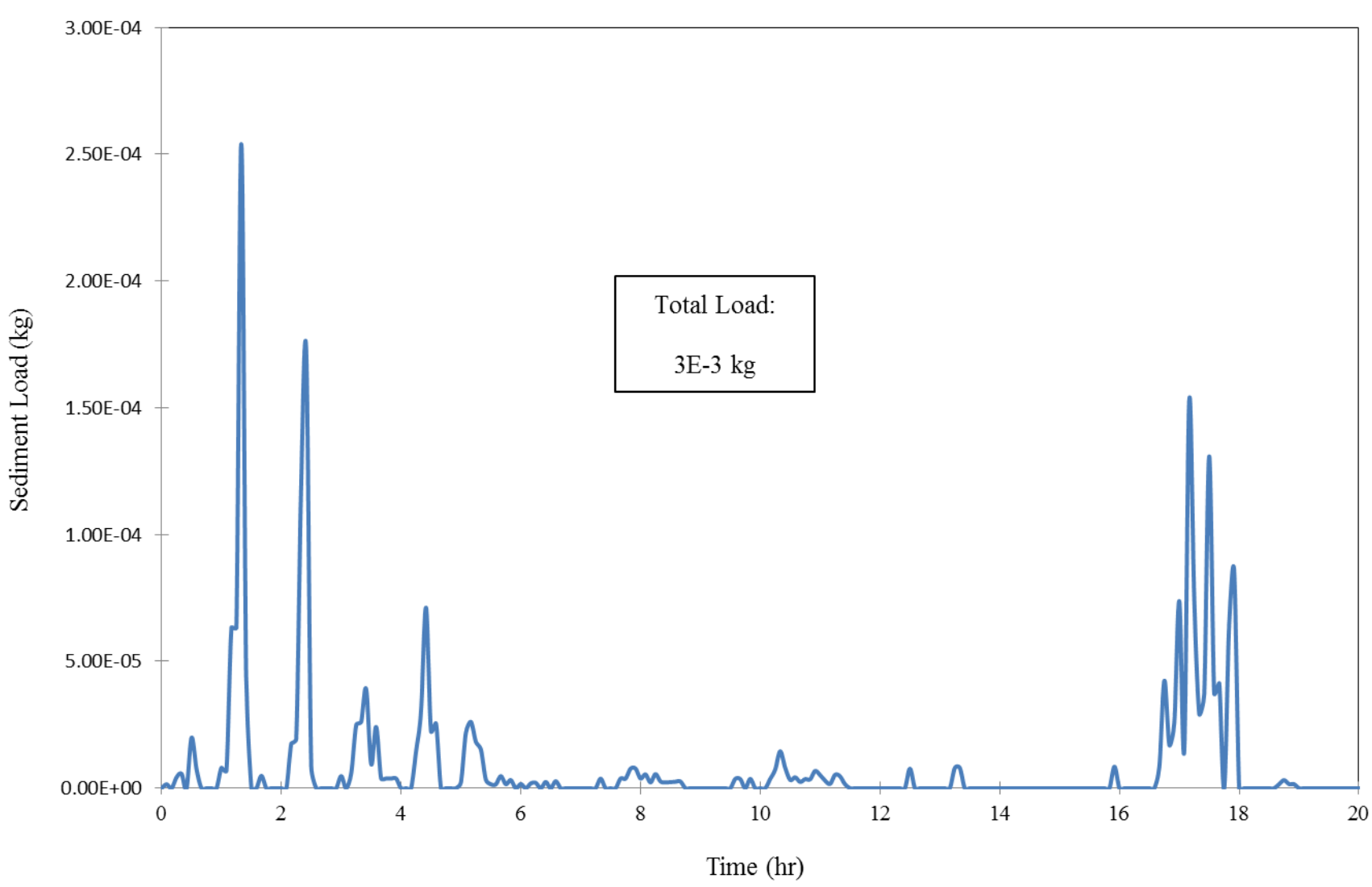

Figure 6.6. Sediment load on the Bloomington site during the May 23 storm.

where Q is the flow rate and C is the concentration of sediment in the runoff.

Figure 6.6 shows the sediment load in tons for the May 23rd storm in Bloomington. To determine the total sediment load passing the monitoring location, the product of flow rate and concentration is simply integrated over the storm duration using the following integral:

$$Total\ Sediment\ Load\ = \int_o^t Q(t)\ C(t)\ dt \tag{6.3}$$

Integrating to find the area under the curve in Figure 6.6 determined that the monitoring location on the Bloomington site had a sediment load of approximately 3.5 kg during the May 23rd storm.

6.5. Impact of a Non-linear Turbidity-Concentration Relationship

Several studies, previously mentioned in Chapter 2, concluded that turbidity and concentration vary linearly. Our analysis of turbidity-concentration relationships for Minnesota construction soils resulted in non-linear power functions. To evaluate the implication of a non-linear relationship, two scenarios will be discussed. First, let's consider a percent reduction in turbidity to meet a turbidity standard. Implementation of sediment control practices is likely required to meet this standard. We are therefore interested in differences in the corresponding percent reductions in sediment concentrations using a linear or non-linear relationship. A single flow –weighted sample is often collected for a given storm to reduce the cost of water quality analysis. Our second scenario examines the error obtained estimating the average turbidity for the storm using the single sample if turbidity varies linearly or nonlinearly with concentration. The first scenario was evaluated using the laboratory concentration and turbidity data for the Arden Hills subsoil. Both linear and nonlinear relationships for this soil are shown in Figure 6.7. The second analysis used the turbidity and estimated concentration data for the May 23rd storm in Bloomington.

For the first scenario, three turbidity values were chosen for the analysis: 4000, 2000, and 500 NTUs. The concentrations corresponding to each turbidity value were calculated with both the linear and non-linear relationship for the soil. The percent reduction was

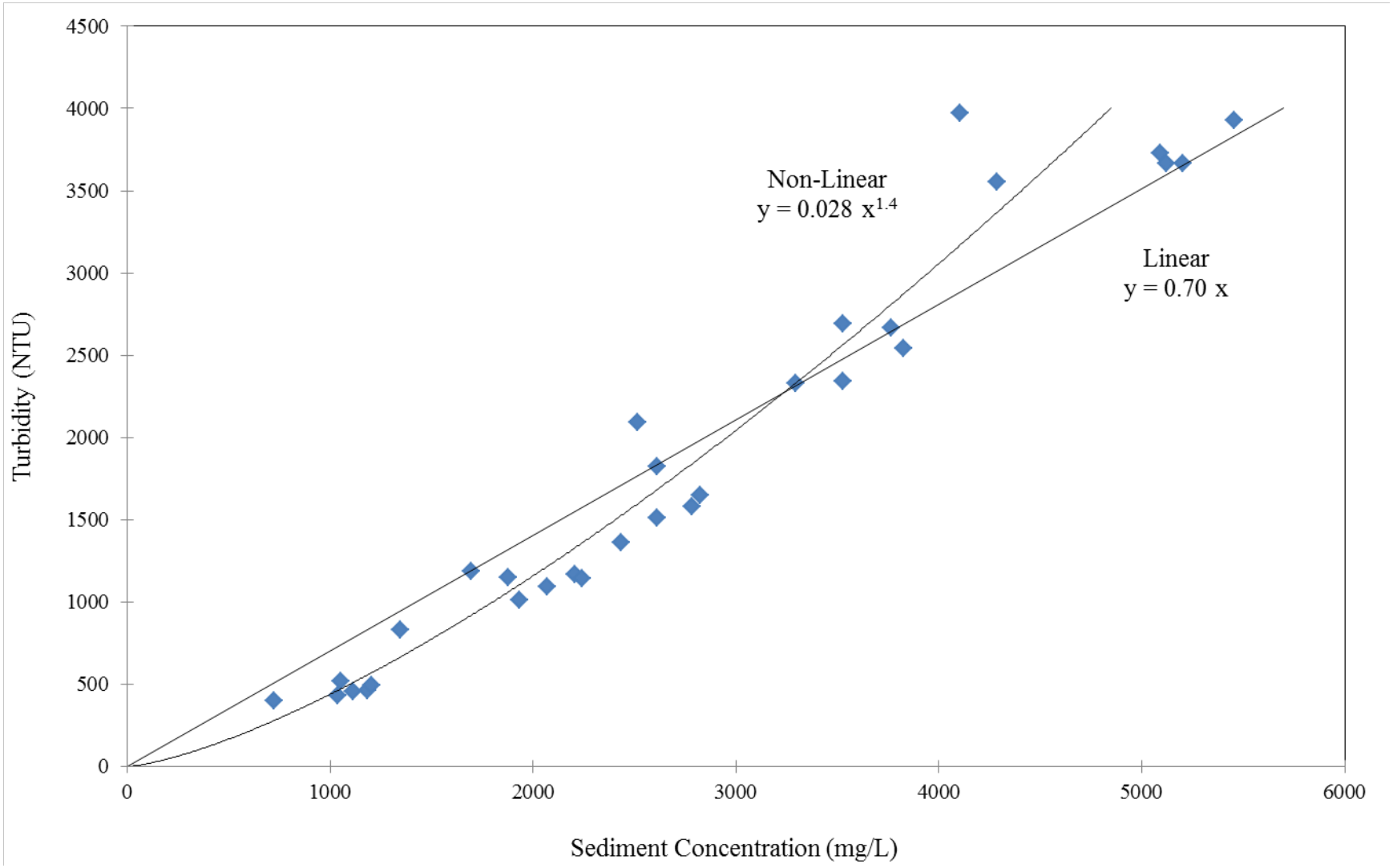

Figure 6.7. Linear and non-linear relationships for Arden Hills subsoil.

calculated assuming the turbidity was reduced from 4000 NTU to 2000 NTU and from 4000 NTU to 500 NTU. The percent reduction was found with the following equation:

$$\%\, reduction = 100\ \left(1 - \frac{reduced\ value}{inital\ value}\right) \tag{6.4}$$

The results of this analysis are shown in Table 6.1.

Table 6.1. Percent reduction in concentration with specified reductions in turbidity for a linear and non-linear relationship.

Turbidity (NTU)	Linear		Non-Linear		
Actual	% Reduction	Concentration (mg/L)	% Reduction	Concentration (mg/L)	% Reduction
4000	-	5698.0	-	4846.3	-
2000	50.0	2849.0	50.0	2953.9	39.0
500	87.5	712.3	87.5	1097.4	77.4

As expected, the percent reduction in sediment concentration for the linear relationship is exactly equal to that of turbidity. However for our non-linear function, the percent reduction in concentration is less than the percent reduction in turbidity. If turbidity standards are adopted, then the difference between a linear and non-linear relationship could have important implications on the selection of target goals of sediment control practices.

For the second scenario, the monitored turbidity for the May 23rd storm on the Bloomington site and the estimated hydrograph discussed in Section 6.4.2 were used to determine a flow-weighted mean turbidity for the storm. The estimated concentration using a site specific linear and non-linear turbidity-concentration relationship developed from the data in Figure 6.2 are shown in Figure 6.8. The flow-weighted mean for both sets of data was computed. The mean concentration was also estimated with the same linear and non-linear relationship using the single flow-weighted mean turbidity value. The percent error between the actual and estimated values was calculated as

$$\%\, Error = 100\ \frac{|Estimated - Actual|}{Actual} \tag{6.5}$$

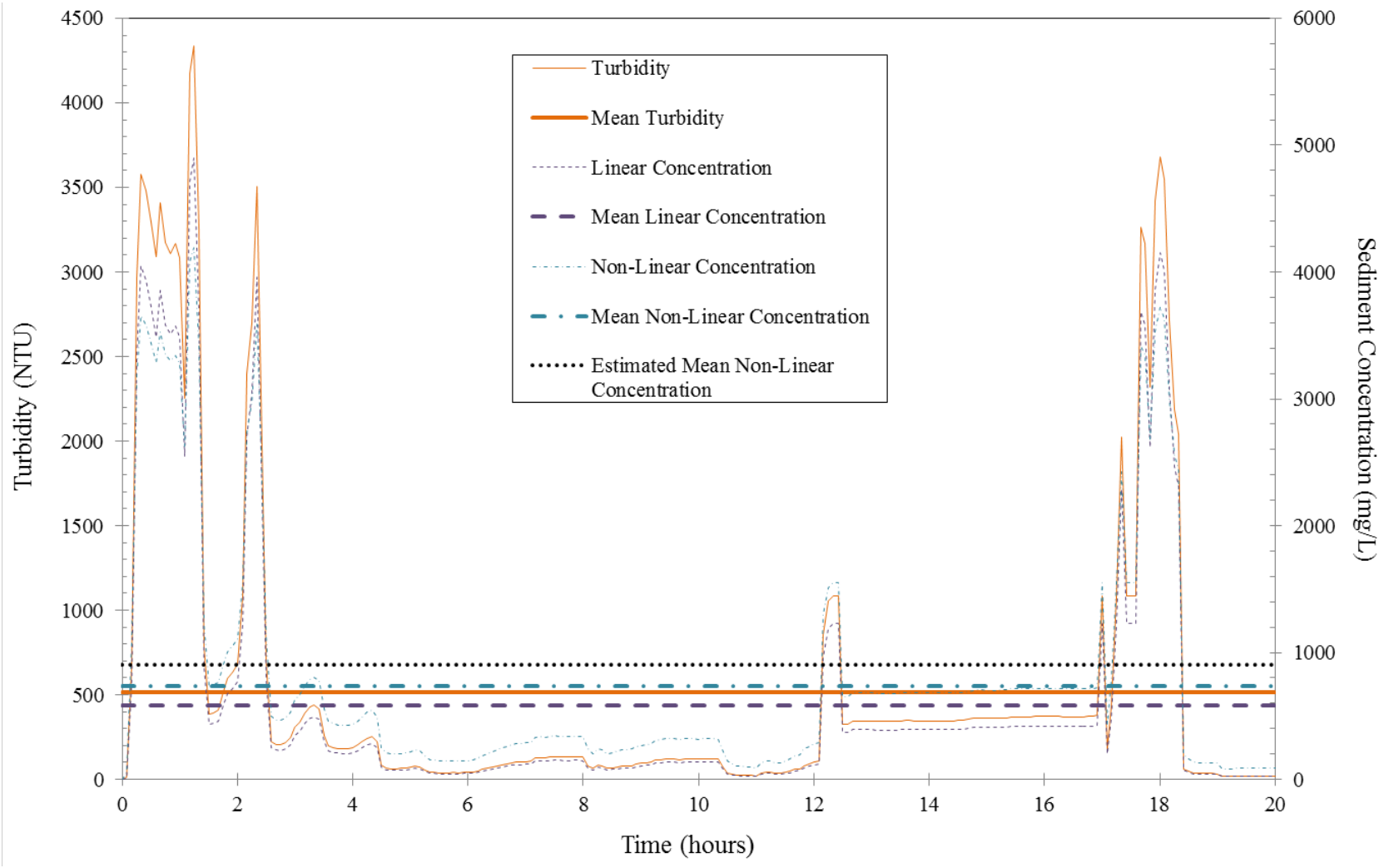

Figure 6.8. Turbidity data from Bloomington site plotted with linear and non-linear estimates of concentration. Flow-weighted mean turbidity and concentration are also plotted.

As expected, the linear function exactly predicted the flow-weighted mean concentration. The non-linear function over-predicted the flow-weighted mean concentration by 18%. If turbidity, in fact, varies linearly with concentration, then a single flow-weighted average concentration can be used to determine the average turbidity for the storm. On the other hand, if the relationship is nonlinear, as indicated by this study, then the use of the single flow-weighted average concentration to determine the actual average turbidity can result in substantial error.

6.6 Summary

The laboratory analyses were evaluated and applied using limited information collected at two construction sites. Comparisons of laboratory and field data suggest that the power relationship is valid for samples collected on construction sites. The prediction of α based on laboratory data is a reasonable first approximation to field values, especially considering possible changes in sediment sizes with deposition. Using the experimental relationship developed for Minnesota soils, turbidity and concentration can easily be estimated from field data with Equation 4.1 and a proper α value determined from Model 1 or Model 2. Once concentration is estimated for a site, the total sediment load can be determined using a hydrograph for the discharge point. Through a simple integration, the total sediment load can be determined at discharge point on a site and the needed sediment removal can be determined based on a turbidity standard. From there, proper erosion control practices can be chosen based on sediment removal needs. The impact of using a non-linear turbidity-concentration relationship instead of a linear relationship was evaluated. Results showed that less reduction in concentration is needed to reduce turbidity by a specified amount when using a non-linear relationship. There was also less error when using a non-linear relationship to estimate average turbidity and concentration values.

Chapter 7
Summary and Conclusions

In 2009, a turbidity standard of 280 NTUs was set by the EPA for construction sites disturbing 10 or more acres. This standard was challenged and is currently pending due to misinterpreted data used to set the limit (EPA, 2011). In response to the original turbidity regulation and because of the need for appropriate data to set a new limit, the MN DOT funded a project to evaluate turbidities from construction sites in Minnesota. Through this project, soils from construction sites around the state of Minnesota were used to determine a soil dependent relationship between turbidity and sediment concentration using a well-defined set of laboratory measurements. The impact of particle settling on the relationship was evaluated through a separate laboratory experiment. A field study on two construction sites in the Twin Cities of Minnesota was performed during the project duration. The field study allowed for a comparison of turbidity data from real runoff and synthetic runoff, as well as providing insight into the application of relationships obtained from laboratory data.

Through the use of a rainfall simulator in the laboratory, fourteen Minnesota construction site soils were rained on and runoff was collected and analyzed. A strong power relationship between turbidity and TSS concentration was found to represent all of the time dependent runoff samples collected for each soil. The power value, β, was relatively constant, only varying slightly between soils. A single β value of 7/5 was chosen to represent all of the Minnesota soils in the final relationship for turbidity and TSS. The intercept on a log-log graph, α, varied significantly between soils, but only varied slightly within soils. A relationship for α was determined through an extensive multiple linear regression using soil properties for each site. The results of this regression determined a relationship using percent silt, maximum abstraction, and interrill erodibility (Model 1) that explained nearly 65% of the variability in α. Because of the complexities involved in evaluating maximum abstraction and interrill erodibility, a simple relationship using only percent silt (Model 2) was also determined. Both models showed promise in determining α for the laboratory soils. Model 1and Model 2 had R^2 values of 0.70 and 0.55,

respectively. Model 1 had a small Relative Mean Error and a considerably smaller Normalized Mean Square Error.

Once a suitable relationship for turbidity and TSS concentration was determined for Minnesota construction site soils, the effect of particle settling was evaluated. A pipette test was performed on the total runoff sample from each soil. This test created a particle size distribution for the runoff samples. Samples were thoroughly mixed and then allowed to settle. While particles settled, small samples were extracted at a specific depth. The turbidity and concentration of each sample were determined for primary particles: sand, silt, and clay. From these samples, an extensive analysis was performed to determine how α and β changed with particle settling. Relationships for the dimensionless correction factors ν_d and ω_d with fraction finer were determined. With these parameters, the turbidity for each particle class can be estimated.

Clay has been considered a significant element of turbidity because it is difficult to remove from suspension. Clay was not found to be an important variable in determining the scaling factor α. However, our statistical analysis is limited by soils that have low fractions of clay in the runoff. On average, the primary particles of soil used were comprised of 9% clay prior to runoff but only 4% of that clay was eroded as aggregates during the ½ hour rainfall event. However, data in Chapter 5 suggests that clay can have an impact on the turbidity-concentration relationship. When clay was alone in suspension, the change in the α_d and β_d parameters was relatively large. This suggests that clay can have an important impact on turbidity and that its insignificance in our regression models for α is likely consequence of our experimental design.

Grab samples were collected from the two field sites in the Twin Cities and laboratory procedures were repeated to determine the turbidity and TSS relationship for field samples. The relationship for the field samples varied only slightly from the relationship determined in the laboratory for the same soil. Field samples had a strong power relationship with β values near 7/5 but α values that were slightly higher than laboratory soils. Particle settling can potentially explain the discrepancies in α.

The relationship created through the laboratory procedure shows great potential for several field applications. It can simply estimate turbidity values from known or estimated concentration data. More importantly, it can estimate concentration from continuously monitored turbidity data collected on a site. With estimated concentration data and known flow rates at the monitoring location, sediment load can be determined through a simple integration. Sediment reduction can then be calculated from based on a turbidity standard for the site. Knowing this information allows for better erosion control BMP planning and execution on a construction site. Ultimately, proper use of this relationship will reduce water impairments due to sediment loads from construction sites in Minnesota, alleviating stress on biota and improving the aesthetics of the water bodies.

References

Anderson, C. W. (2005). Turbidity. *U.S. Geological Survey techniques of water-resourcesiInvestigations* (A6.6). Retrieved from water.usgs.gov

Ankcorn, P. D. (2003). Clarifying turbidity – the potential and limitations of turbidity as a surrogate for water-quality monitoring. *Georgia Water Resources Conference.* Athens, GA: Georgia Water Science Center Publications.

ASTM Standard D5907. (2010). "Standard test methods for filterable matter (total dissolved solids) and nonfilterable matter (total suspended solids) in water. ASTM International, West Conshohocken, PA, 2010, DOI: 10.1520/D5907-10.

ASTM Standard D422. (2007). "Standard test method for particle-size analysis of soils. ASTM International, West Conshohocken, PA, 2010, DOI: 10.1520/D0422-63R07.

Coduto, D. P., Yeung, M. R., & Kitch, W. A. (2010). *Geotechnical engineering: Principles and practices.* Saddle River, NJ: Prentice Hall.

Elliot, W. J., Licbenow, A. M., Laflen, J. M., & Kohl, K. D. (1989). *A compendium of soil erodibility data from WEPP cropland soil field erodibility experiments 1987 & 1988.* Ohio State University & USDA Agricultural Research Service.

Faucette, L. B., Jordan, C. F., Risse, L. M., Cabrera, M., Coleman, D. C., & West, L. T. (2005). Evaluation of stormwater from compost and conventional erosion control practices in construction activities. *Journal of Soil and Water Conservation,* 60(6), 288-297.

Ferguson, R. J. & Church, M. (2004). A simple universal equation for grain settling velocity. *Journal of Sedimentology Research,* 74(6), 933-937.

Holliday, C. P., Rasmussen, T. C., & Miller, W. P. (2003). Establishing the relationship between turbidity and total suspended sediment concentration. *Georgia Water Resources Conference*. Athens, GA: Georgia Water Science Center Publications.

Holman, J. P. (1989). *Experimental methods for engineers.* St. Louis, MO: McGraw-Hill.

Jastram, J. D., Zipper, C. E., Zelazny, L. W., & Hyer, K. E. (2009). Increasing precision of turbidity-based suspended sediment concentration and load estimates. *Journal of Environmental Quality*, 39, 1306-1326.

Klute, A. (Ed.). (1986). *Methods of Soil Analysis Part 1: Physical and Mineralogical Methods.* Madison, WI: Soil Science Society of America.

Marshall, J. S. & Palmer, W. M. (1948). The distribution of raindrops with size. *Shorter Contributions,* 165-166.

Neter, J., Kutner, M., Wasserman, W., & Nachtsheim, C. (1996). *Applied linear statistical models*. New York, NY: McGraw-Hill/Irwin.

Omar, A. F. B. & MatJafri, M. Z. B. (2009). Turbidimeter design and analysis: A review on optical fiber sensors for the measurement of water turbidity. *Sensors*, 9(10), 8311-8335.

Omega Engineering, Inc. *Technical reference and selection guide.* Retrieved from www.omega.com/techref/

Onstad, C. A., Radke, J. K., & Young, R. A. (1981). An outdoor portable rainfall erosion laboratory. *Florence Symposium*. Florence, Italy: IAHS.

Packman, J. J., Cornings, K. J., & Booth, D. B. (1999). Confronting uncertainty: Managing change in water resources and the environment. *Canadian Water Resources Association Annual Meeting.* Vancouver, BC.

Patil, S. S., Barfield, B. J., & Wilber, G. G. (2011). Turbidity modeling based on the concentration of total suspended solids for stormwater runoff from construction and development sites. *World Environmental and Water Resources Congress 2011*. Palm Springs, FL: ASCE.

Rasmussen, P. P., Gray, J. R., Glysson, G. D., & Ziegler, A.C. (2009). Guidelines and procedures for computing time-series suspended-sediment concentrations and loads from in-stream turbidity-sensor and stream flow data. Reston, VA: U.S. Geological Survey.

Sadar, M. (2007). Turbidity revealed. *Opflow*, 33(1), 24-26.

Sadar, M. Turbidity measurement: A simple, effective indicator of water quality change. Retrieved from www.hacchhydromet.com

Sheppard, B. E. (1990). Measurements of raindrop size distributions using a small Doppler radar. *Journal of Atmospheric and Oceanic Technology*, 7, 255-268.

Tolhurst, T. J., Black, K. S., Shayler, S. A., Mather, S., Black, I, Baker, K., & Paterson, M. D. (1999). Measuring the *in situ* erosion shear stress of intertidal sediment with the cohesive strength meter (CSM). *Estuarine, Coastal and Shelf Science*, 49, 281-294.

United States Department of Agriculture. (1978). *Predicting rainfall erosion losses: A guide to conservation planning.* Washington, DC: GPO.

United States Environmental Protection Agency. (1999). *EPA guidance manual: Turbidity provisions.* Washington, DC: GPO.

United States Environmental Protection Agency. (2011). Industry effluent guidelines: Construction and development. Retrieved from water.epa.gov

United States Environmental Protection Agency. (2013). Minnesota impaired waters and TMDL Information. Retrieved from iaspub.epa.gov/tmdl

United States Weather Bureau. (1961). Rainfall atlas of the United States. Technical paper no. 40. Washington, DC: GPO.

Wilson, B. N., B. J. Barfield, A. D. Ward, & I. D. Moore. (1984). A hydrology and sedimentology watershed model. Part I: Operational format and hydrologic component. *Transactions of the ASAE,* 27(5), 1370-1377.

Wilson, B. N., B. J. Barfield, I. D. Moore, & R. C. Warner. (1984). A hydrology and sedimentology watershed model. Part II: Operational format and hydrologic component. *Transactions of the ASAE,* 27(5), 1378-1384.

Wilson, B. N., A. Y. Sheshukov, & R. Pulley. (2006). Erosion risk assessment tool for construction sites (Minnesota Department of Transportation Research Report No. MN/RC-2006-27).

Wilson, B. N., A. Y. Sheshukov, & A. Mendez. (2008). Design tool for controlling runoff and sediment from highway construction (Minnesota Department of Transportation Research Report No. MN/RC-2008-35).

Wurbs, R. A. & James, W. P. (2001). *Water resources engineering.* Saddle River, NJ: Prentice Hall.

Appendix A
Rainfall Simulator Calibration

To calibrate the rainfall simulator (pictured in Figure 3.2), each needle needed to be evaluated to determine if the simulator was raining over the surface evenly. The volume of rain from each needle was collected over a 10 minute period. This was done once without fans and once with the fans. These values can be seen in Table A.1 and Table A.2. The goal of the fans is distribute the rainfall between the needles. These tables show that the fans are successful in achieving a more even raindrop distribution over the surface.

Raindrop rates for each needle were determined by counting each raindrop that fell from a needle over a minute. These rates can be seen in Table A.3.

The average raindrop diameters for raindrops falling from each needle were determined using equations 3.2 and 3.3. These diameters can be seen in Table A.4.

The x's in these tables represent needles that data could not be collected for.

Table A.1. Rain volumes for each needle without fans.

Rainfall Volumes (mL), no fans, 10 minutes										
23.40	37.68	41.19	41.00	35.57	41.22	38.12	38.64	37.45	38.11	38.76
0	0	0	0	0	0	0	0	0	0	0
38.42	44.37	42.28	44.08	41.05	38.24	37.98	38.26	40.06	36.53	37.11
0	0	0	0	0	0	0	0	0	0	0
41.82	46.63	46.44	x	41.19	39.45	40.61	38.55	40.06	35.07	42.73
0	0	0	0	0	0	0	0	0	0	0
25.53	24.41	39.23	43.72	27.43	39.47	39.77	38.55	36.54	40.27	40.43
0	0	0	0	0	0	0	0	0	0	0
45.04	46.56	47.53	43.28	44.85	36.19	40.62	36.62	40.49	40.51	40.46
0	0	0	0	0	0	0	0	0	0	0
37.57	43.94	47.46	42.90	42.95	36.19	40.62	39.71	40.34	40.40	43.49
0	0	0	0	0	0	0	0	0	0	0
47.28	34.41	46.92	47.38	44.09	38.07	39.87	44.98	37.89	42.02	40.16
0	0	0	0	0	0	0	0	0	0	0
38.16	44.80	46.92	46.58	x	43.95	43.79	43.27	42.93	43.86	38.52

Table A.2. Rain volumes for each needle with fans.

Rainfall Volumes (mL), with fans, 10 minutes										
32.39	40.06	34.23	25.50	31.12	20.29	25.43	28.82	24.02	25.39	24.16
35.80	30.41	33.09	19.34	x	27.80	42.86	40.26	34.54	34.84	33.78
40.22	39.67	38.08	38.18	50.02	34.77	37.78	35.20	27.59	36.41	27.50
35.49	35.35	33.72	17.58	38.28	36.33	32.58	41.96	x	19.84	35.85
39.29	43.51	38.41	11.13	36.16	39.45	36.49	29.66	27.59	34.28	47.50
41.98	37.31	24.72	23.53	31.53	26.74	33.17	37.78	28.83	31.28	36.30
38.48	32.28	42.79	36.30	30.08	39.69	41.42	29.66	28.35	35.17	29.09
38.43	38.35	35.67	37.39	28.60	46.43	34.03	x	34.54	37.74	x
45.37	43.40	42.82	26.98	36.95	35.27	41.42	29.78	30.39	38.92	29.05
33.53	39.31	28.22	41.42	34.67	37.11	x	37.65	x	39.82	30.18
33.33	44.18	36.52	46.68	44.06	25.38	25.67	36.39	39.76	42.67	29.53
30.17	36.96	36.34	40.57	35.91	x	31.23	35.18	34.23	32.48	23.97
22.90	40.06	53.89	32.98	44.95	25.38	25.67	34.97	38.86	33.75	28.27
38.90	32.94	44.44	29.91	34.55	32.79	31.37	30.02	33.95	30.83	30.34
42.17	34.96	38.93	32.54	23.93	31.13	27.83	26.75	34.32	30.71	39.00

Table A.3. Raindrop rates for each needle.

Raindrop rates (drops/minute)										
186	186	198	180	165	149	178	188	189	160	191
204	192	192	180	167	159	165	148	181	167	197
198	186	192	x	166	164	158	167	179	187	197
180	198	180	198	163	175	165	160	176	132	190
180	186	204	198	x	173	159	169	175	186	191
156	174	180	167	150	174	168	167	163	181	146
186	192	186	167	157	170	169	172	157	167	156
198	204	180	196	156	154	142	179	161	160	142

Table A.4. Raindrop diameters for each needle.

Average Raindrop Diameter (mm)										
2.89	3.38	3.41	3.52	3.45	3.75	3.45	3.40	3.36	3.57	3.38
3.30	3.53	3.48	3.60	3.61	3.58	3.53	3.67	3.48	3.47	3.30
3.43	3.63	3.59	x	3.62	3.58	3.66	3.53	3.50	3.30	3.46
3.00	2.87	3.47	3.48	3.18	3.51	3.58	3.58	3.41	3.88	3.44
3.63	3.63	3.54	3.47	x	3.42	3.65	3.46	3.54	3.46	3.43
3.58	3.64	3.69	3.66	3.80	3.41	3.59	3.57	3.62	3.49	3.85
3.65	3.25	3.64	3.78	3.77	3.50	3.56	3.68	3.59	3.64	3.66
3.33	3.47	3.68	3.57	x	3.79	3.89	3.59	3.71	3.74	3.73

Appendix B
Soil Properties

Section 3.9 explains the soil properties that were used in the regression performed to determine α. This appendix includes Table B.1 that has the soil property values for each soil used in the regression analysis. Figures B.1 through B.16 are the particle distributions for each soil that were determined using a standard hydrometer test. These figures were used to determine the percent sand, silt, and clay of each soil. Figures B.17 through B.27 show the proctor test results. This information was used to determine the optimum moisture content of each soil. The final pages of this appendix contain the information for Soil A and B, which were attained from the MN DOT. These soils were already evaluated by the MN DOT to obtain a particle size distribution and optimum moisture content.

Table B.1. Soil property values for each soil.

Soil Name	USDA Classification	β	α	α, β=1.4	% Sand	% Silt	% Clay	I (in/hr)	BD (g/cm^3)
AHS	Silt Loam	1.40	0.037	0.036	45.9	54.1	0.0	1.29	1.30
AHS 2	Silt Loam	1.39	0.028	0.025	45.9	54.1	0.0	1.31	1.29
AHT	Loam	1.48	0.011	0.021	47.6	34.7	17.6	1.29	1.28
AHT 2	Loamy Sand	1.39	0.013	0.012	74.2	25.8	0.0	1.22	1.16
AHT 3	Loamy Sand	1.44	0.008	0.011	73.3	25.6	1.1	1.22	1.54
AHT 4	Loamy Sand	1.40	0.008	0.008	71.0	28.0	1.1	1.22	1.55
AHT 5	Sandy Loam	1.43	0.006	0.008	67.2	31.8	1.0	1.22	1.64
CTYS	Sandy Loam	1.35	0.033	0.023	49.5	48.5	2.1	1.31	1.46
CTYT	Loam	1.39	0.015	0.014	42.7	37.5	19.8	1.38	1.27
DulS	Silt Loam	1.37	0.062	0.050	33.3	59.1	7.5	1.31	1.60
DulT	Loamy Sand	1.12	0.040	0.004	79.7	12.2	8.1	1.38	1.56
HastS	Sandy Loam	1.39	0.007	0.006	61.9	34.5	3.6	1.29	1.72
HastT	Sandy Loam	1.30	0.016	0.007	70.4	23.5	6.2	1.43	1.65
OVS	Silt Loam	1.44	0.062	0.080	23.5	73.5	3.1	1.36	1.37
OVT	Silt Loam	1.36	0.050	0.037	43.4	56.6	0.0	1.29	1.23
Soil A	Silt	1.40	0.007	0.009	7.5	84.0	8.5	1.43	1.59
Soil B	Silt Clay Loam	1.35	0.016	0.049	7.5	66.5	26.0	1.43	1.58
THS	Sandy Loam	1.48	0.010	0.014	69.7	19.1	11.2	1.43	1.49
THT	Loam	1.44	0.072	0.023	34.3	47.5	18.2	1.43	1.20

Soil Name	K_i ($kg\text{-}s/m^4$)	CN	S (in)	w (%)	OMC (%)	TES (g)	τ (Pa)	V_t (mL)	Q (in^3/hr)
AHS	1.08E+06	96.79	0.33	29.61	13.0	15.55	1.50	1975	241.04
AHS 2	1.76E+06	98.34	0.17	26.26	13.0	26.08	1.50	2625	320.37
AHT	1.32E+06	96.17	0.40	23.51	11.0	19.05	1.30	1780	217.24
AHT 2	1.34E+06	95.57	0.46	23.42	12.0	17.21	1.65	1465	178.80
AHT 3	1.68E+06	95.59	0.46	26.94	12.0	21.66	1.67	1470	179.41
AHT 4	2.13E+06	97.11	0.30	27.07	12.0	27.44	1.37	1920	234.33
AHT 5	3.07E+06	98.33	0.17	26.58	12.0	39.48	1.27	2390	291.69
CTYS	3.32E+06	98.72	0.13	25.21	14.5	49.35	1.82	2800	341.73
CTYT	1.68E+06	98.21	0.18	29.26	15.5	27.71	1.62	2744	334.90
DulS	1.64E+06	97.09	0.30	18.63	13.0	24.35	1.23	2125	259.35
DulT	1.33E+06	96.32	0.38	18.46	11.0	21.94	1.40	2030	247.76
HastS	4.06E+06	97.79	0.23	11.37	9.0	58.53	1.23	2340	285.59
HastT	1.27E+06	97.00	0.31	16.69	7.3	22.48	0.87	2380	290.47
OVS	7.04E+05	89.56	1.17	35.96	12.0	11.27	0.87	665	81.16
OVT	9.93E+04	86.29	1.59	19.58	20.0	1.43	1.63	300	36.61
Soil A	2.81E+06	96.73	0.34	24.32	11.3	49.75	1.28	2285	278.88
Soil B	1.27E+06	97.01	0.31	30.60	16.7	22.47	1.03	2385	291.08
THS	1.55E+06	99.20	0.08	16.60	10.1	27.38	1.03	3179	387.99
THT	1.02E+06	95.94	0.42	22.10	14.7	18.03	1.35	1870	228.23

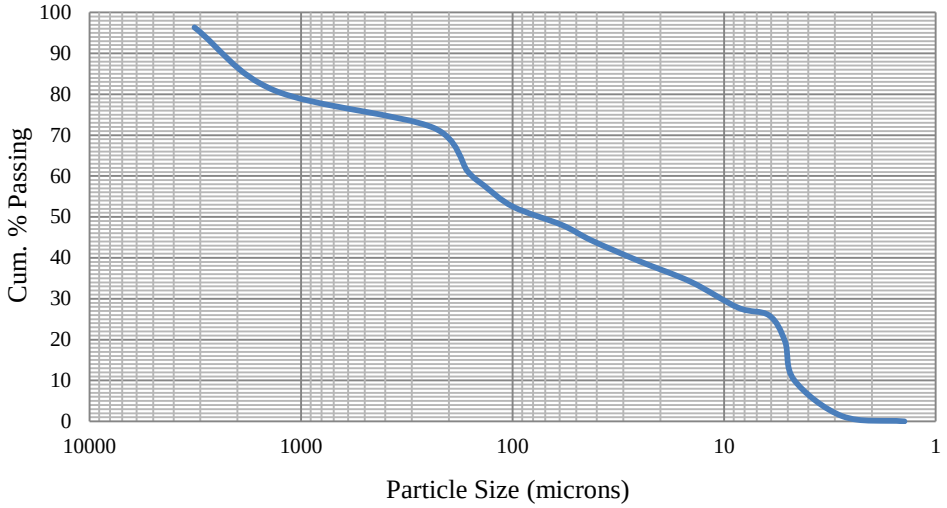

Figure B.1. Hydrometer Test, AH - S

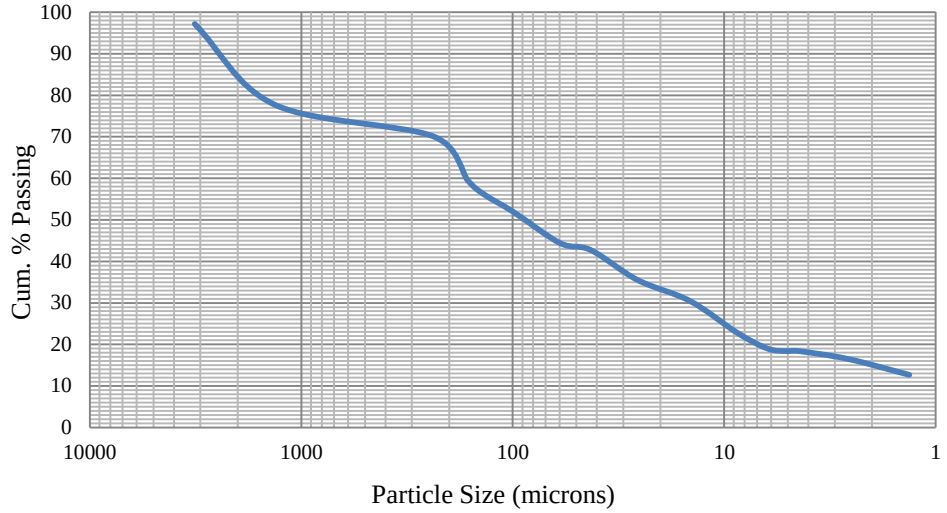

Figure B.2. Hydrometer Test, AH - T

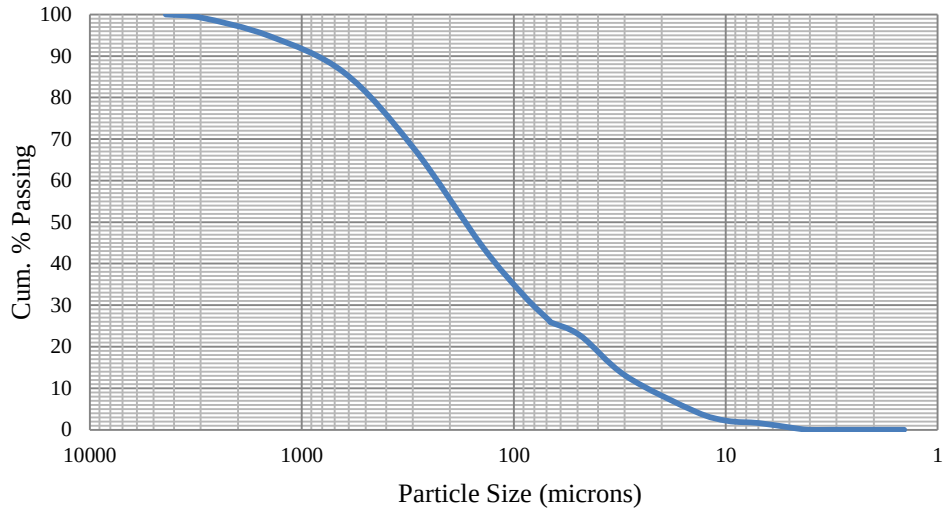

Figure B.3. Hydrometer Test, AH - T 2

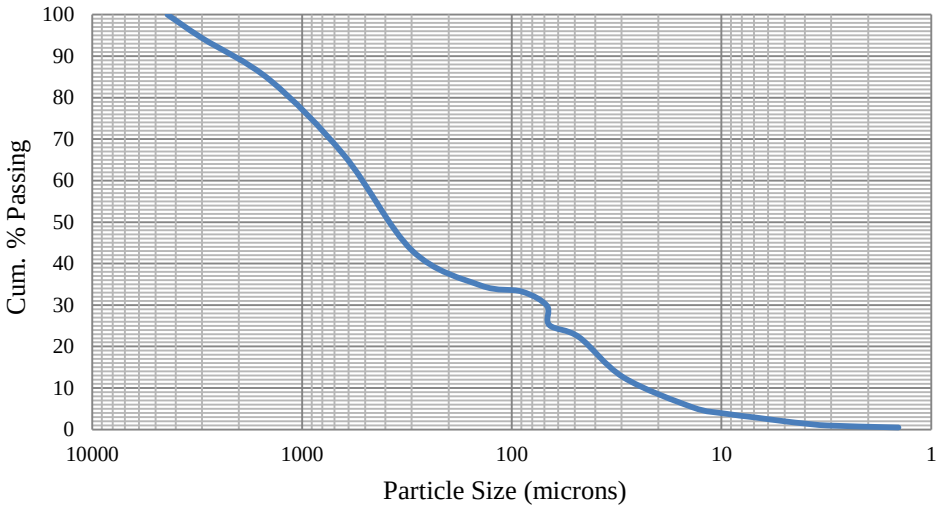

Figure B.4. Hydrometer Test, AH - T 3

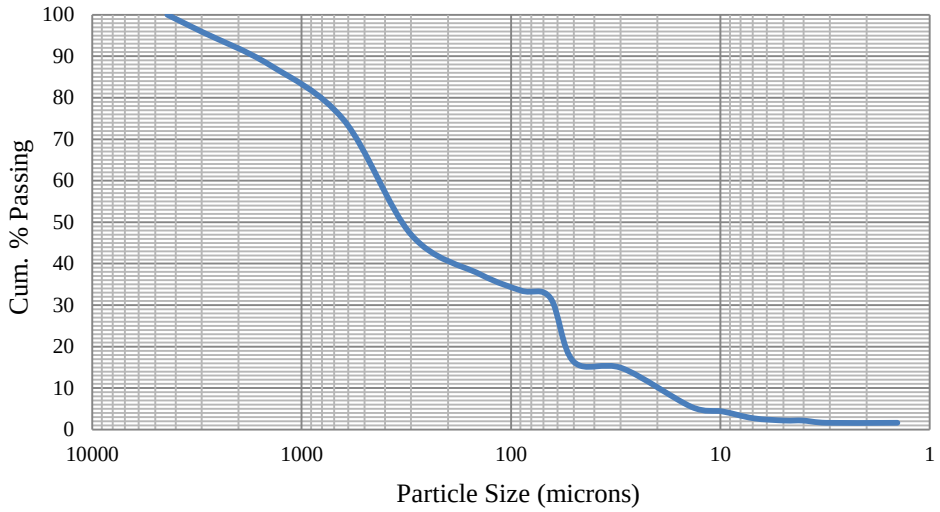

Figure B.5. Hydrometer Test, AH - T 4

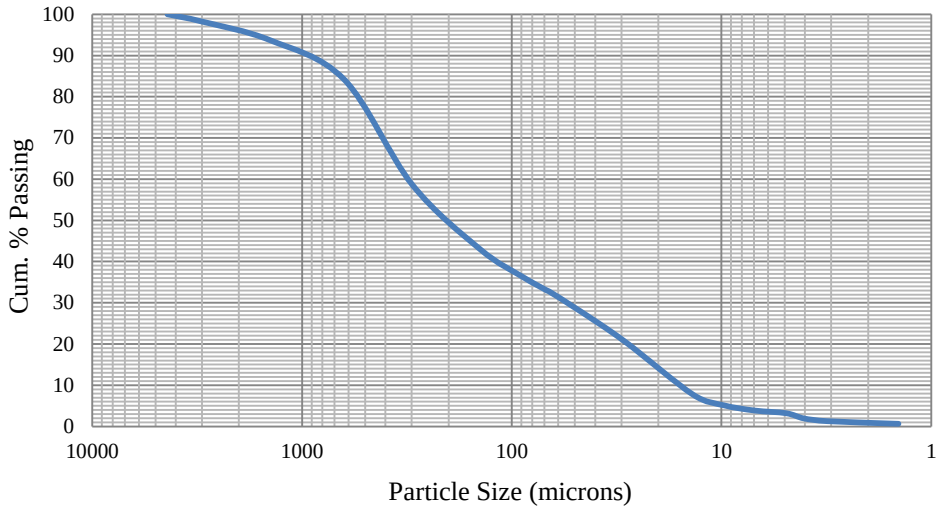

Figure B.6. Hydrometer Test, AH - T 5

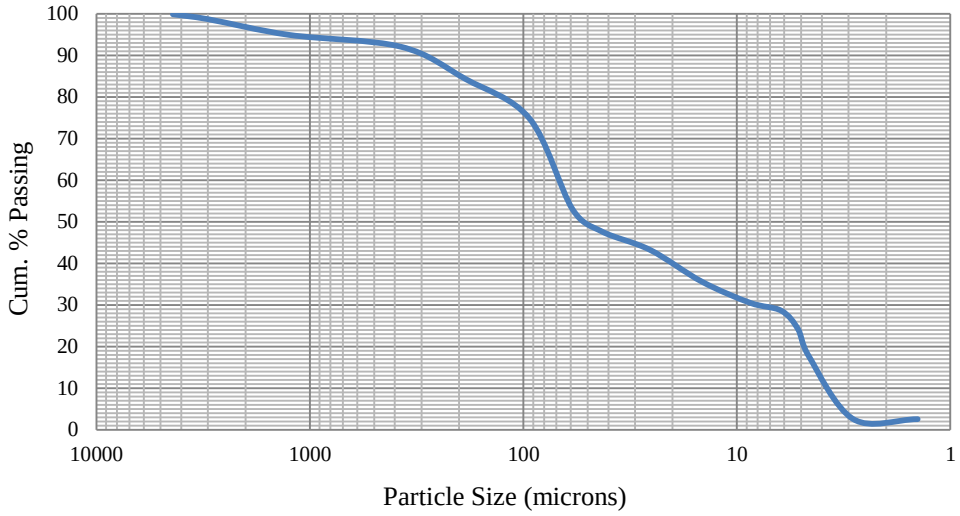

Figure B.7. Hydrometer Test, CTY 14 - S

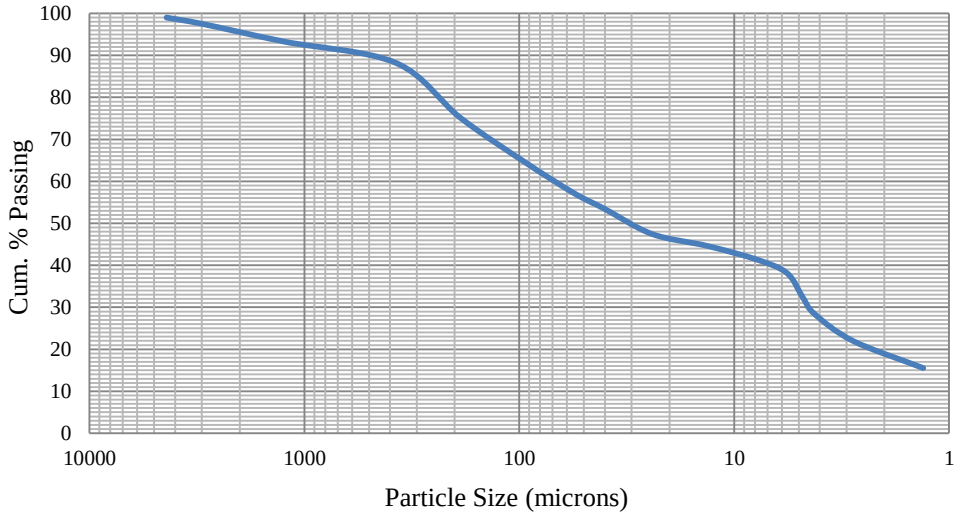

Figure B.8. Hydrometer Test, CTY 14 - T

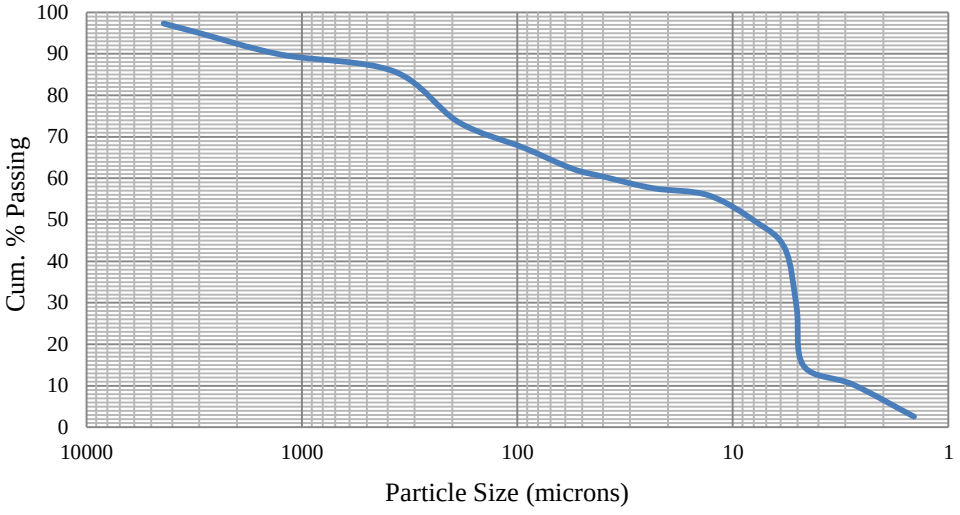

Figure B.9. Hydrometer Test, Duluth - S

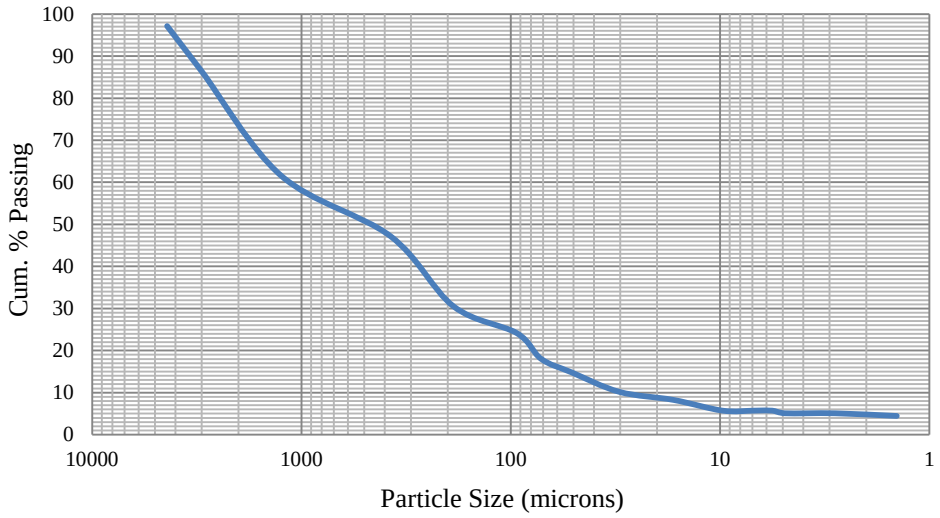

Figure B.10. Hydrometer Test, Duluth - T

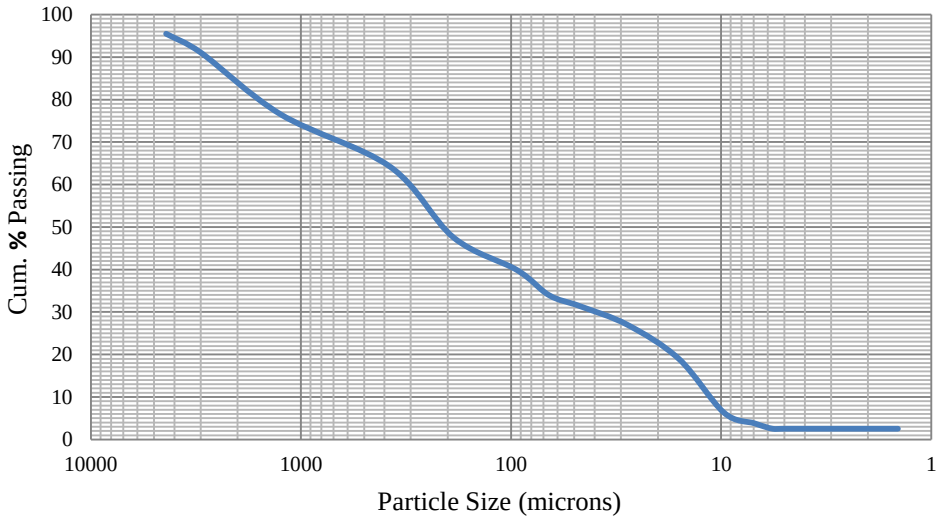

Figure B.11. Hydrometer Test, Hastings - S

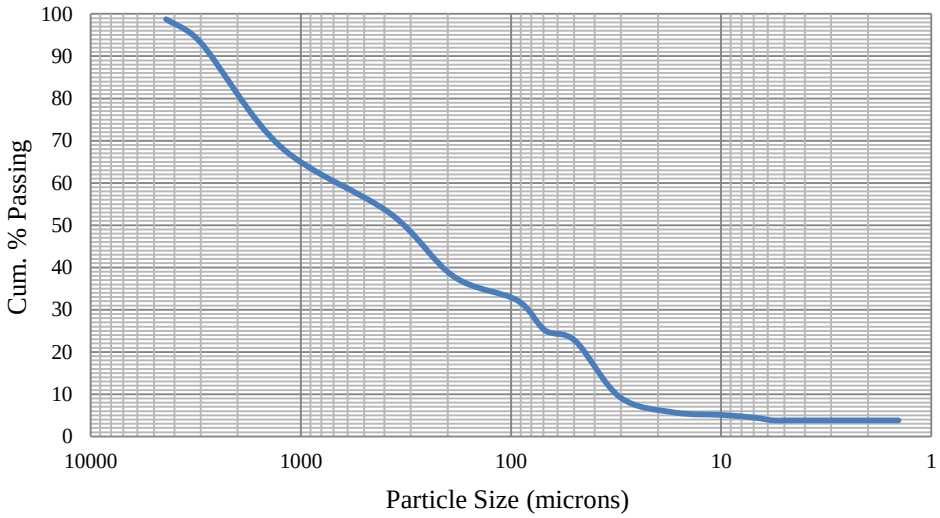

Figure B.12. Hydrometer Test, Hastings - T

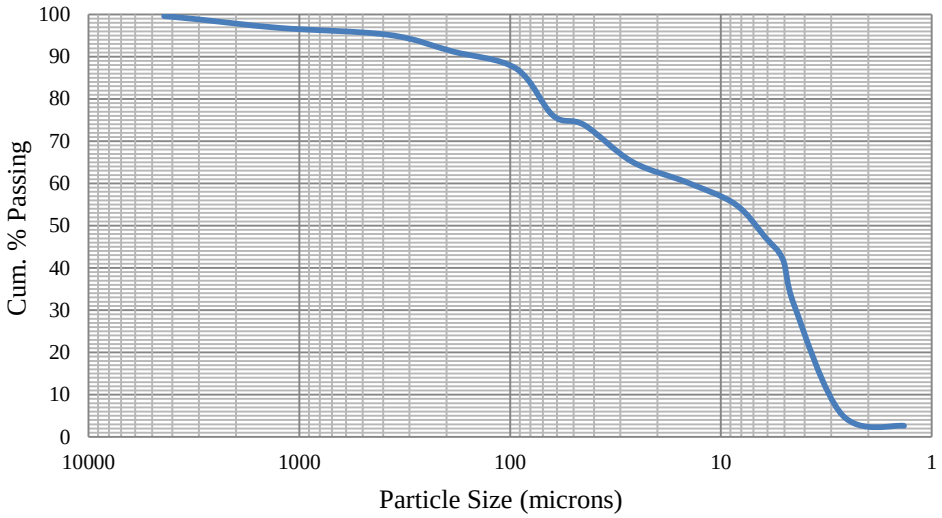

Figure B.13. Hydrometer Test, OV - S

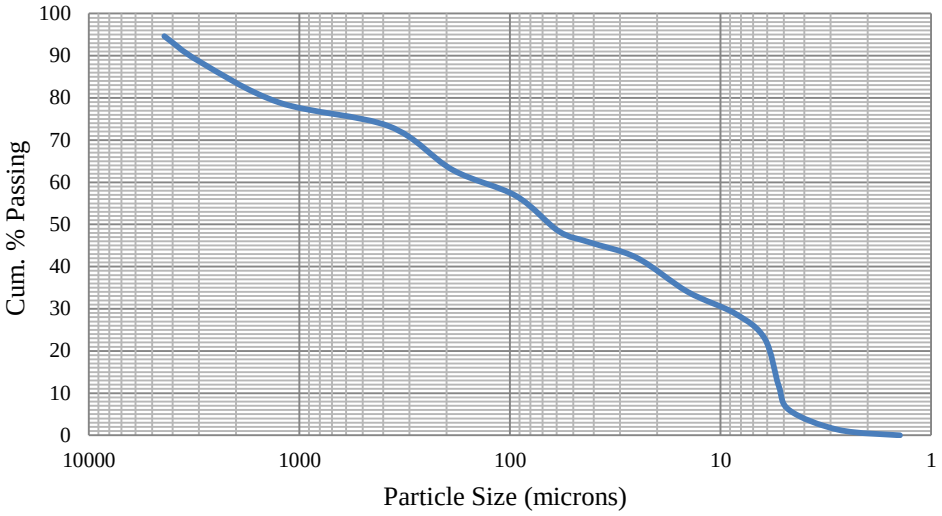

Figure B.14. Hydrometer Test, OV - T

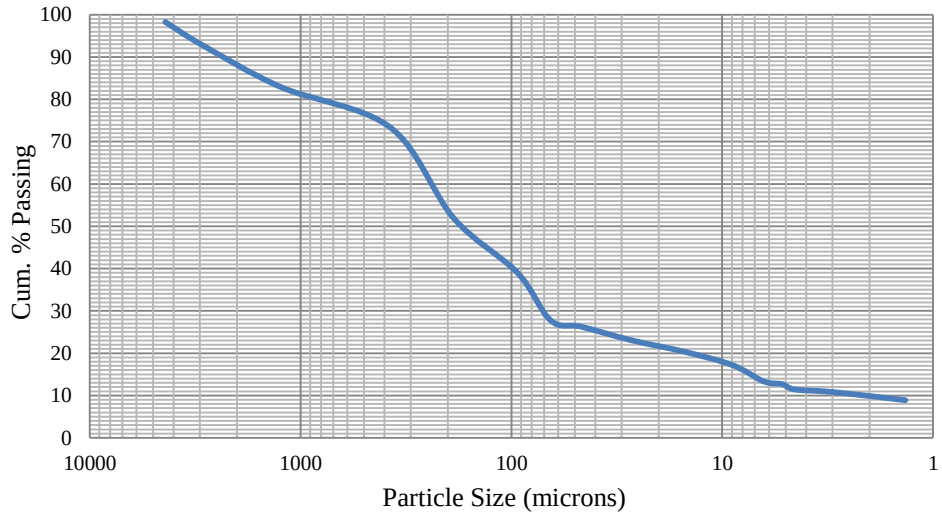

Figure B.15. Hydrometer Test, TH23 - S

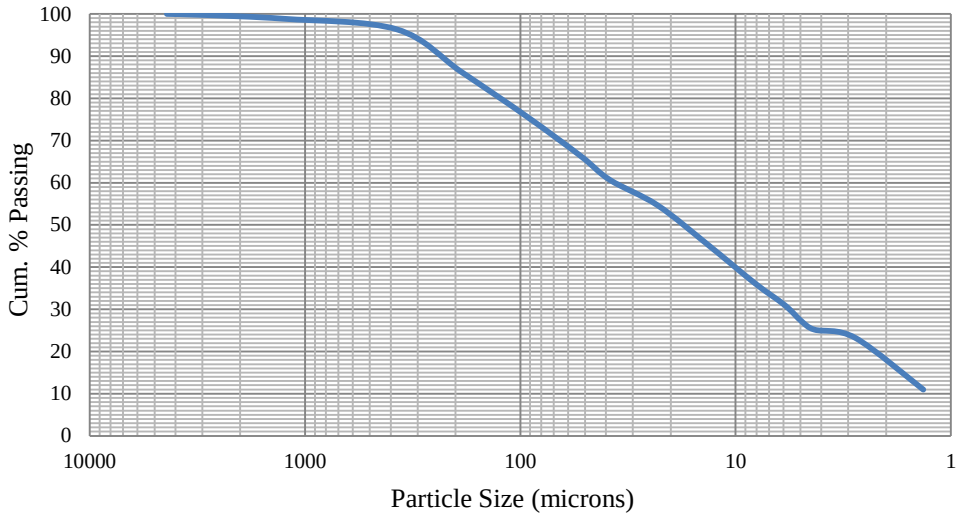

Figure B.16. Hydrometer Test, TH23 - T

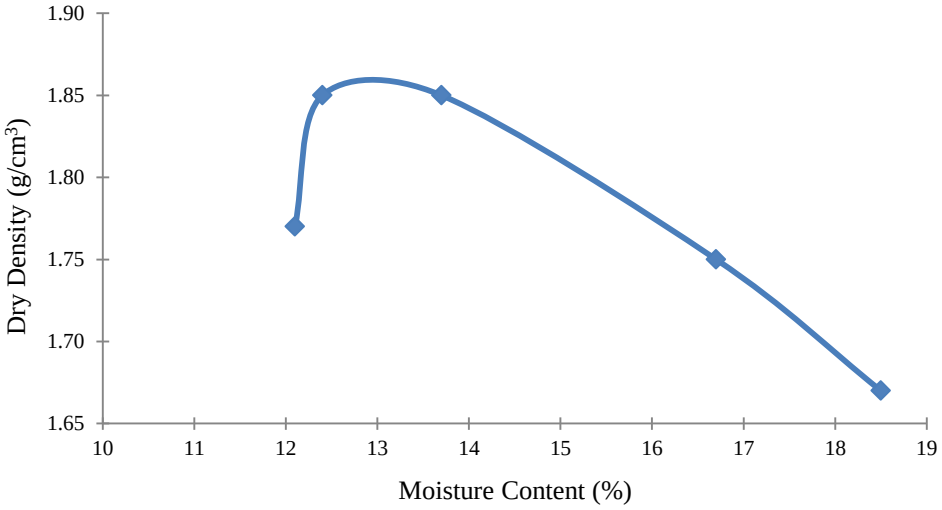

Figure B.17. Proctor Test, AH - S

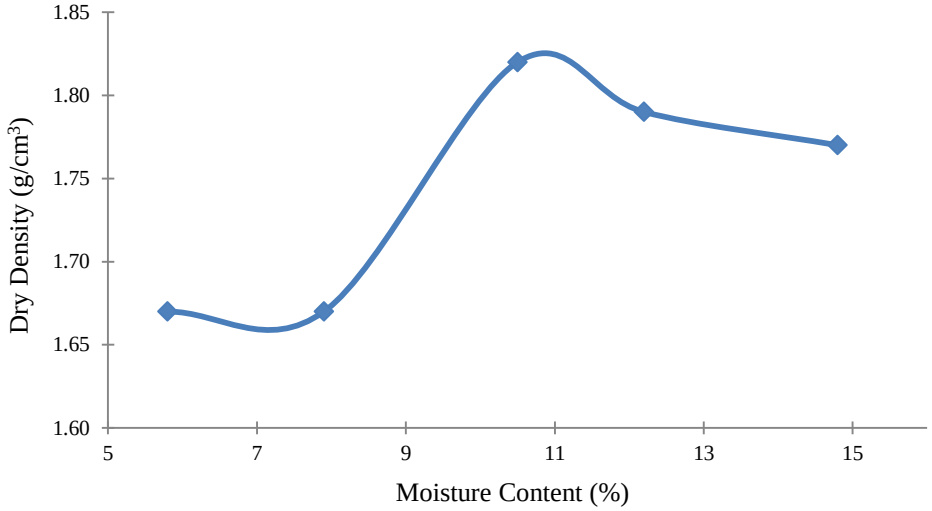

Figure B.18. Proctor Test, AH - T

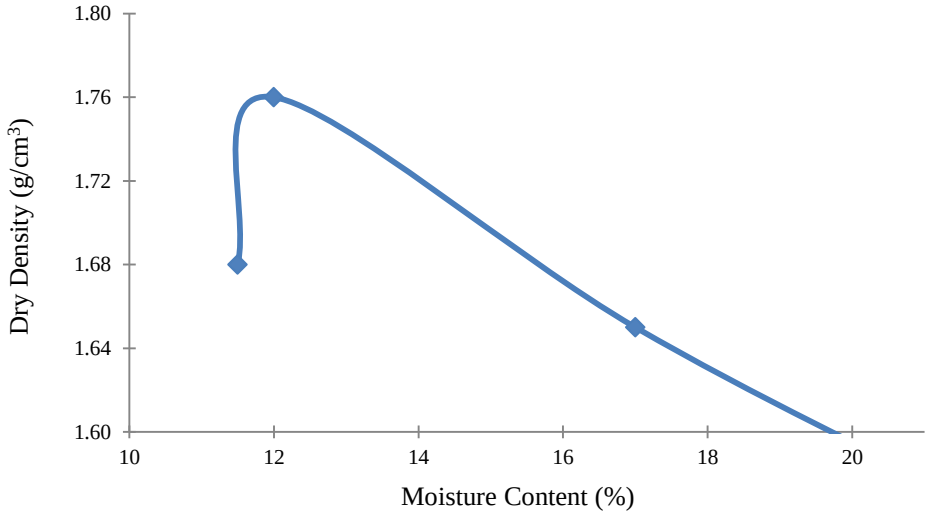

Figure B.19. Proctor Test, AH - T rep

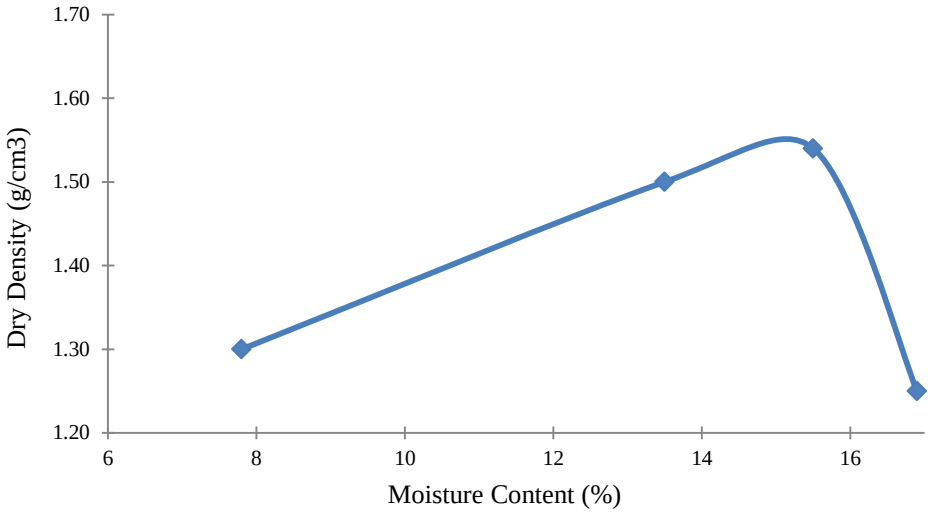

Figure B.20. Proctor Test, CTY14 - T

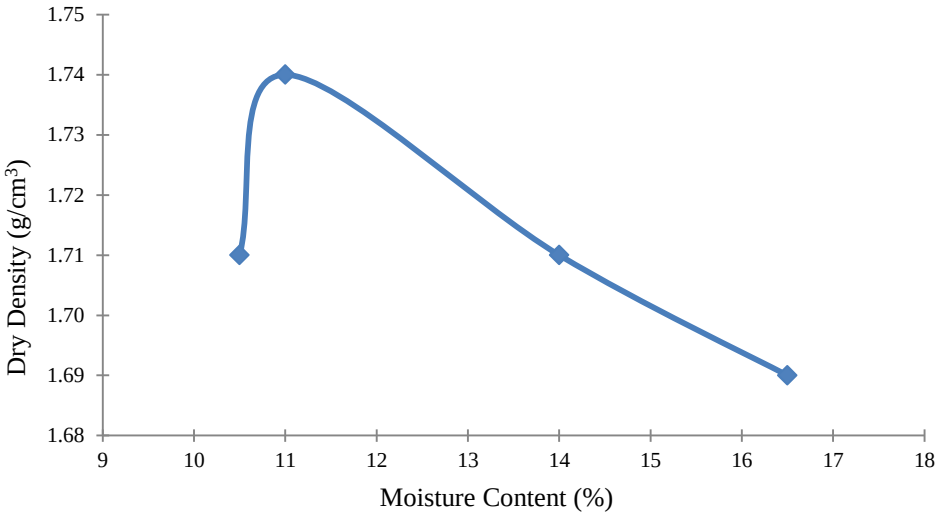

Figure B.21. Proctor Test, Dul - T

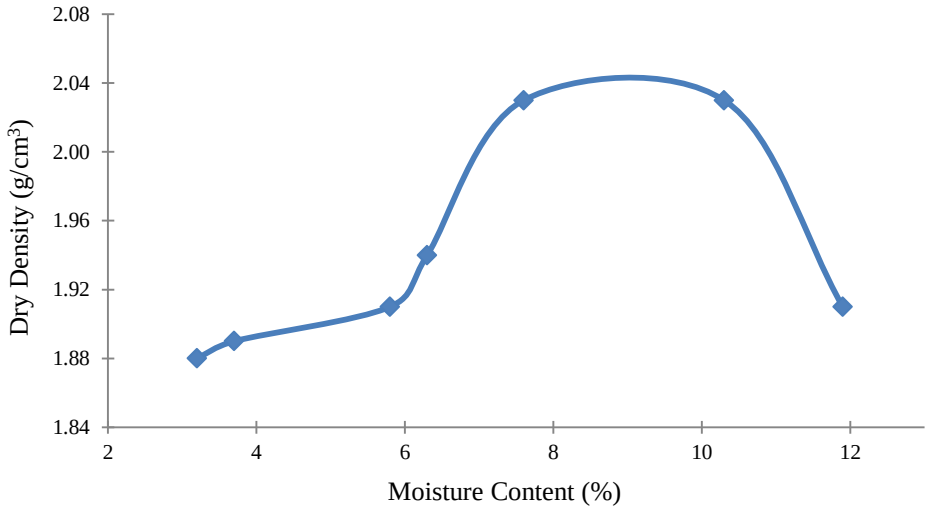

Figure B.22. Proctor Test, Hast - S

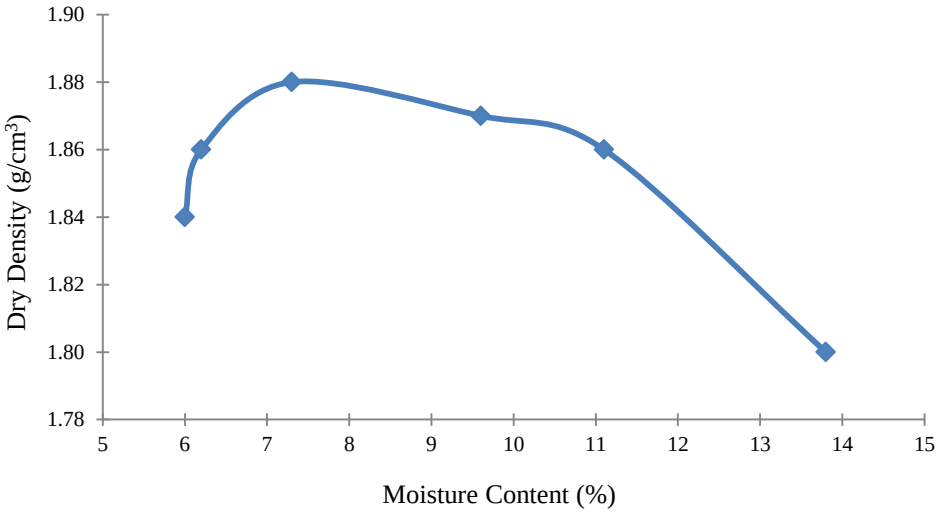

Figure B.23. Proctor Test, Hast - T

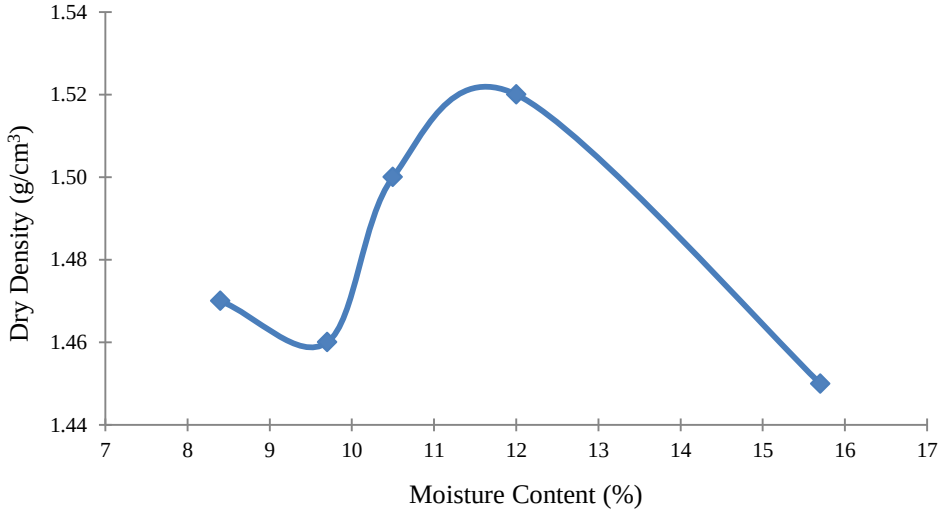

Figure B.24. Proctor Test, OV - S

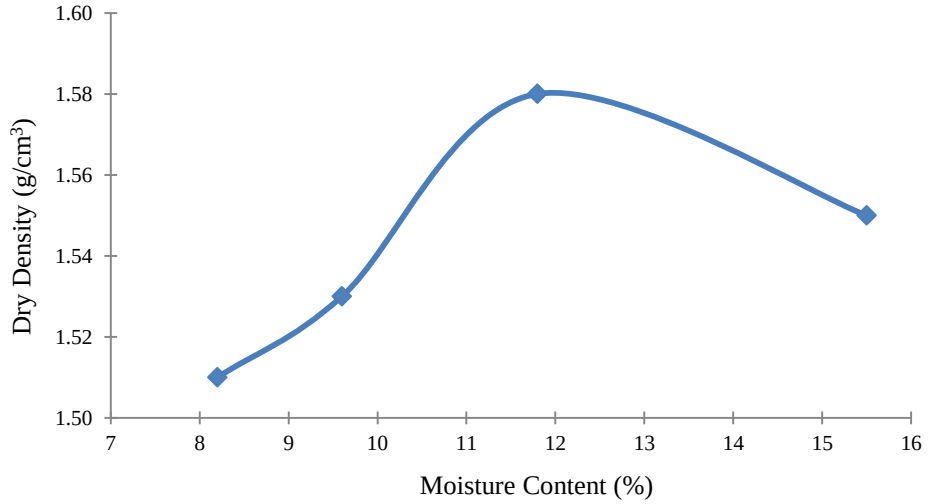

Figure B.25. Proctor Test, OV - T

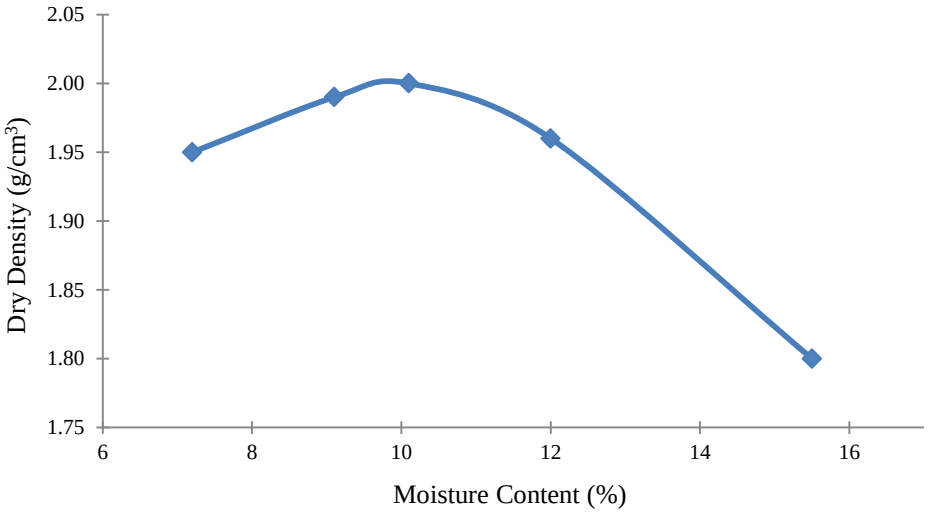

Figure B.26. Proctor Test, TH23 - S

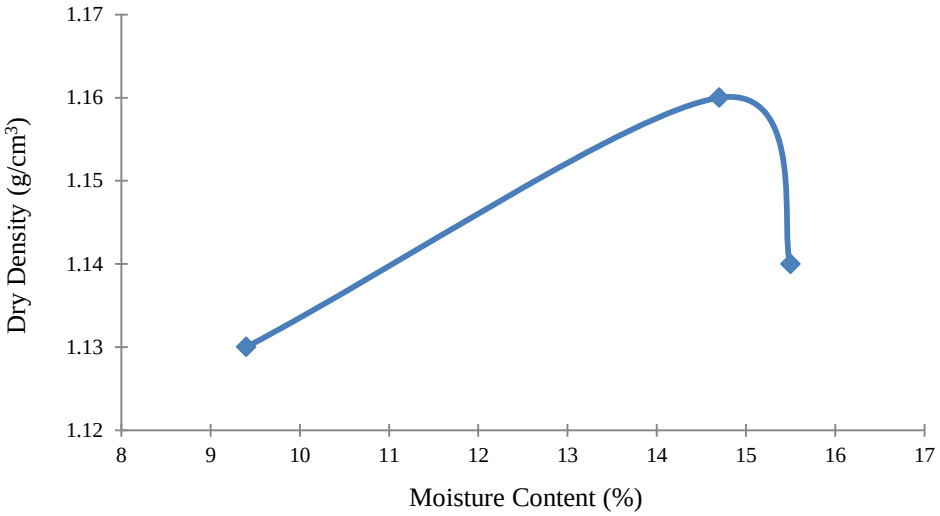

Figure B.27. Proctor Test, TH23 - T

Minnesota Department Of Transportation

TEST REPORT ON SAMPLE OF SUBSOIL

Office of Materials and Road Research
1400 Gervais Avenue
Maplewood, MN 55109

Sample ID:	**CO-SS12-0179**	Depth:	
Project No.:	**99008-9**	Field ID:	**UMA**
T.H. Number:		Field Classification:	
Submitted By:	**JOHN SIEKMEIER**	Date Sampled:	**2/14/2012**
Proj. Eng.:	**JOHN SIEKMEIER**	Date Received:	**2/17/2012**
Point Number:		Report Approved:	**03/15/2012 13:14**
Tests Required:	**G,PI,P,R-V,SPG**		
Sample Taken From:			

Sieves

Sieve Size	*Percent Passing*
2" (50 mm)	100.0
1" (25.0 mm)	100.0
3/4" (19.0 mm)	100.0
3/8" (9.5 mm)	100.0
#4 (4.75 mm)	100.0
#10 (2.00 mm)	99.4
#20 (850 um)	98.5
#40 (425 um)	97.3
#60 (250 um)	96.1
#100 (150 um)	94.8
#200 (75 um)	92.2

Other Soil Tests

Test	*Result*
Plasticity Index	NP
Mn/DOT Class (Entire Sample)	Si
Clay (Entire Sample) %	8.5
Silt (Entire Sample) %	83.7
Sand (Entire Sample) %	7.8
Mn/DOT Class (Minus 10)	Si
Clay (Minus 10) %	8.5
Silt (Minus 10) %	84.2
Sand (Minus 10) %	7.2
AASHTO Group	A-4
Group Index	0
Optimum Moisture (% dry wt)	11.3
Max Density (lb/cubic ft)	113.1
R-Value (at 240 psi)	45.8
Soil SpG	2.699

Test Procedures: AASHTO T87, T88, T89, T90, T99 Method "C"(M), T100, T190 (M), T-265 M = Mn/DOT Modified

Comments:

Copies To:

JOHN SIEKMEIER - METRO

Charge Out: 1037, 1038, 1041, 1046

Rod Patrin

REVIEWED BY

Minnesota Department Of Transportation

SubSoil Sample Worksheet

Sample ID:	CO-SS12-0179	Submitted By:	JOHN SIEKMEIER
Project No.:	99008-9	Source:	
Date Sampled:	2/14/2012	Date Received:	2/17/2012

Hydrometer Analysis

Time	Temp	Read	Size (mm)	% Finer
2 min	71.0	28.0	0.03328	43.9
5 min	71.0	23.0	0.02232	33.8
15 min	71.0	16.0	0.01343	19.6
30 min	71.0	14.0	0.00906	15.5
60 min	71.0	13.0	0.00675	13.6
250 mi	69.0	12.0	0.00334	10.7
24 hr	70.0	10.0	0.00140	7.1

Liquid Limit

Type	Weight 1	Weight 2
Liquid Limit	0.0%	

Particle Size

%	Particle
7.8	Sand and Gravel (Entire Sample)
83.7	Silt (Entire Sample)
8.5	Clay (Entire Sample)

Hygroscopic Moisture

Content Type	Weight
Air Dry + Can	25.90
Oven Dry + Can	25.72
Can	14.57
Corr. Factor	0.984%

Plastic Limit

Type	Weight 1	Weight 2
Plastic Limit	0.0%	
Plasticity Ind	0.0	

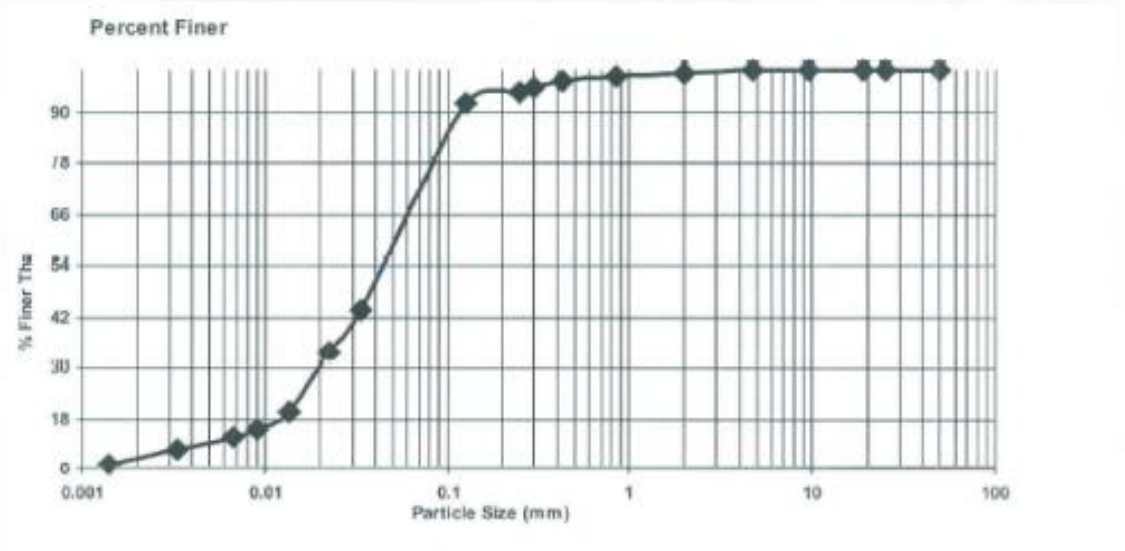

State of Minnesota Department of Transportation

MOISTURE-DENSITY RELATIONSHIP

Sample ID: CO-SS12-0179 Proj Eng : JOHN SIEKMEIER Submitted by: JOHN SIEKMEIER

Sample From : Project No.: 99008-9 Report Approved : 03/09/2012 08:17

Test Number:	1	2	3	4	5	6	7	8
Wet Soil Mold:	5915.90	6007.60	6104.10	6078.30				
Mold:	4204.90	4204.90	4204.90	4204.90				
Wet Soil Pan:	917.60	911.40	995.70	983.40				
Dry Soil Pan:	885.50	867.00	931.30	905.20				
Pan:	351.70	354.60	353.00	357.20				
%Moisture-Dry:	6.01	8.67	11.14	14.27				
Dry Density:	106.76	109.73	113.04	108.44				

Maximum Density: 113.1 lb/cu.ft.

Optimum Moisture: 11.3 %

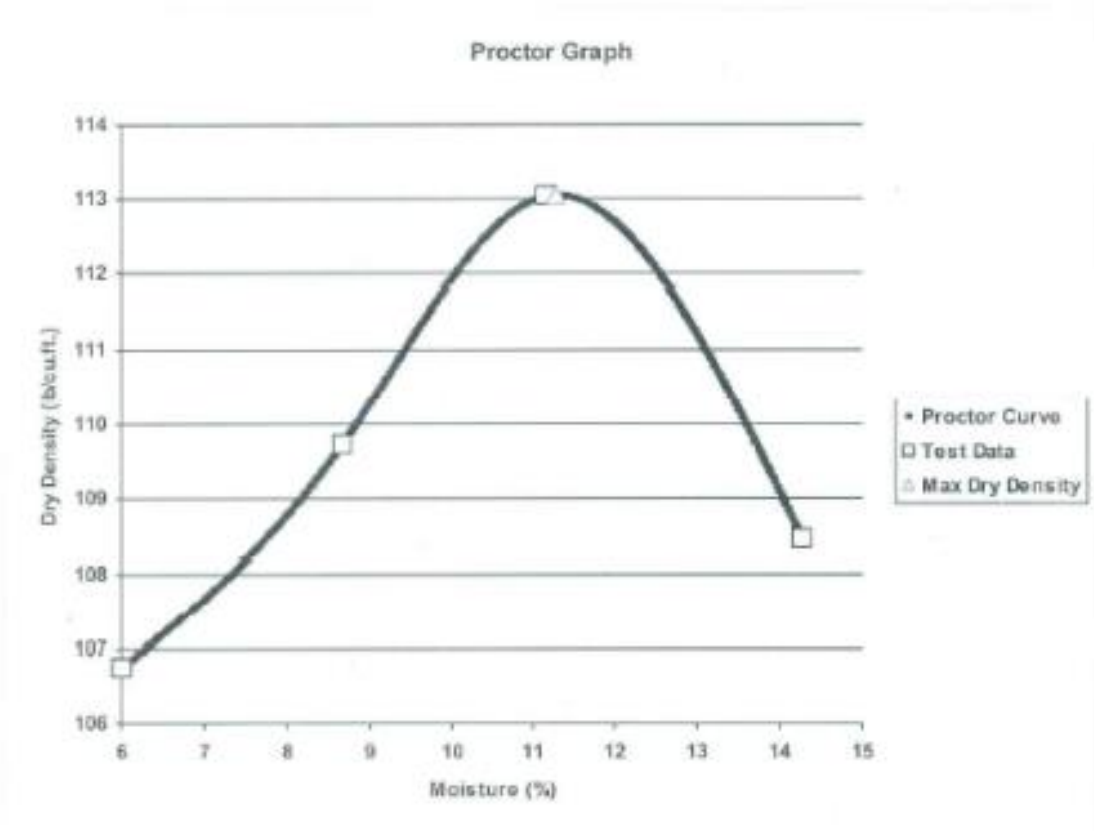

State of Minnesota Department of Transportation

R-Value Worksheet

Sample ID: **CO-SS12-0179** Soils Lab No.: RV Initials: RV Date:

% Passing 3/8": **60.0** % Passing #4: **100.0** Mn/DOT Class: **SI** AASHTO Group: **A-4**

Opt. Moisture: **11.3** Max Density: **113.1** Est Orig Moisture: **2** Report Approved: **03/15/2012 12:49**

Mold No:	1	2	3	4
Batching Data				
Water Added (Init):	64	82	137	119
Water Added (Final):	32	41	69	59
Initial Moisture (%):	5	6	10	9
Moisture Added (%):	7.0	9.0	15.0	13.0
Total Moisture (%):	9.0	11.0	17.0	15.0
Orig. Wt. of Batch:	1400			
Corr. Wt. of Batch:	1372			
Dry Spec. Wt:	933			
Wet Spec. Wt:	1017	1035	1091	1073
Moisture Data				
Wet Weight:		675.9	718.8	682.7
Dry Weight:		633.2	648.2	623.6
Pan Tare Wt.:	183.0	186.2	195.8	184.0

Mold No:	1	2	3	4
Stabilometer Test				
Exudation Pressure:		800	200	350
Wt. of Briq. + Mold:		3162.9	3143.1	3134.8
Wt. of Mold:	2050.2	2129.3	2055.8	2065.3
Height of Briquette:		2.60	2.61	2.57
Dial Reading (.0001):		6	10	15
Expansion Pressure:		0.2	0.3	0.4
Stabil - 1000lb:		19	35	25
Stabil. - 2000lb:		38	64	48
Turns Displacement:		4.18	6.32	4.39
Calculated Information				
Moisture Loss:		42.7	70.6	59.1
Dry Soil Wt.		447.0	452.4	439.6
Moisture at Compact.		9.6	15.6	13.4
Wet Wt. of Briq.:		1034	1087	1070
R-Value (Corr)		68.0	39.8	59.3
R-Value at 240 psi:	45.8			

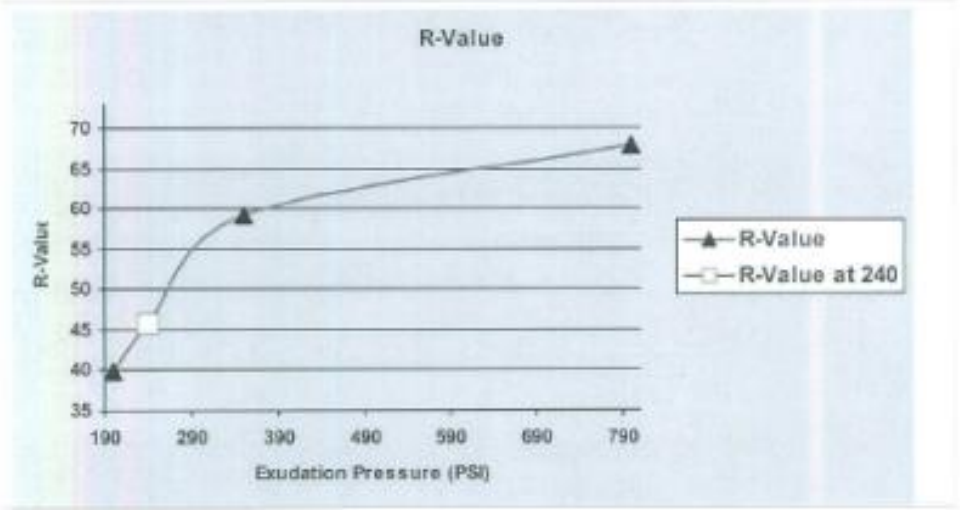

Minnesota Department Of Transportation

TEST REPORT ON SAMPLE OF SUBSOIL

Office of Materials and Road Research
1400 Gervais Avenue
Maplewood, MN 55109

Sample ID:	CO-SS12-0180	Depth:	
Project No.:	99008-9	Field ID:	UMB
T.H. Number:		Field Classification:	
Submitted By:	JOHN SIEKMEIER	Date Sampled:	2/14/2012
Proj. Eng.:	JOHN SIEKMEIER	Date Received:	2/17/2012
Point Number:		Report Approved:	03/15/2012 13:15
Tests Required:	G,PI,P,R-V,SPG		
Sample Taken From:			

Sieves

Sieve Size	*Percent Passing*
2" (50 mm)	100.0
1" (25.0 mm)	100.0
3/4" (19.0 mm)	100.0
3/8" (9.5 mm)	100.0
#4 (4.75 mm)	99.9
#10 (2.00 mm)	99.1
#20 (850 um)	98.8
#40 (425 um)	98.3
#60 (250 um)	97.8
#100 (150 um)	97.2
#200 (75 um)	92.5

Other Soil Tests

Test	*Result*
Liquid Limit (%)	31.5
Plastic Limit (%)	20.2
Plasticity Index	11.3
Mn/DOT Class (Entire Sample)	SiCL
Clay (Entire Sample) %	26.2
Silt (Entire Sample) %	66.4
Sand (Entire Sample) %	7.5
Mn/DOT Class (Minus 10)	SiCL
Clay (Minus 10) %	26.4
Silt (Minus 10) %	67
Sand (Minus 10) %	6.7
AASHTO Group	A-6
Group Index	10
Optimum Moisture (% dry wt)	16.7
Max Density (lb/cubic ft)	105.3
R-Value (at 240 psi)	24.1
Soil SpG	2.692

Test Procedures: AASHTO T87, T88, T89, T90, T99 Method "C" (M), T100, T190 (M), T-265 M = Mn/DOT Modified

Comments:

Copies To:

JOHN SIEKMEIER - METRO

Charge Out: 1037, 1038, 1041, 1046

Rod Patrin

REVIEWED BY

Minnesota Department Of Transportation

SubSoil Sample Worksheet

Sample ID:	CO-SS12-0180	Submitted By:	JOHN SIEKMEIER
Project No.:	99008-9	Source:	
Date Sampled:	2/14/2012	Date Received:	2/17/2012

Hydrometer Analysis

Time	Temp	Read	Size (mm)	% Finer
2 min	71.0	37.0	0.03138	62.8
5 min	71.0	34.0	0.02081	56.6
15 min	71.0	28.0	0.01248	44.4
30 min	71.0	25.0	0.00848	38.3
60 min	71.0	23.0	0.00635	34.2
250 mi	69.0	21.0	0.00317	29.2
24 hr	70.0	18.0	0.00134	23.5

Liquid Limit

Type	Weight 1	Weight 2
No. Blows	18	27
Wet + Can	30.10	28.90
Dry + Can	26.24	25.47
Can	14.51	14.43
Liquid Limit	31.5%	

Particle Size

%	Particle
7.5	Sand and Gravel (Entire Sample)
66.4	Silt (Entire Sample)
26.2	Clay (Entire Sample)

Hygroscopic Moisture

Content Type	Weight
Air Dry + Can	24.64
Oven Dry + Can	24.34
Can	14.33
Corr. Factor	0.970%

Plastic Limit

Type	Weight 1	Weight 2
Wet + Can	18.54	18.91
Dry + Can	17.80	18.18
Can	14.2	14.5
Plastic Limit	20.2%	
Plasticity Ind	11.3	

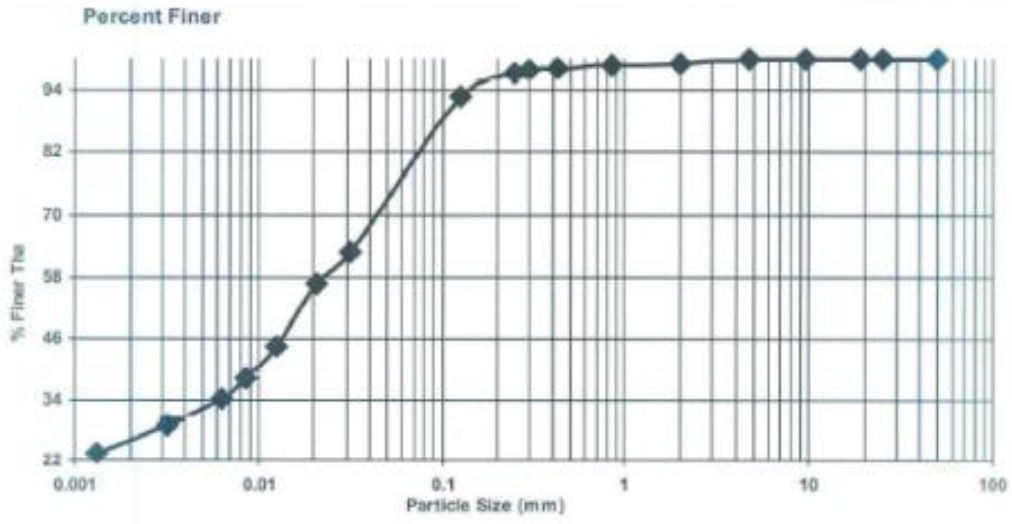

State of Minnesota Department of Transportation

MOISTURE-DENSITY RELATIONSHIP

Sample ID:	CO-SS12-0180	Proj Eng :	JOHN SIEKMEIER	Submitted By:	JOHN SIEKMEIER			
Sample From :		Project No.:	99008-9	Report Approved :	03/09/2012 08:18			

Test Number:	1	2	3	4	5	6	7	8
Wet Soil Mold:	5898.50	5973.30	6064.80	6032.60				
Mold:	4204.90	4204.90	4204.90	4204.90				
Wet Soil Pan:	947.90	995.60	1041.50	1054.70				
Dry Soil Pan:	893.20	921.00	942.30	931.20				
Pan:	349.20	359.80	353.60	358.40				
%Moisture-Dry:	10.06	13.29	16.85	21.56				
Dry Density:	101.79	103.25	105.28	99.45				

Maximum Density: 105.3 lb/cu.ft.

Optimum Moisture: 16.7 %

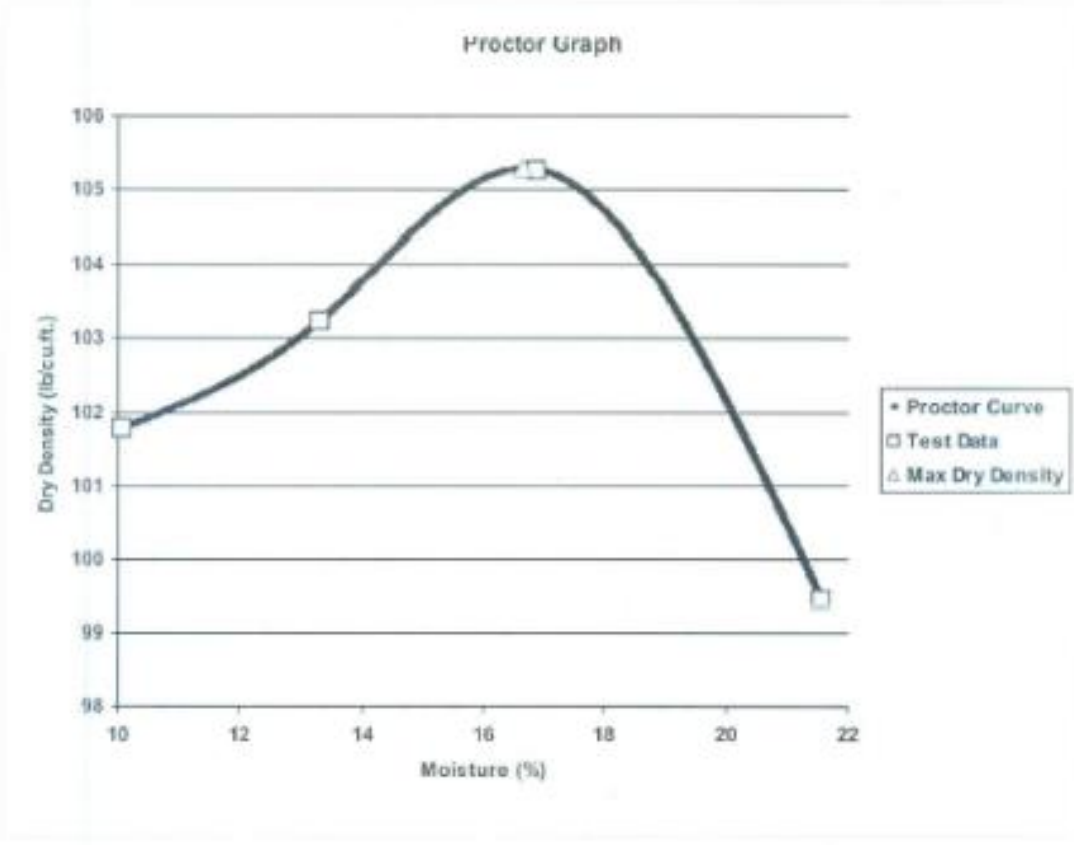

State of Minnesota Department of Transportation

R-Value Worksheet

Sample ID: CO-SS12-0180 Soils Lab No.: RV Initials: RV Date:

% Passing 3/8": 60.0 % Passing #4: 99.9 Mn/DOT Class: SiCL AASHTO Group: A-6

Opt. Moisture: 16.7 Max Density: 105.3 Est Orig Moisture: 4 Report Approved : 03/15/2012 14:54

Mold No:	5	6	7	8
Batching Data				
Water Added (Init):	119	137	156	174
Water Added (Final):	59	69	78	87
Initial Moisture (%):	9	10	11	13
Moisture Added (%):	13.0	15.0	17.0	19.0
Total Moisture (%):	15.0	17.0	19.0	21.0
Orig. Wt. of Batch:	1400			
Corr. Wt. of Batch:	1372			
Dry Spec. Wt:	868			
Wet Spec. Wt:	999	1016	1033	1051
Moisture Data				
Wet Weight:	785.9	763.5		815.2
Dry Weight:	707.9	677.2		709.5
Pan Tare Wt.:	197.1	177.2	199.5	191.2

Mold No:	5	6	7	8
Stabilometer Test				
Exudation Pressure:	800	332		180
Wt. of Briq. + Mold:	3069.4	3075.6		3112.0
Wt. of Mold:	2070.5	2062.0	2123.6	2061.0
Height of Briquette:	2.32	2.45		2.54
Dial Reading (.0001):	183	42		13
Expansion Pressure:	5.5	1.3		0.4
Stabil - 1000lb:	31	42		54
Stabil. - 2000lb:	74	88		126
Turns Displacement:	3.53	3.68		3.52
Calculated Information				
Moisture Loss:	78.0	86.3		105.7
Dry Soil Wt.	510.8	500.0		518.3
Moisture at Compact.	15.3	17.3		20.4
Wet Wt. of Briq.:	989	1014		1051
R-Value (Corr):	40.7	34.6		15.6
R-Value at 240 psi:	24.1			

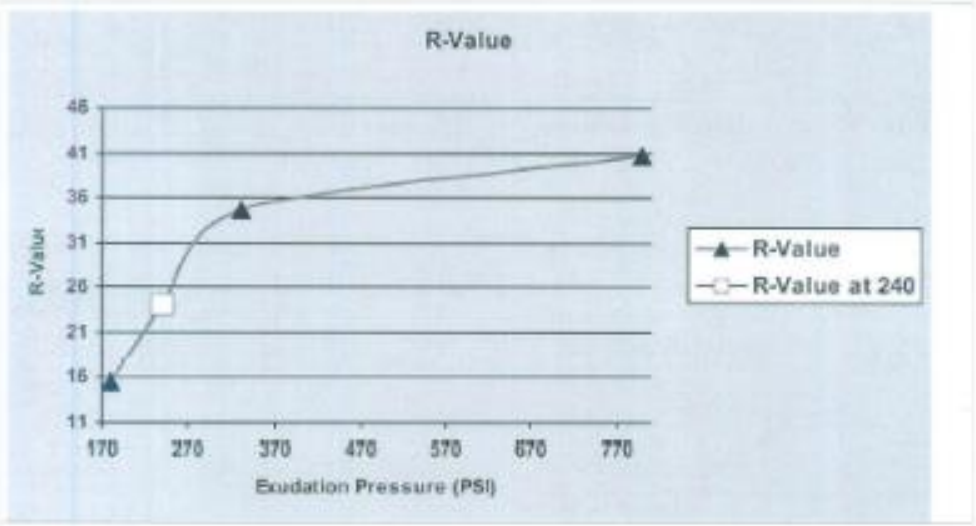

Appendix C
Same Slope Regression Analysis

Figures C.1 through C.22 show the same slope regression analysis done to determine the β values of each soil. This information was to determine a single β value for each soil from the six time dependent turbidity and TSS relationships. This information was also used to determine if the soils reached steady state over the thirty minute of rainfall they were exposed to. If the β values collapse to a single β value over time, the soil was assumed to have reached steady state during the experiment.

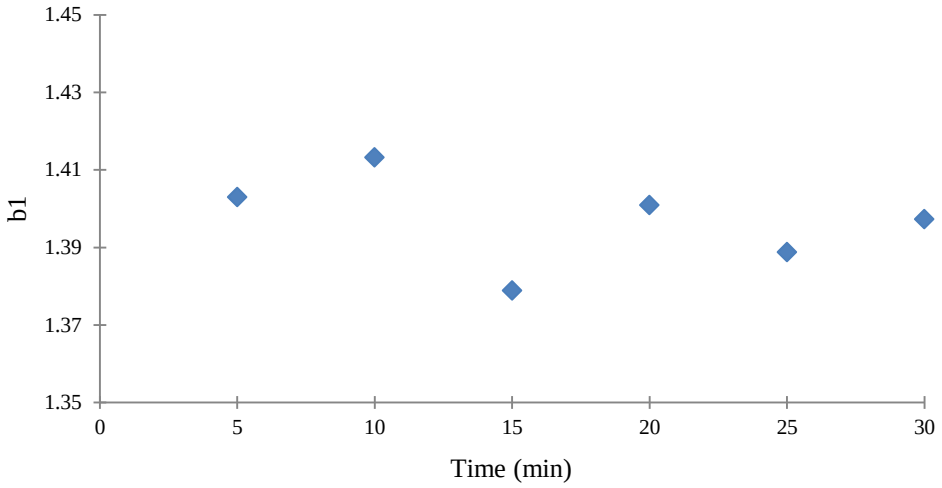

Figure C.1. AH - S (1) b1 Regression

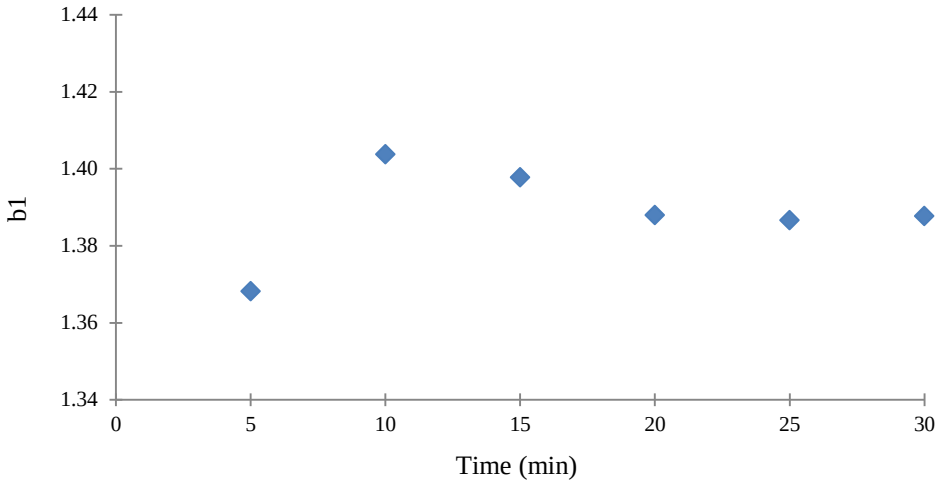

Figure C.2. AH - S (2) b1 Regression

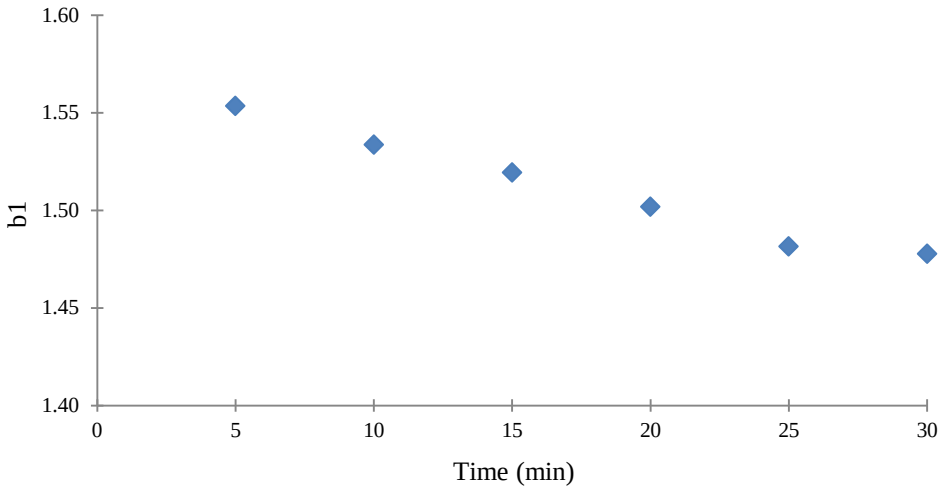

Figure C.3. AH - T (1) b1 Regression

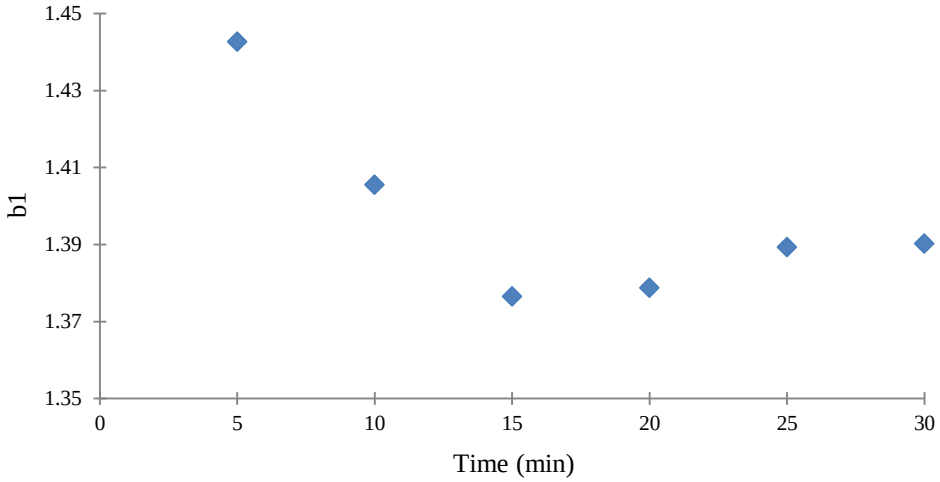

Figure C.4. AH -T (2) b1 Regression

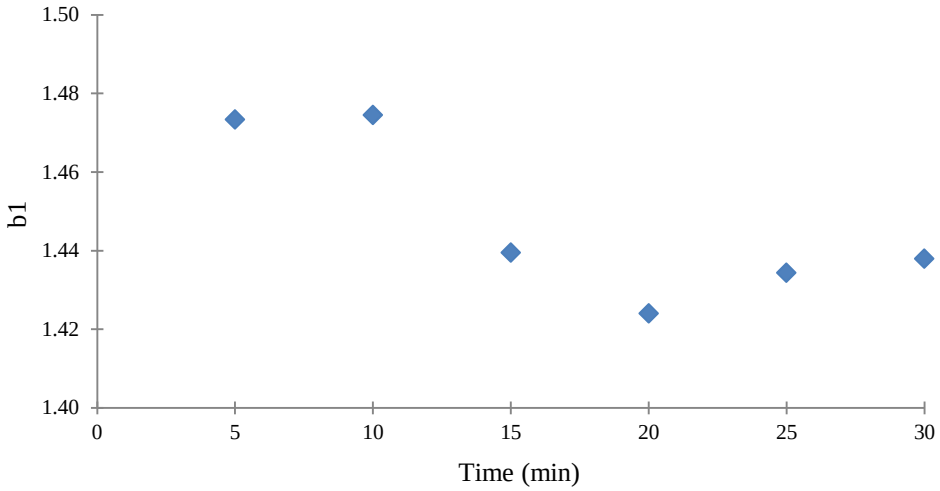

Figure C.5. AH - T (3) b1 Regression

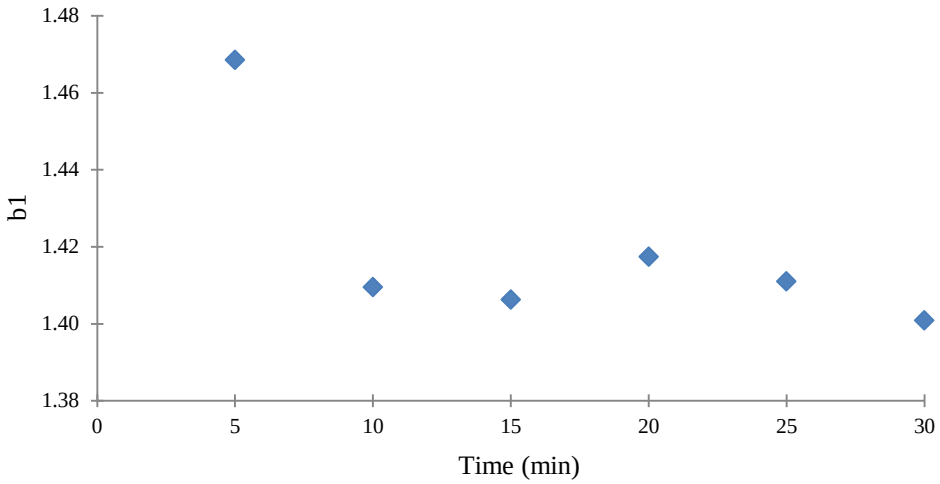

Figure C.6. AH - T (4) b1 Regression

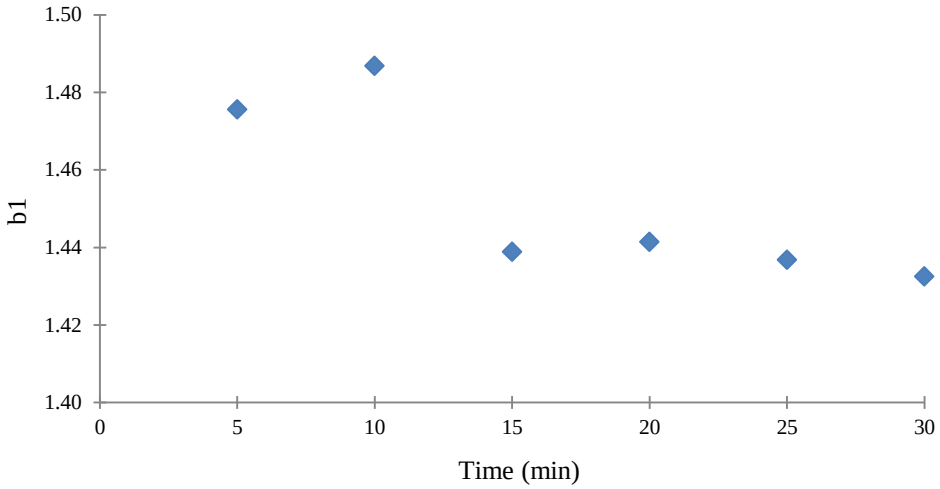

Figure C.7. AH - T (5) b1 Regression

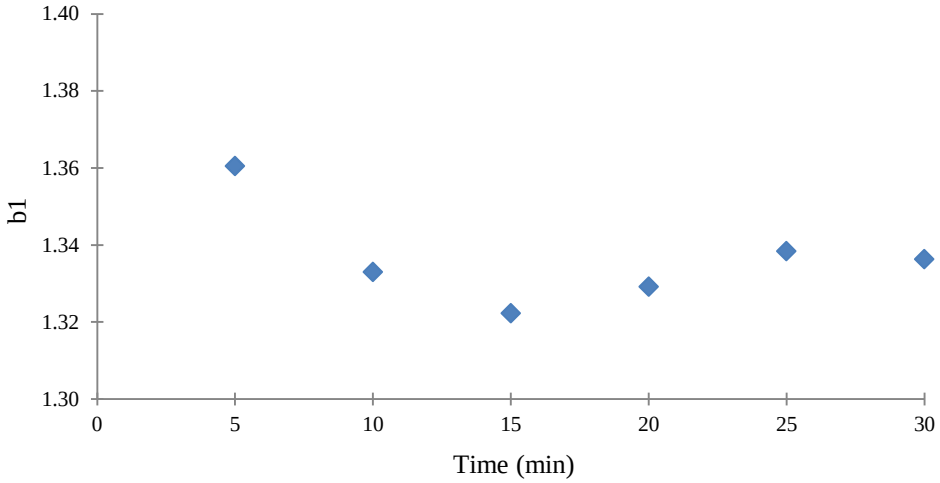

Figure C.8. CTY - S (1) b1 Regression

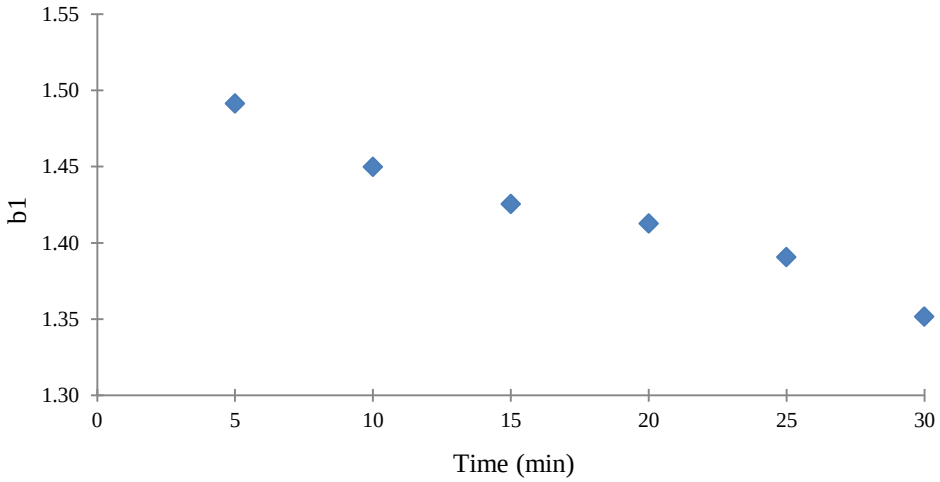

Figure C.9. CTY - S (2) b1 Regression

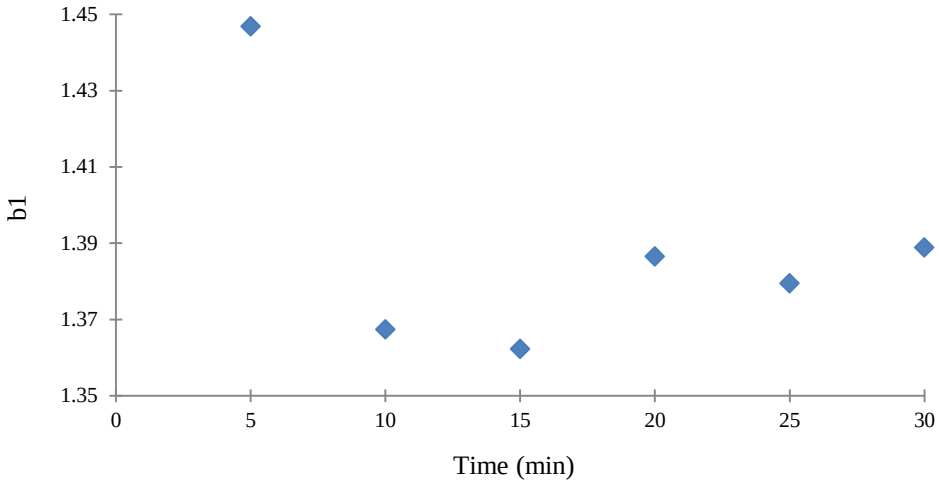

Figure C.10. CTY - T b1 Regression

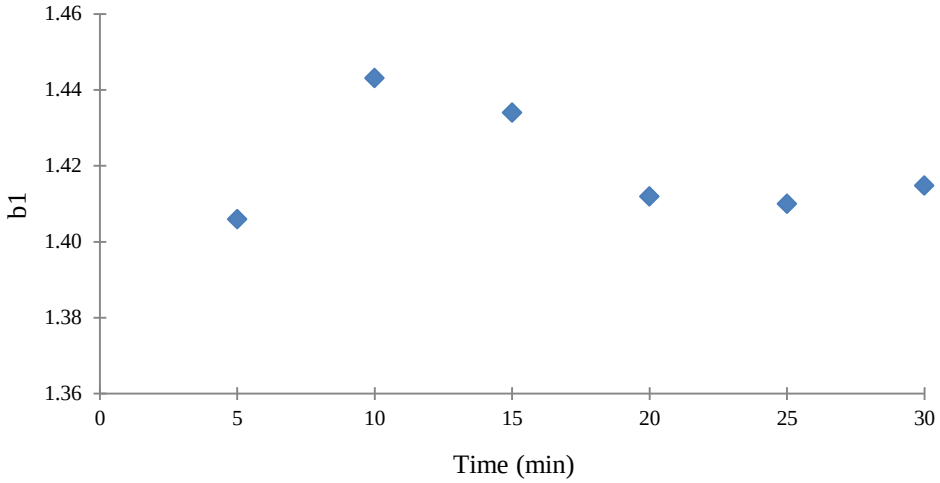

Figure C.11. Dul - S (1) b1 Regression

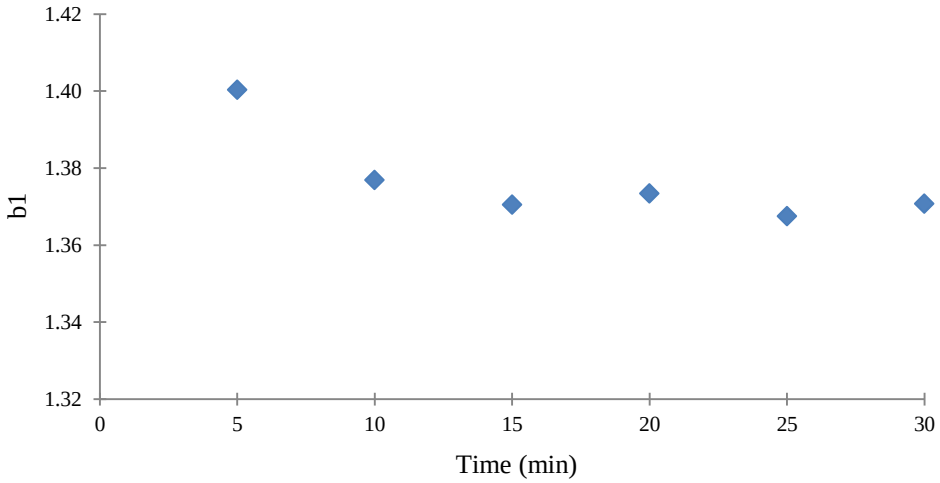

Figure C.12. Dul - S (2) b1 Regression

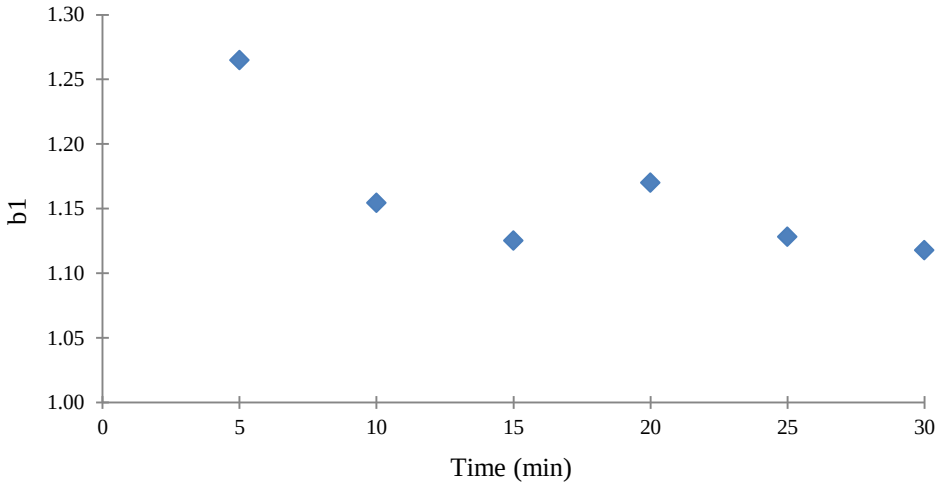

Figure C.13. Dul - T b1 Regression

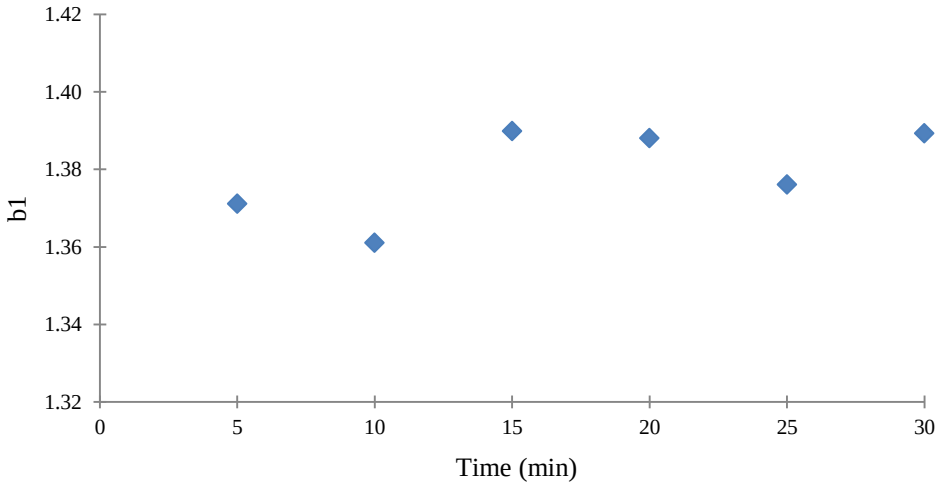

Figure C.14. Hast - S b1 Regression

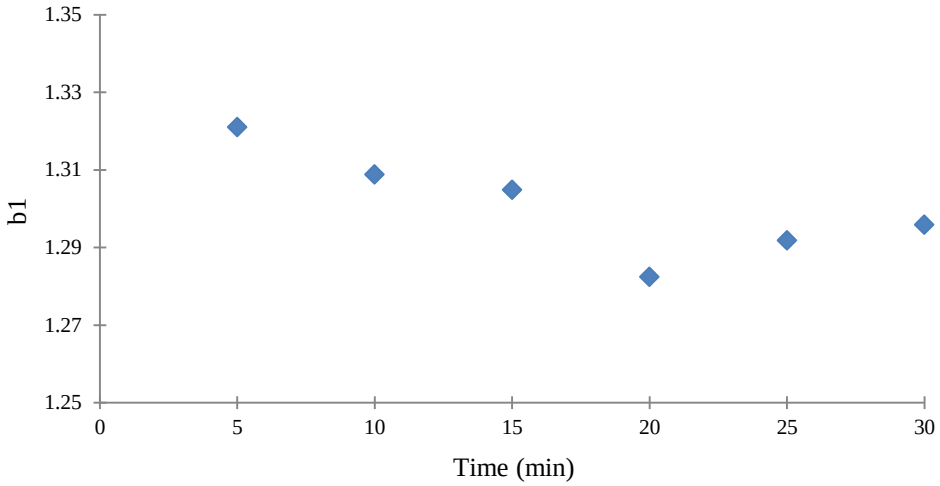

Figure C.15. Hast - T b1 Regression

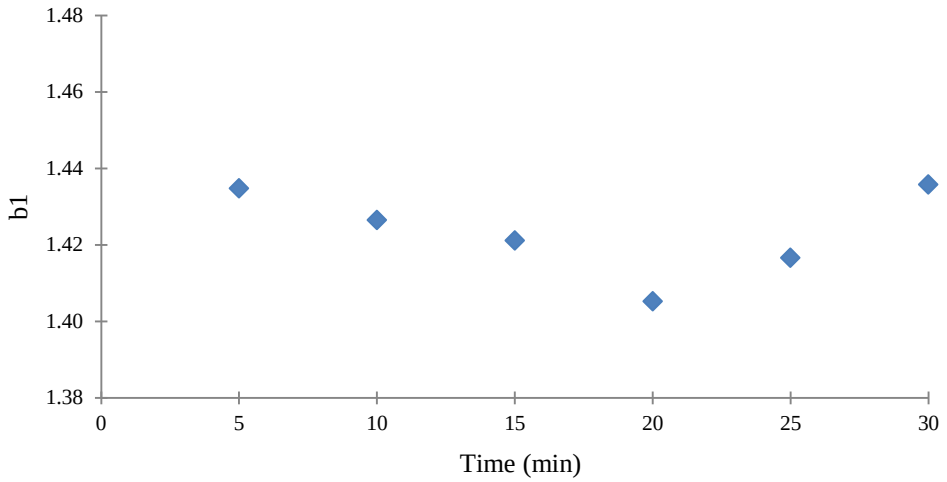

Figure C.16. OV - S (1) b1 Regression

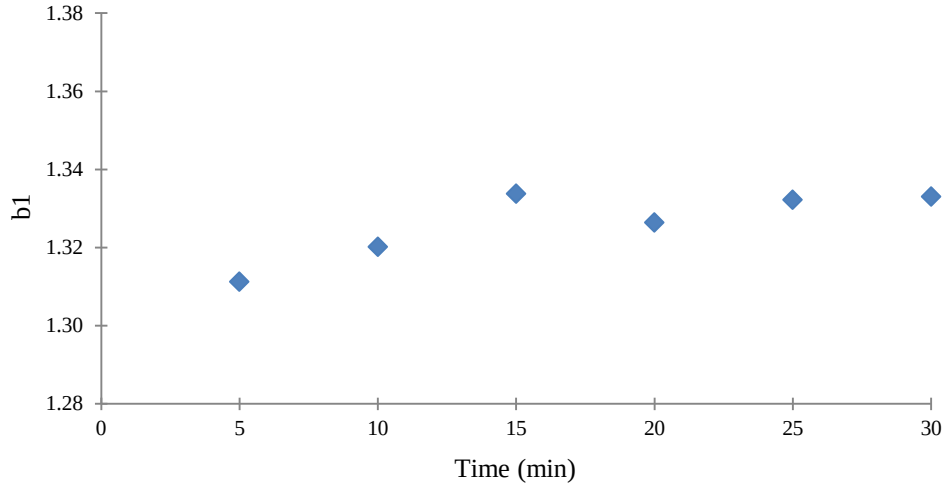

Figure C.17. OV - S (2) b1 Regression

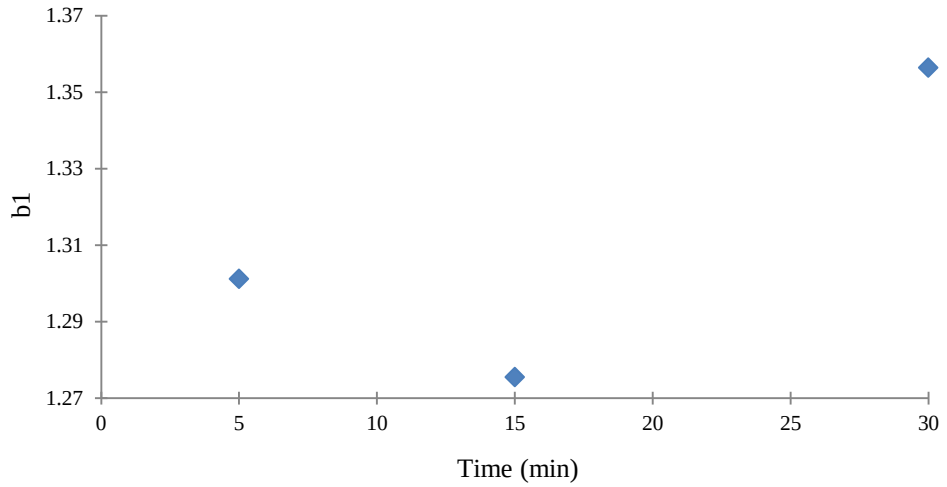

Figure C.18. OV - T b1 Regression

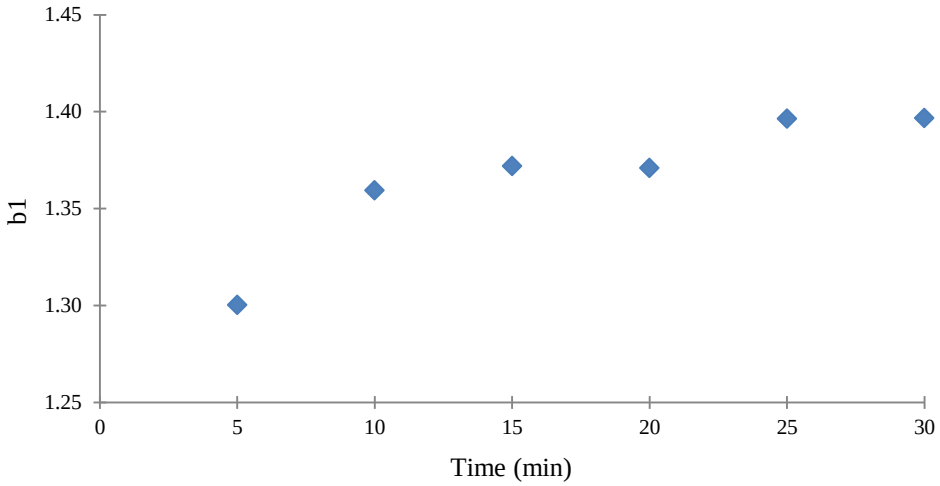

Figure C.19. Soil A b1 Regression

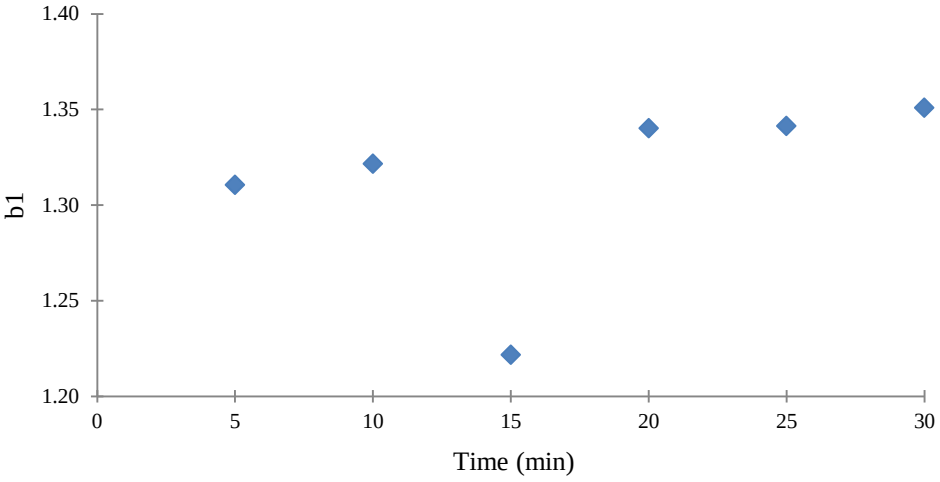

Figure C.20. Soil B b1 Regression

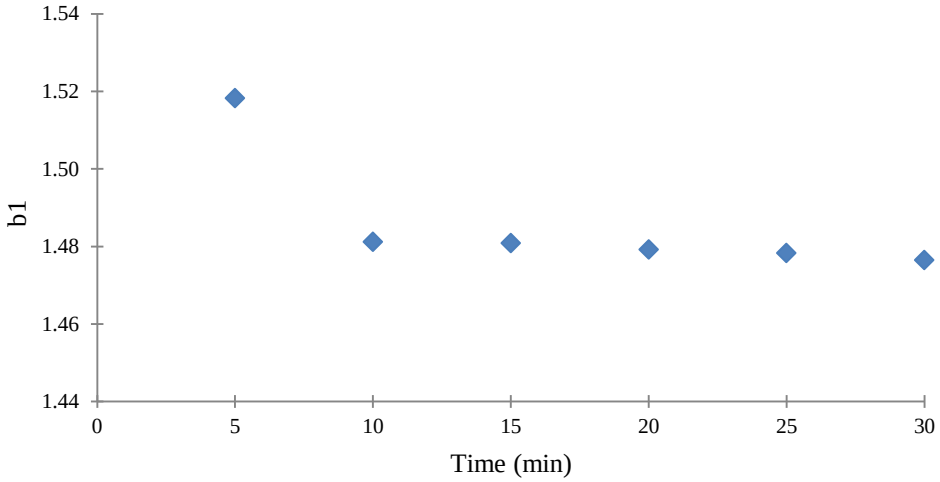

Figure C.21. TH23 - S b1 Regression

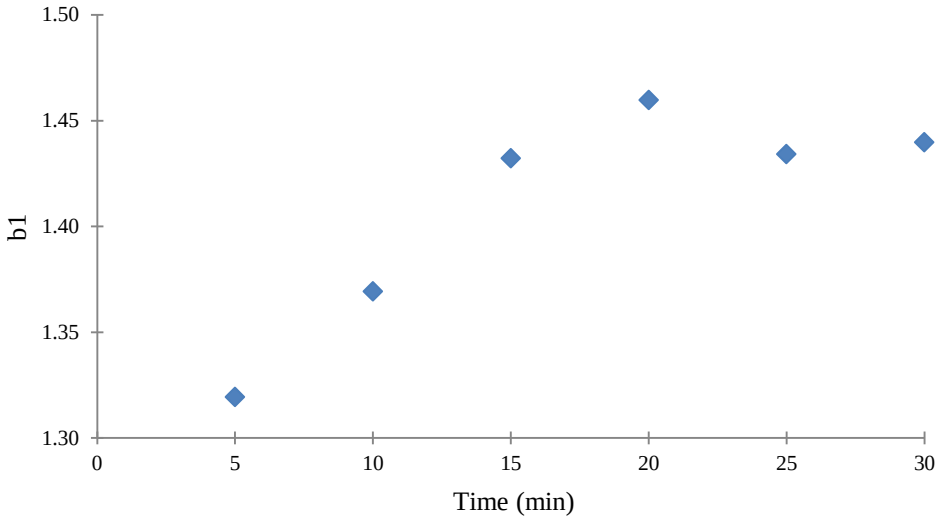

Figure C.22. TH23 - T b1 Regression

Appendix D
Aliquot Sample Dilution Curves

Figures D.1 through D.22 show the aliquot sample analysis for each soil. Each 50 mL sample was diluted 4-6 times to create time dependent, turbidity and TSS relationships. Each soil has six relationships that were further analyzed to determine a general relationship for all of the soils. This is discussed further in Chapter 4.

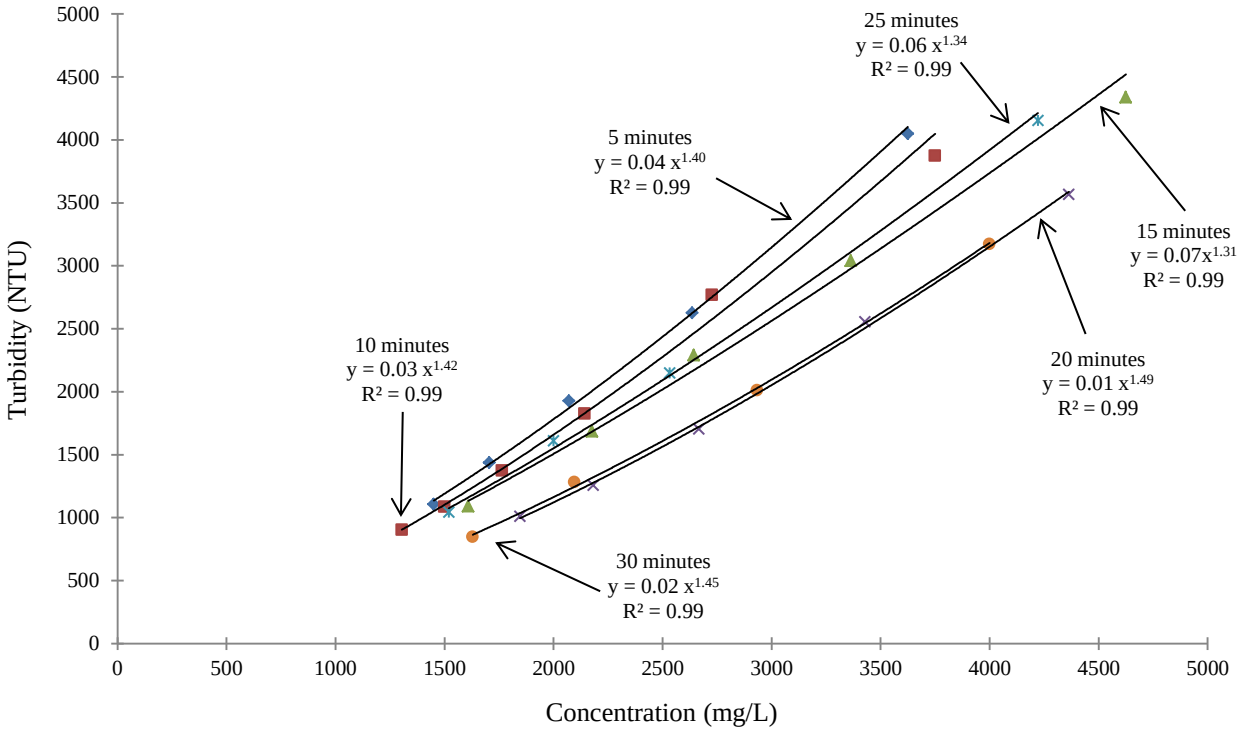

Figure D.1. AH - S (1) Aliquot Samples

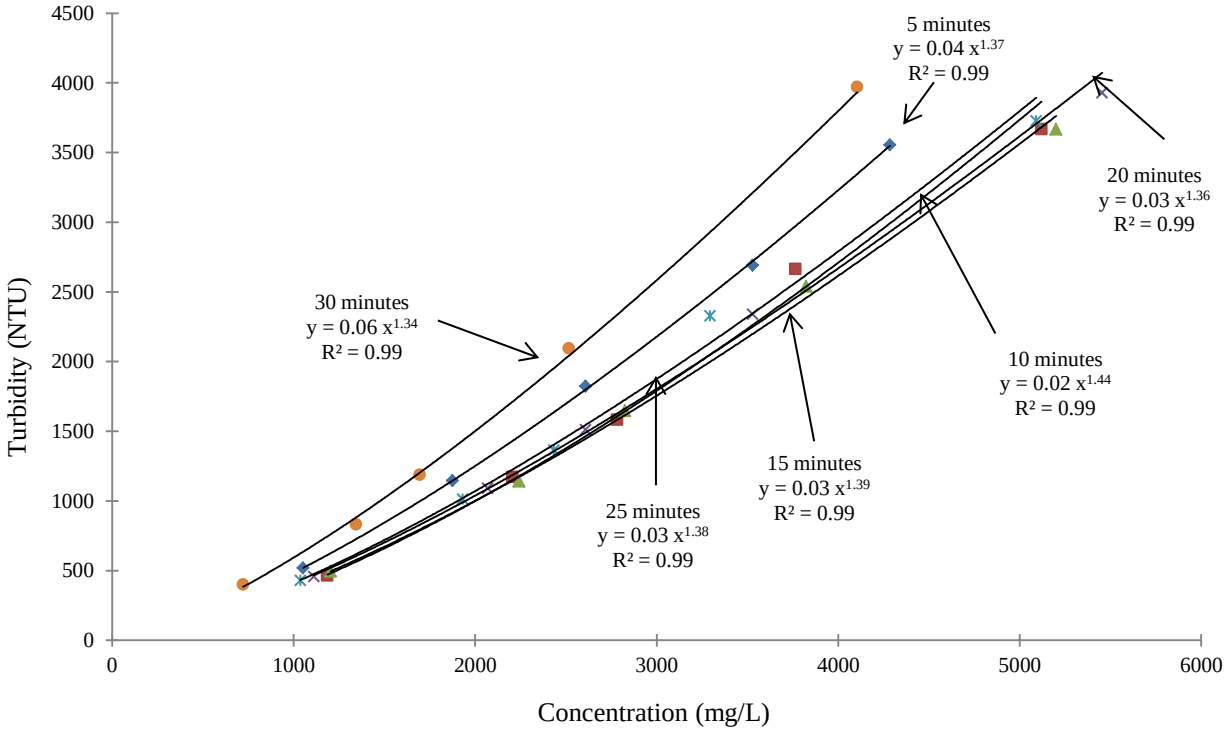

Figure D.2. AH - S (2) Aliquot Samples

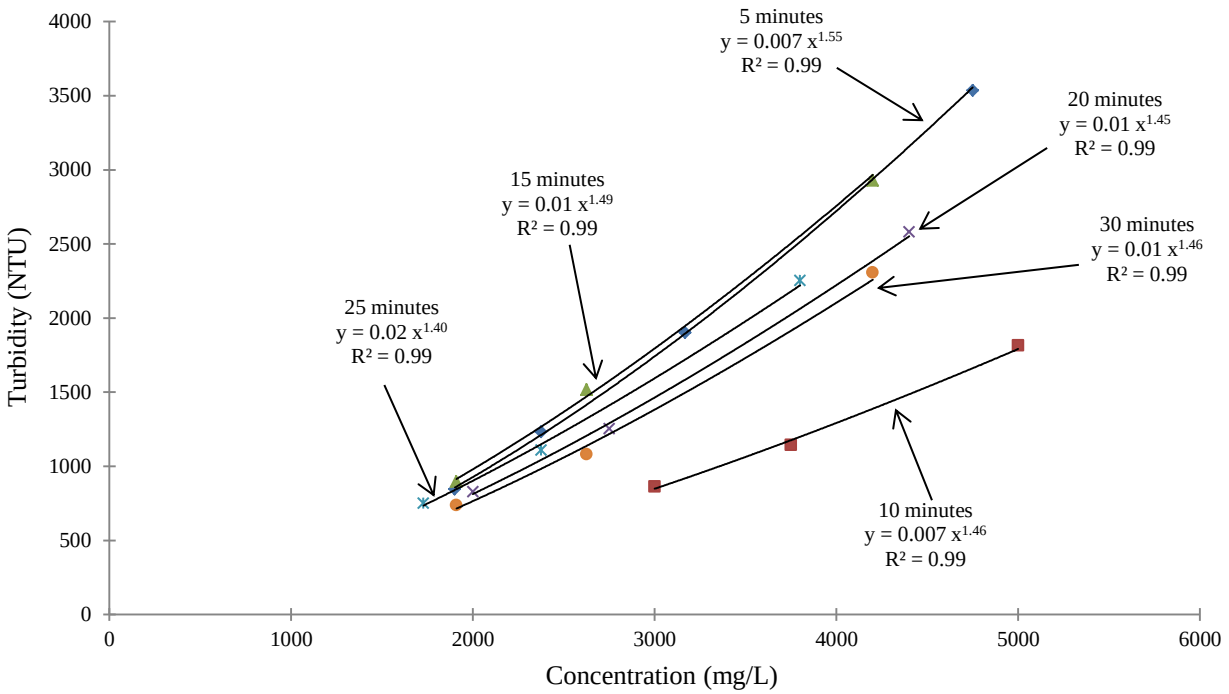

Figure D.3. AH - T (1) Aliquot Samples

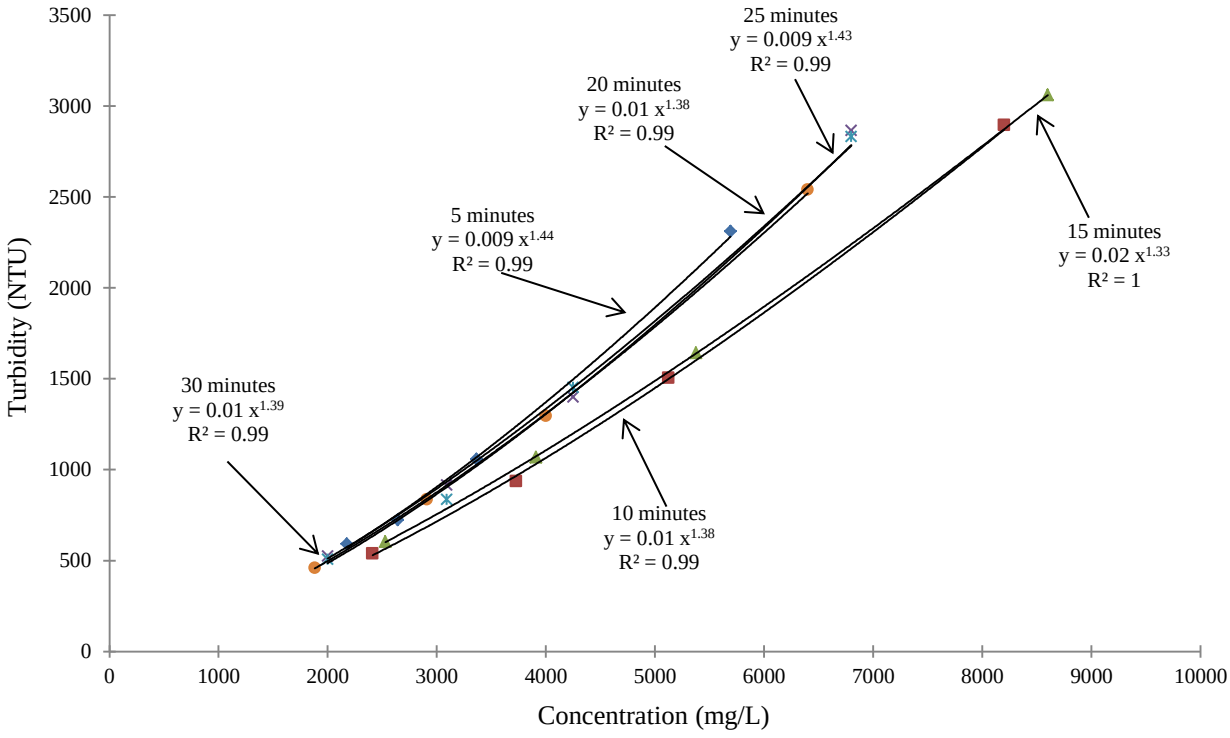

Figure D.4. AH - T (2) Aliquot Samples

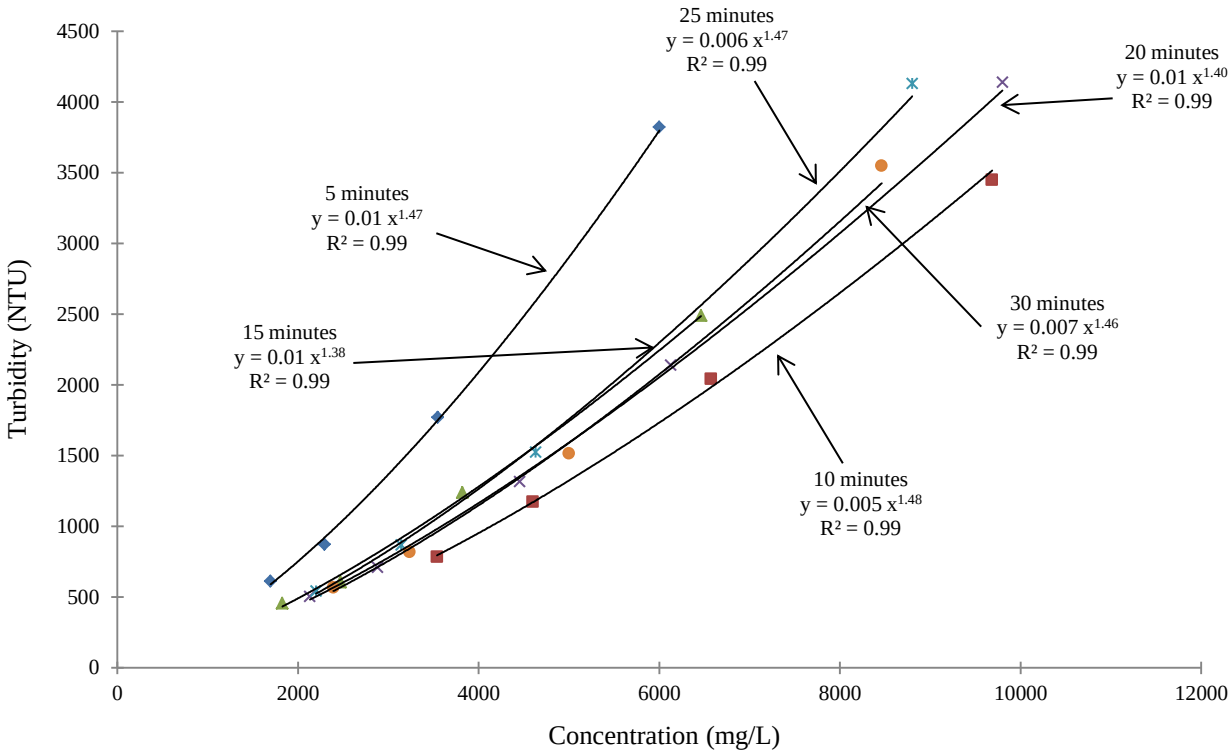

Figure D.5. AH -T (3) Aliquot Samples

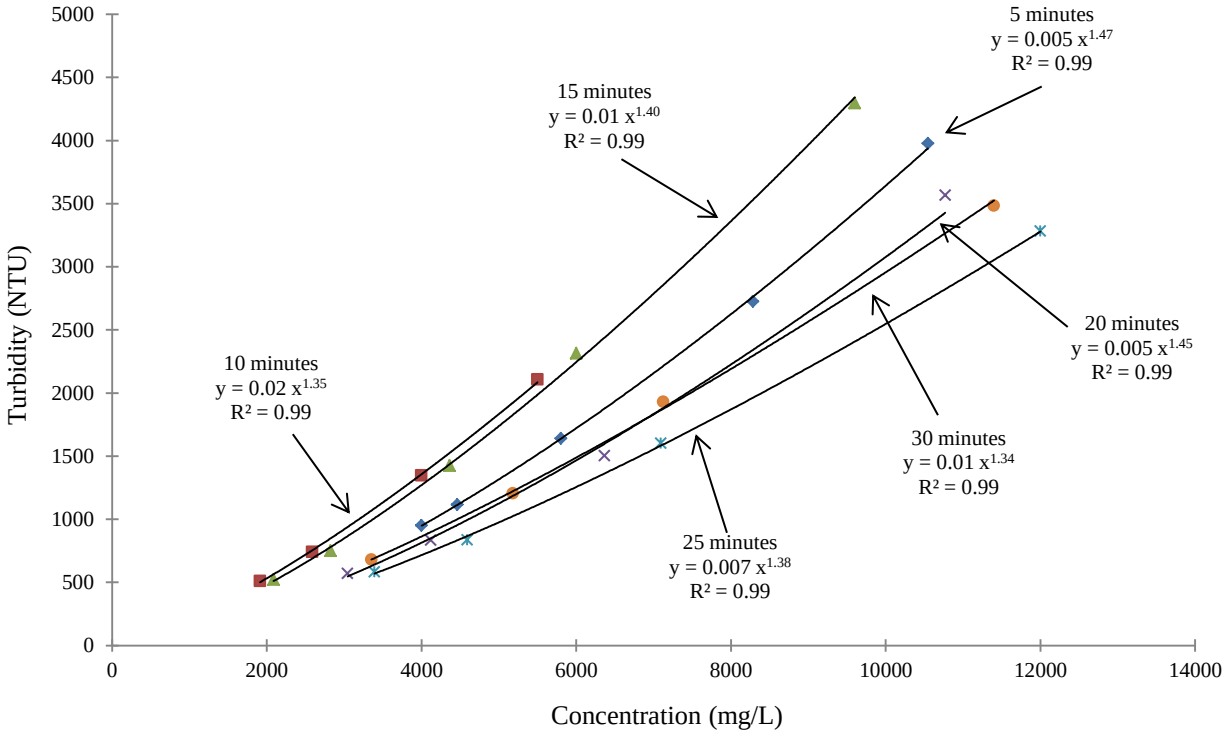

Figure D.6. AH - T (4) Aliquot Samples

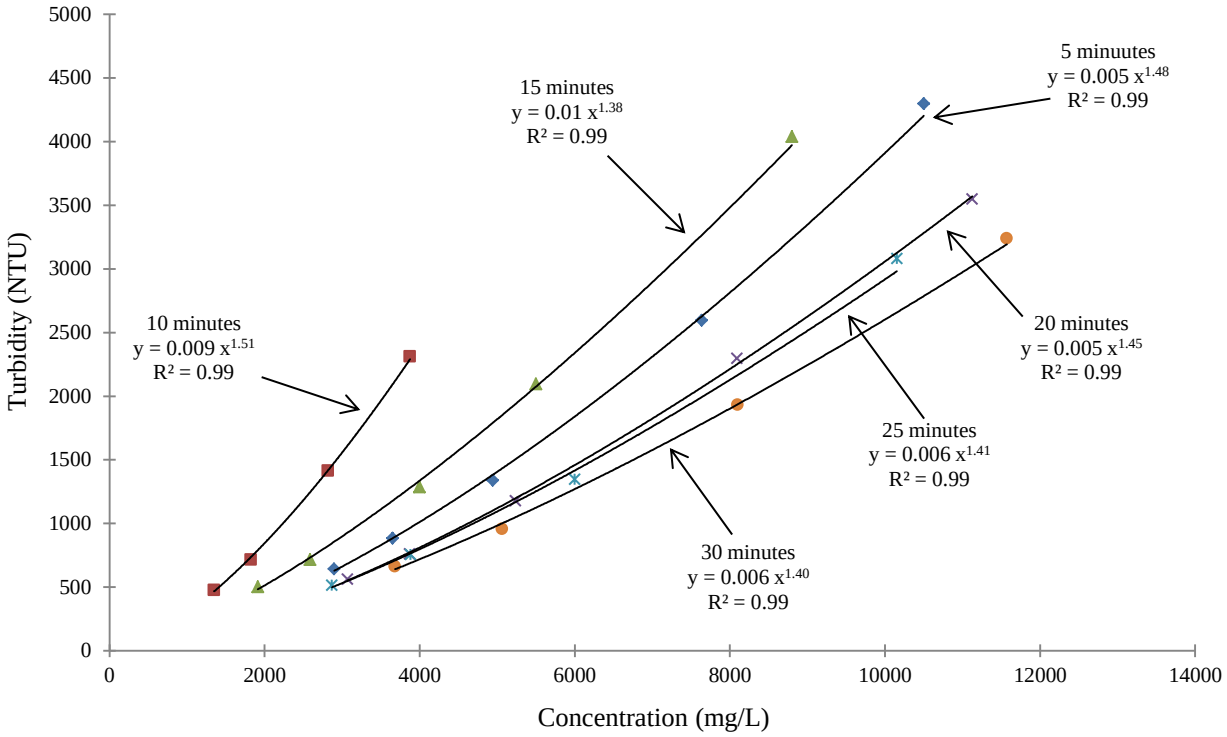

Figure D.7. AH - T (5) Aliquot Samples

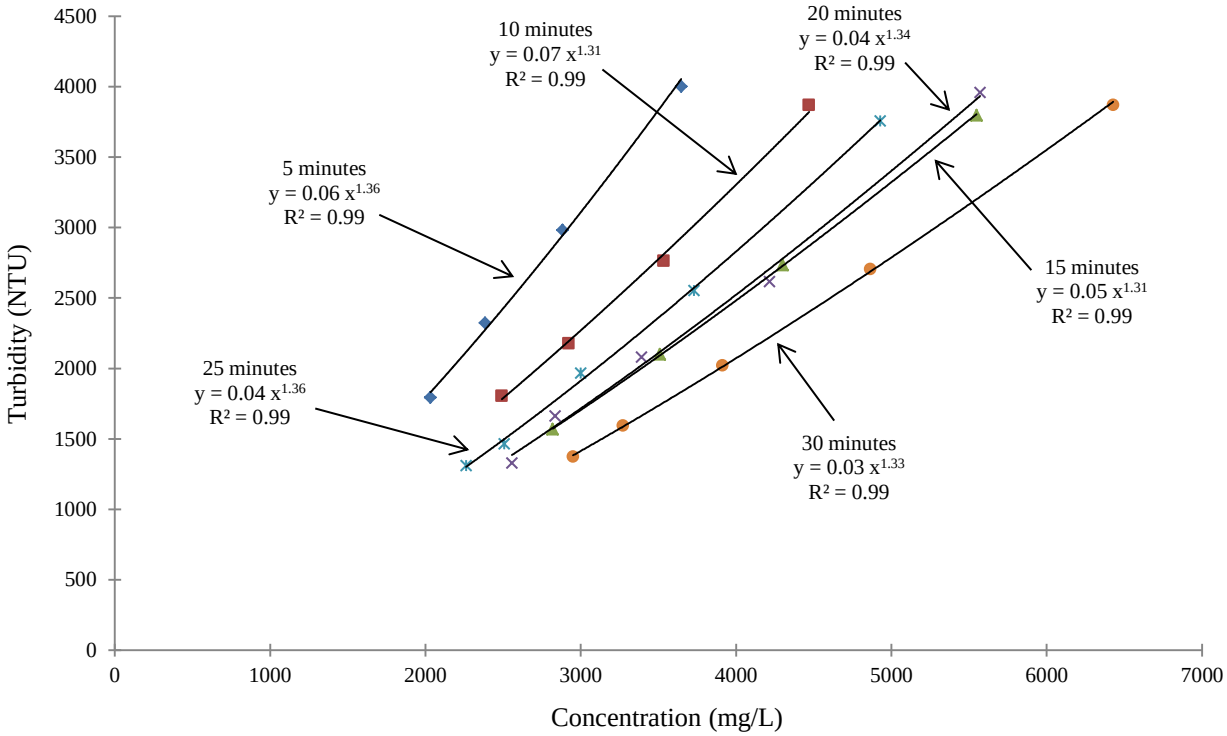

Figure D.8: CTY - S (1) Aliquot Samples

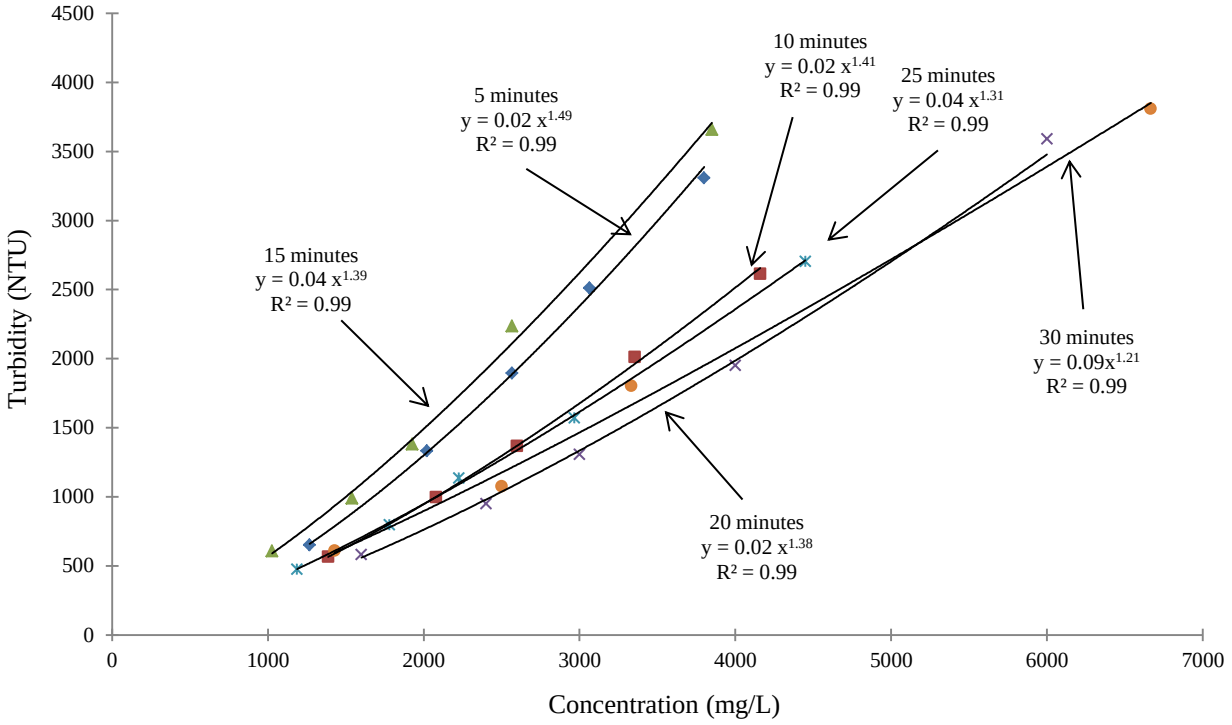

Figure E.9: CTY - S (2) Aliquot Samples

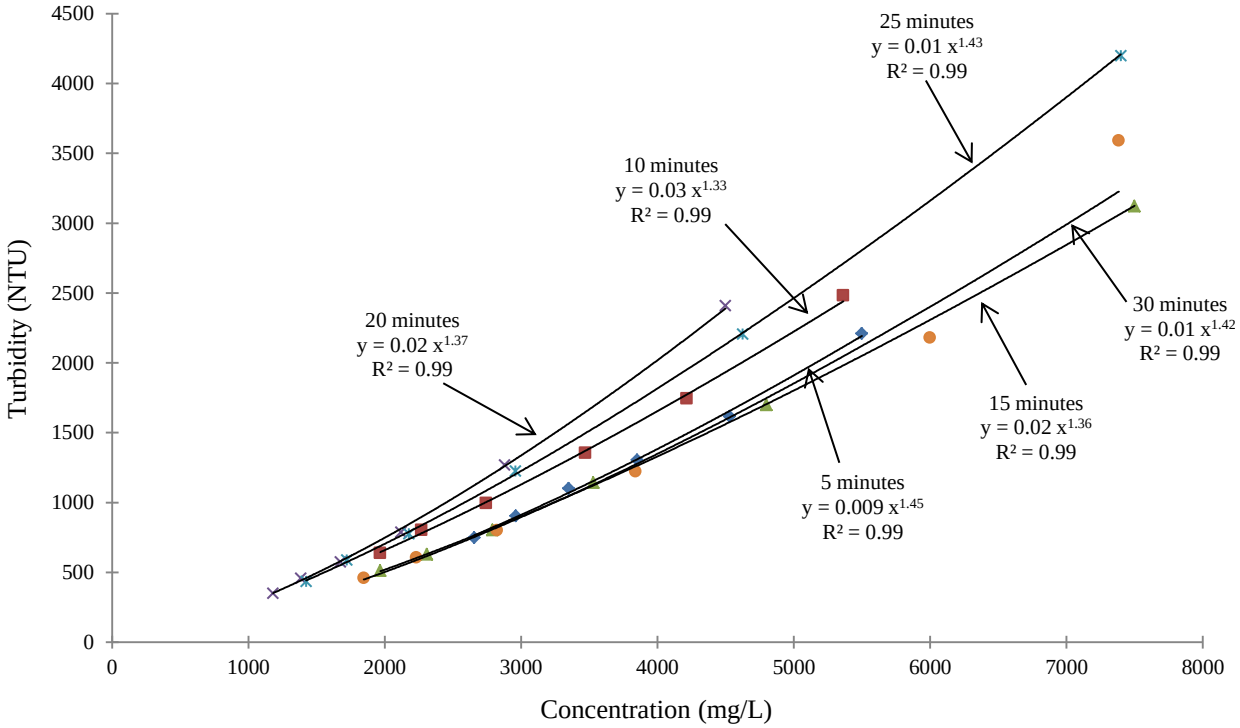

Figure D.10. CTY - T Aliquot Samples

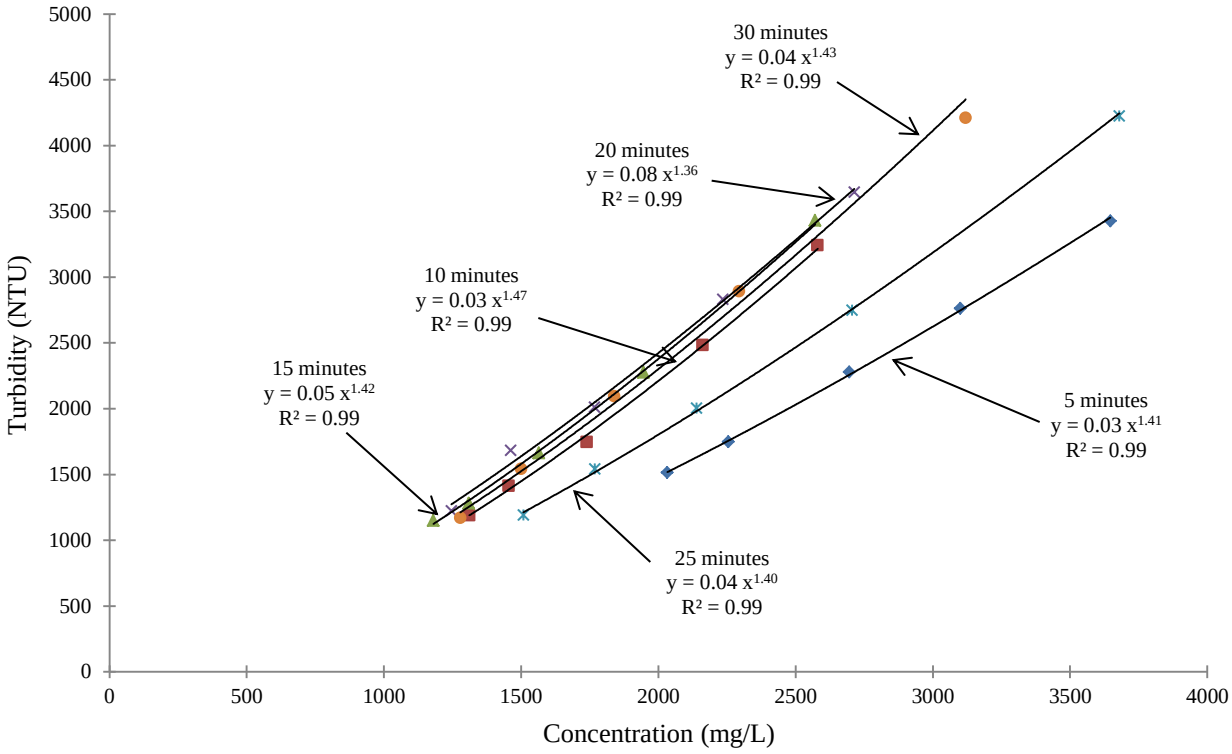

Figure D.11. Dul - S (1) Aliquot Samples

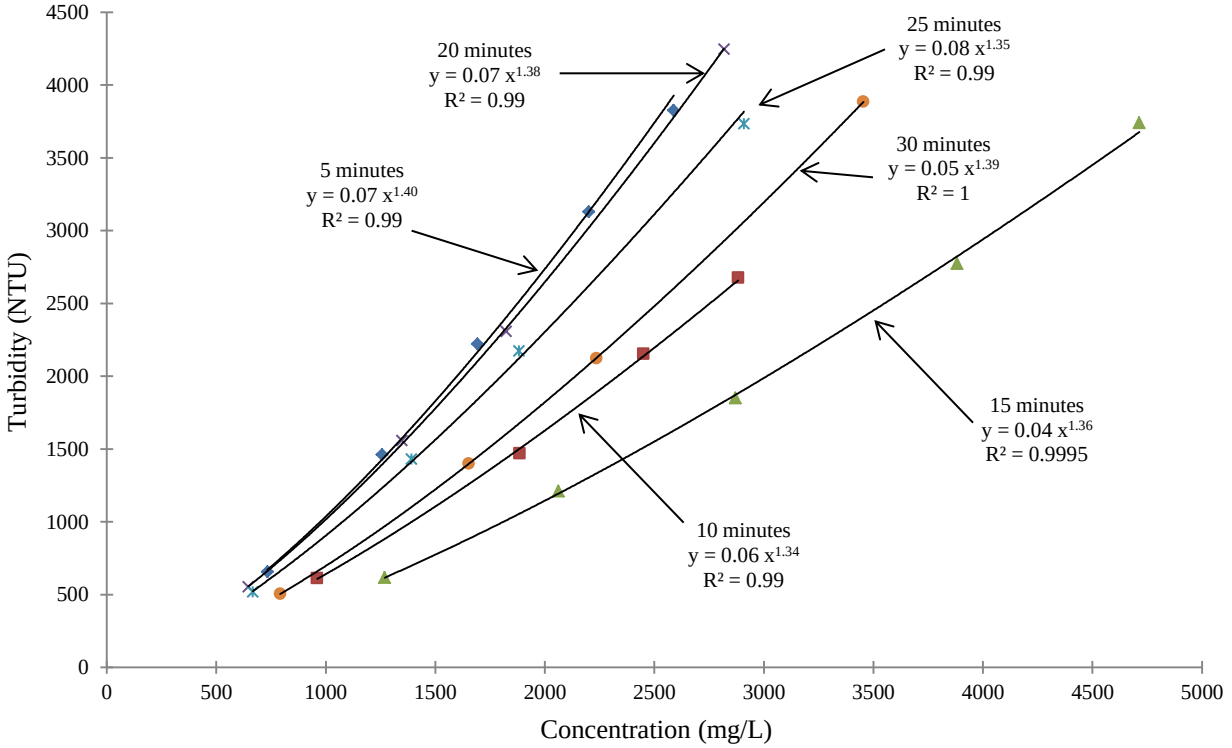

Figure D.12. Dul - S (2) Aliquot Samples

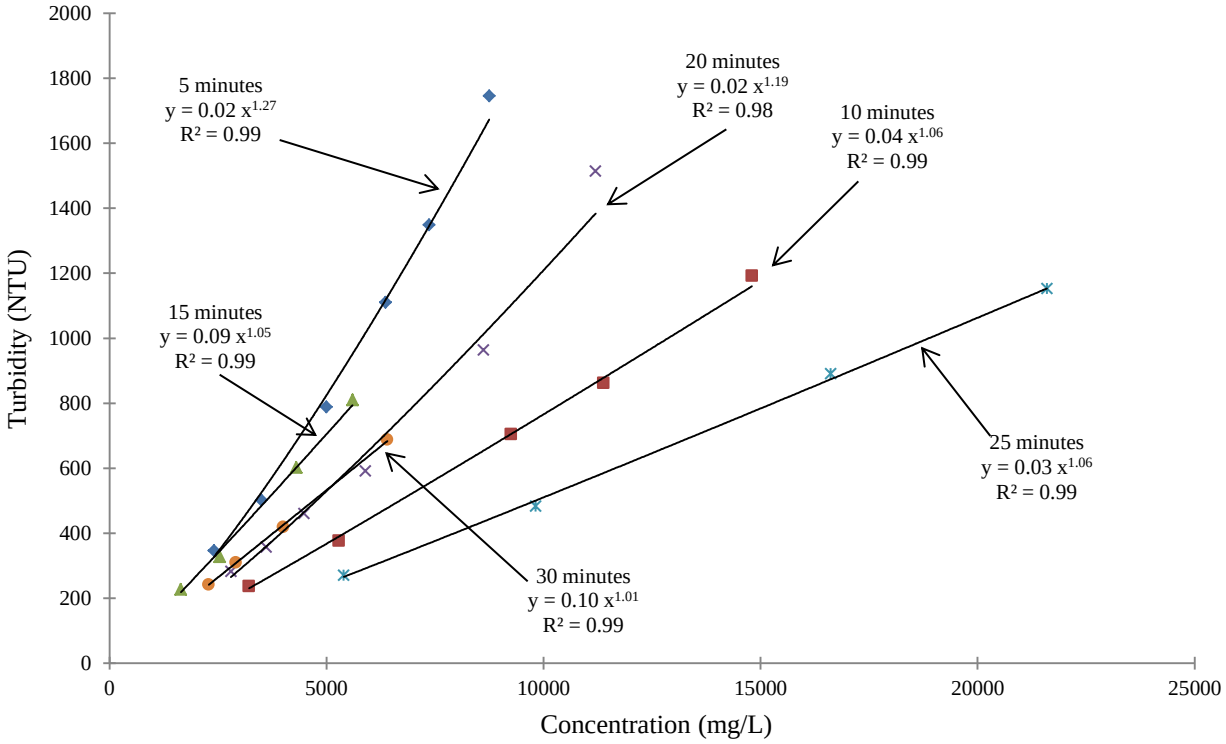

Figure D.13. Dul - T Aliquot Samples

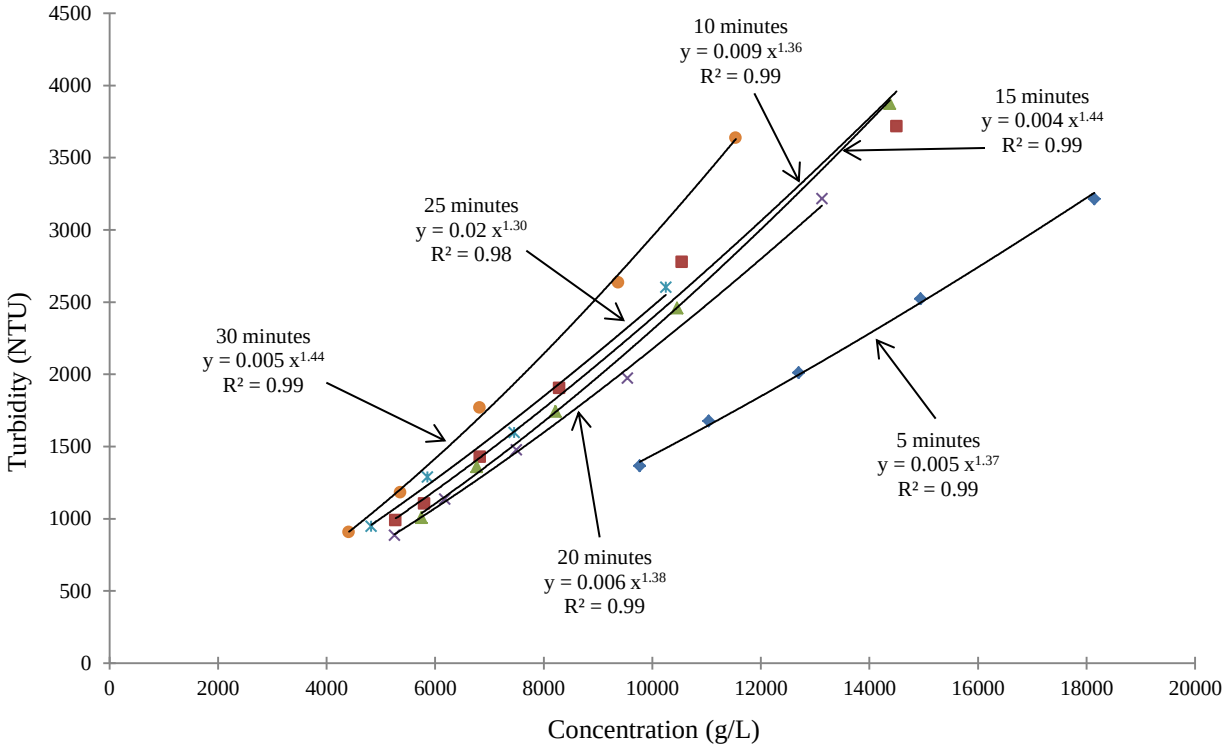

Figure D.14. Hast - S Aliquot Samples

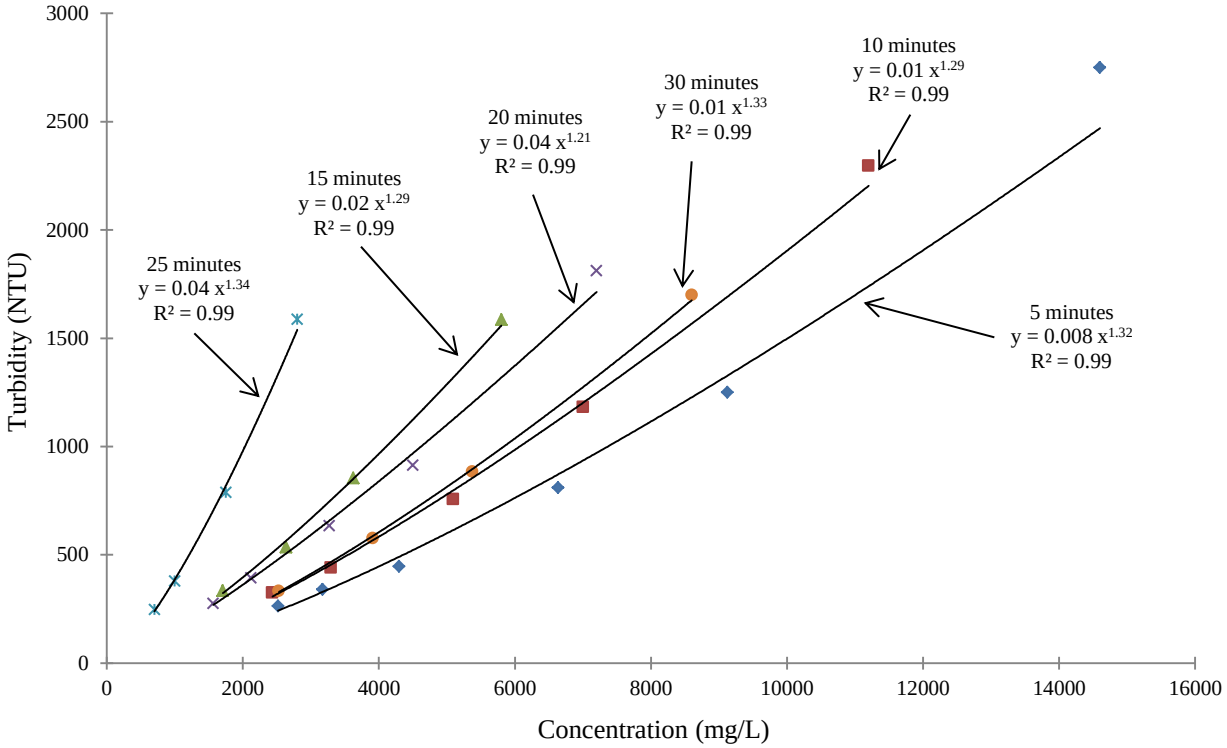

Figure D.15. Hast - T Aliquot Samples

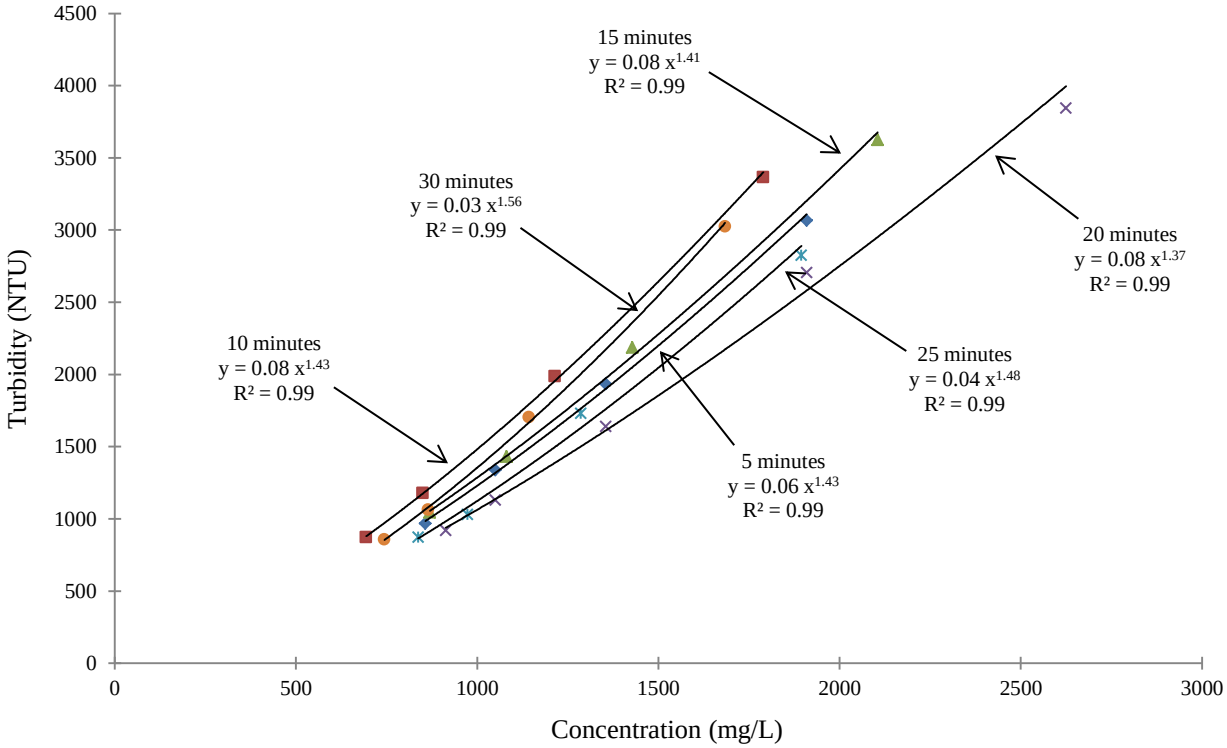

Figure D.16. OV - S (1) Aliquot Samples

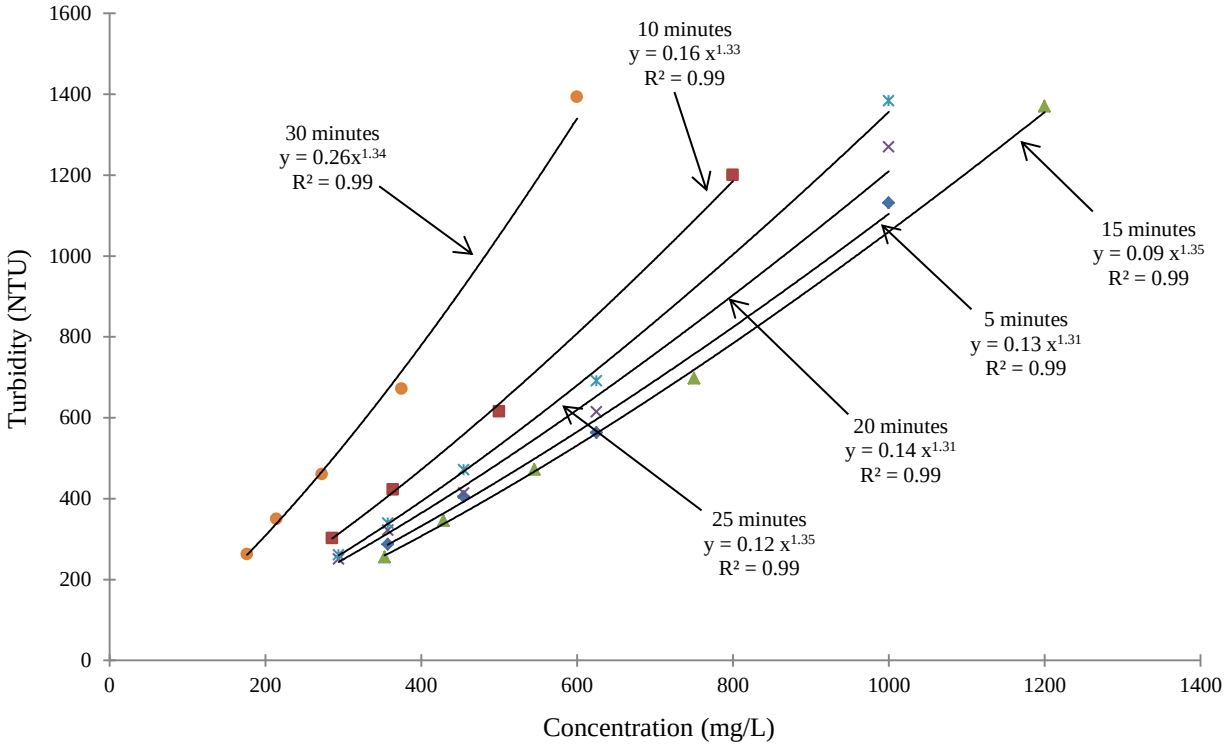

Figure D.17. OV - S (2) Aliquot Samples

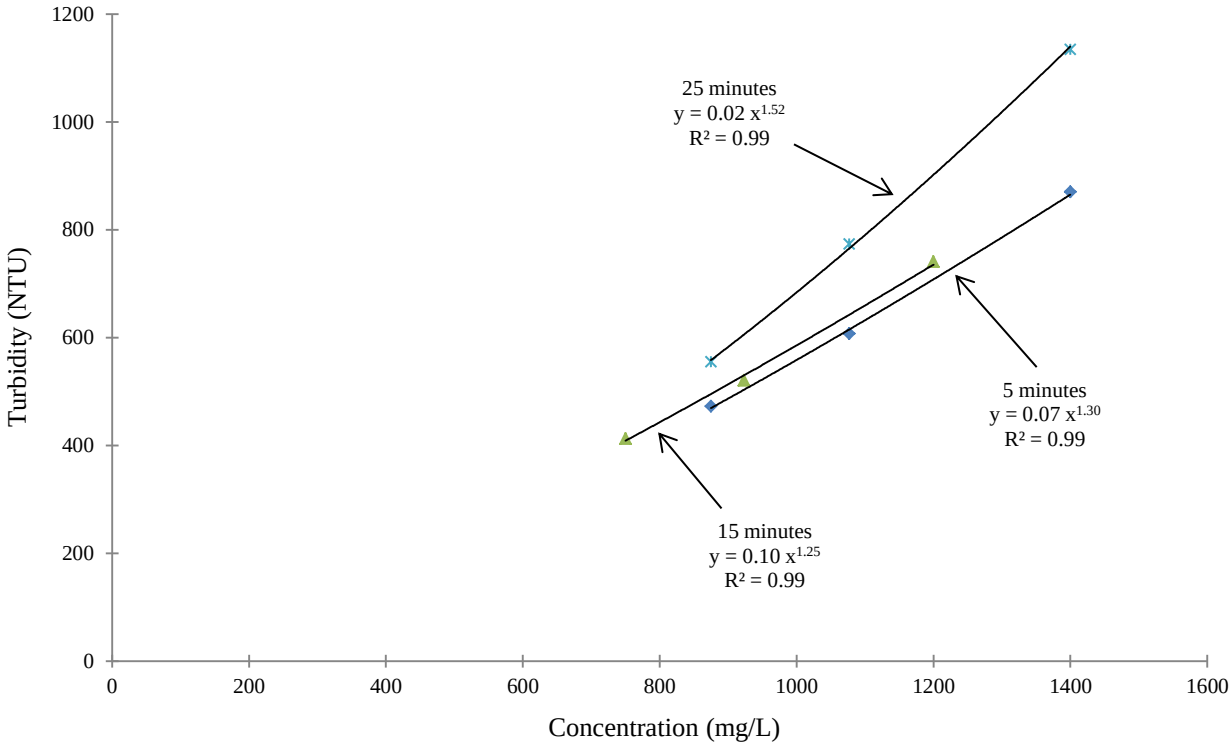

Figure D.18. OV - T Aliquot Samples

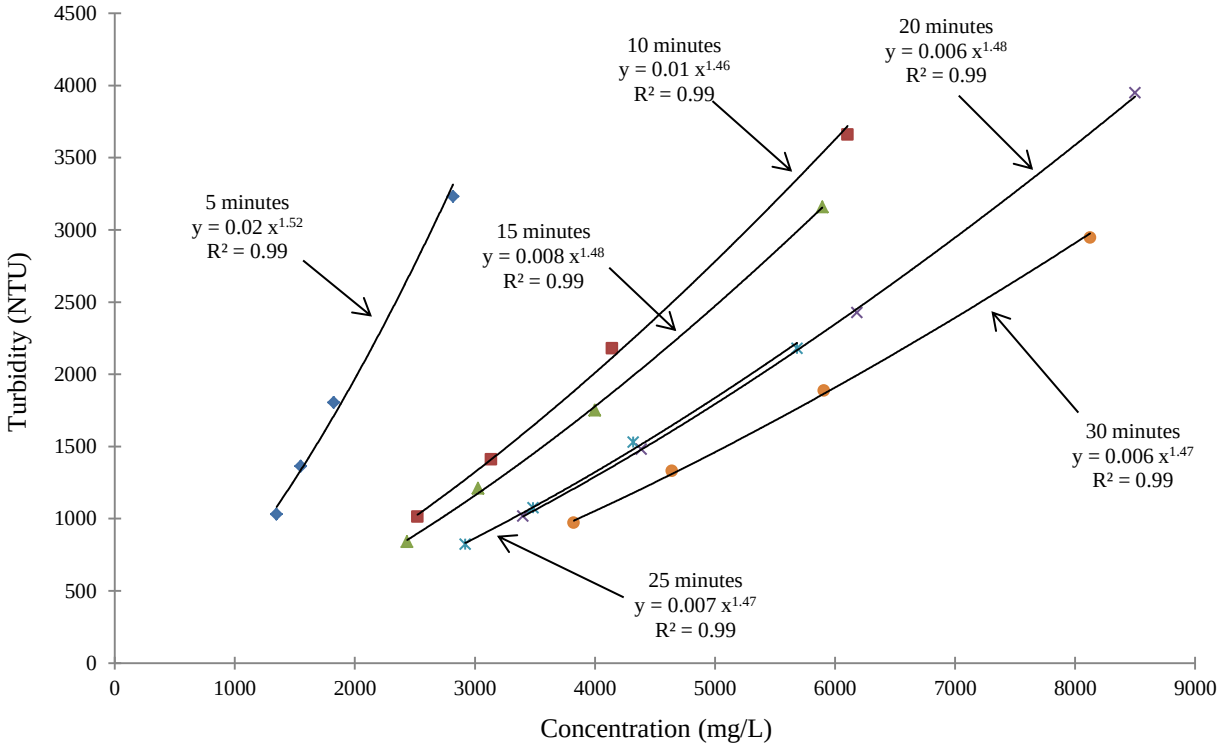

Figure D.21. TH23 - S Aliquot Samples

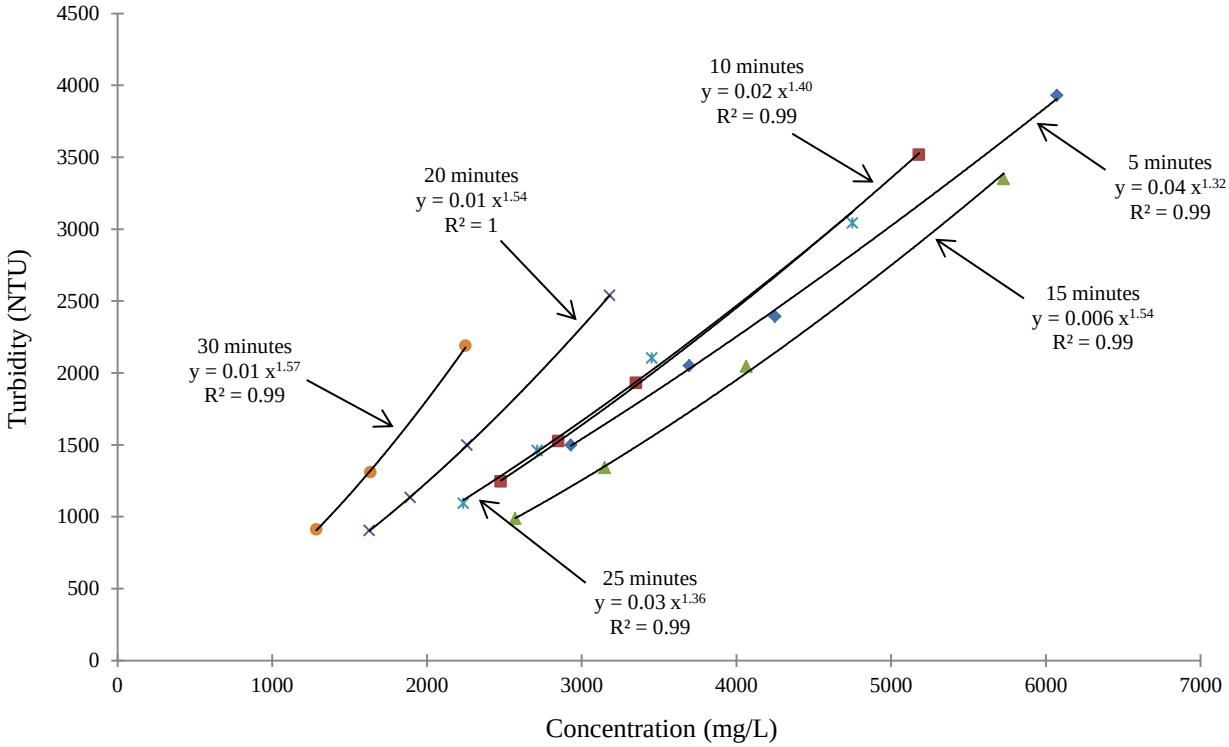

Figure D.22. TH23 - T Aliquot Samples

Appendix E

Regression Analysis of α

Extensive multiple linear regression analyses were performed to determine what soil properties best described the variation in the α parameter of the turbidity and TSS relationship. Table D.1 shows the correlation matrix for the soil properties used in the regression on α. Table D.2 shows the best regression models for α. Chapter 4 describes the chosen models in more detail.

Table D.1. Correlation matrix for soil properties.

	α	β	Sand	Silt	Clay	S+C	I	BD	V_t
α	**1.00**	0.18	-0.64	0.68	0.09	0.64	0.14	-0.24	-0.45
β	0.18	**1.00**	-0.21	0.22	0.04	0.21	-0.22	-0.26	-0.03
Sand	-0.64	-0.21	**1.00**	-0.93	-0.46	-1.00	-0.47	0.12	0.09
Silt	0.68	0.22	-0.93	**1.00**	0.11	0.93	0.27	-0.12	-0.23
Clay	0.09	0.04	-0.46	0.11	**1.00**	0.46	0.65	-0.05	0.31
S+C	0.64	0.21	-1.00	0.93	0.46	**1.00**	0.47	-0.12	-0.09
I	0.14	-0.22	-0.47	0.27	0.65	0.47	**1.00**	0.08	0.33
BD	-0.24	-0.26	0.12	-0.12	-0.05	-0.12	0.08	**1.00**	0.38
V_t	-0.45	-0.03	0.09	-0.23	0.31	-0.09	0.33	0.38	**1.00**
Q	-0.45	-0.03	0.09	-0.23	0.31	-0.09	0.33	0.38	1.00
CN	-0.53	0.02	0.22	-0.33	0.22	-0.22	0.09	0.37	0.93
S	0.53	-0.02	-0.22	0.33	-0.23	0.22	-0.09	-0.37	-0.92
w	0.51	0.27	-0.42	0.45	0.06	0.42	-0.12	-0.32	-0.22
OMC	0.42	0.03	-0.46	0.44	0.18	0.46	-0.03	-0.50	-0.34
TES	-0.46	0.02	0.01	0.01	-0.05	-0.01	0.01	0.60	0.63
τ	-0.30	-0.06	0.22	-0.13	-0.31	-0.22	-0.52	-0.45	-0.08
K_i	-0.47	0.07	0.14	-0.08	-0.18	-0.14	-0.21	0.59	0.56

	Q	CN	S	MC	OMC	TES	Tau	Ki
α	-0.45	-0.53	0.53	0.51	0.42	-0.46	-0.30	-0.47
β	-0.03	0.02	-0.02	0.27	0.03	0.02	-0.06	0.07
Sand	0.09	0.22	-0.22	-0.42	-0.46	0.01	0.22	0.14
Silt	-0.23	-0.33	0.33	0.45	0.44	0.01	-0.13	-0.08
Clay	0.31	0.22	-0.23	0.06	0.18	-0.05	-0.31	-0.18
S+C	-0.09	-0.22	0.22	0.42	0.46	-0.01	-0.22	-0.14
I	0.33	0.09	-0.09	-0.12	-0.03	0.01	-0.52	-0.21
BD	0.38	0.37	-0.37	-0.32	-0.50	0.60	-0.45	0.59
V_t	1.00	0.93	-0.92	-0.22	-0.34	0.63	-0.08	0.56
Q	**1.00**	0.93	-0.92	-0.22	-0.34	0.63	-0.08	0.56
CN	0.93	**1.00**	-1.00	-0.16	-0.46	0.63	0.01	0.61
S	-0.92	-1.00	**1.00**	0.15	0.47	-0.62	0.00	-0.60
w	-0.22	-0.16	0.15	**1.00**	0.36	-0.28	0.09	-0.25
OMC	-0.34	-0.46	0.47	0.36	**1.00**	-0.39	0.46	-0.38
TES	0.63	0.63	-0.62	-0.28	-0.39	**1.00**	0.03	0.97
τ	-0.08	0.01	0.00	0.09	0.46	0.03	**1.00**	0.11
K_i	0.56	0.61	-0.60	-0.25	-0.38	0.97	0.11	**1.00**

Table D.2. Best regression models for α.

Model	Silt	Silt+Clay	CN	S	K_i	MSE	F	R^2
1	#			X	#	0.50	11.44	0.70
2	#		X		#	0.50	11.28	0.69
3	#				#	0.50	16.04	0.67
4		#			#	0.52	14.90	0.65
5		#		0	#	0.53	9.60	0.66
6		#	0		X	0.53	9.37	0.65
7		#	#			0.55	12.53	0.61
8	#		#			0.56	11.86	0.60
9	#					0.57	20.86	0.55
10		#		X		0.57	10.71	0.57
11	#			0		0.57	10.57	0.57
12		#				0.58	19.56	0.54
# = Significant Variable (90% level), X = Significant Variable (70% - 90% level), 0 = Insignificant Variable								

Appendix F
Particle Settling Data

After determining a relationship between turbidity and TSS using the methods described in Chapter 4, the effect of particle settling was explored. Chapter 5 discusses how the settlement of particle sizes over time from suspension effects the α and β coefficients in the turbidity and TSS relationship. Figures F.1. through F.15. show the non-diluted turbidity and TSS values for each sample extracted from a bucket of runoff collected from each soil. The sample for the total turbidity of the bucket, when sand settles out, and when silt settles out, representing the total, silt and clay, and clay particles still in suspension were diluted 5 times to create three independent turbidity and TSS relationships. These relationships were evaluated to determining how the coefficients change as particles settle out.

The raw data that was used to calculate dimensionless turbidity and sand, silt, and clay turbidity for each soil in Chapter 5 is shown in Table F.1.

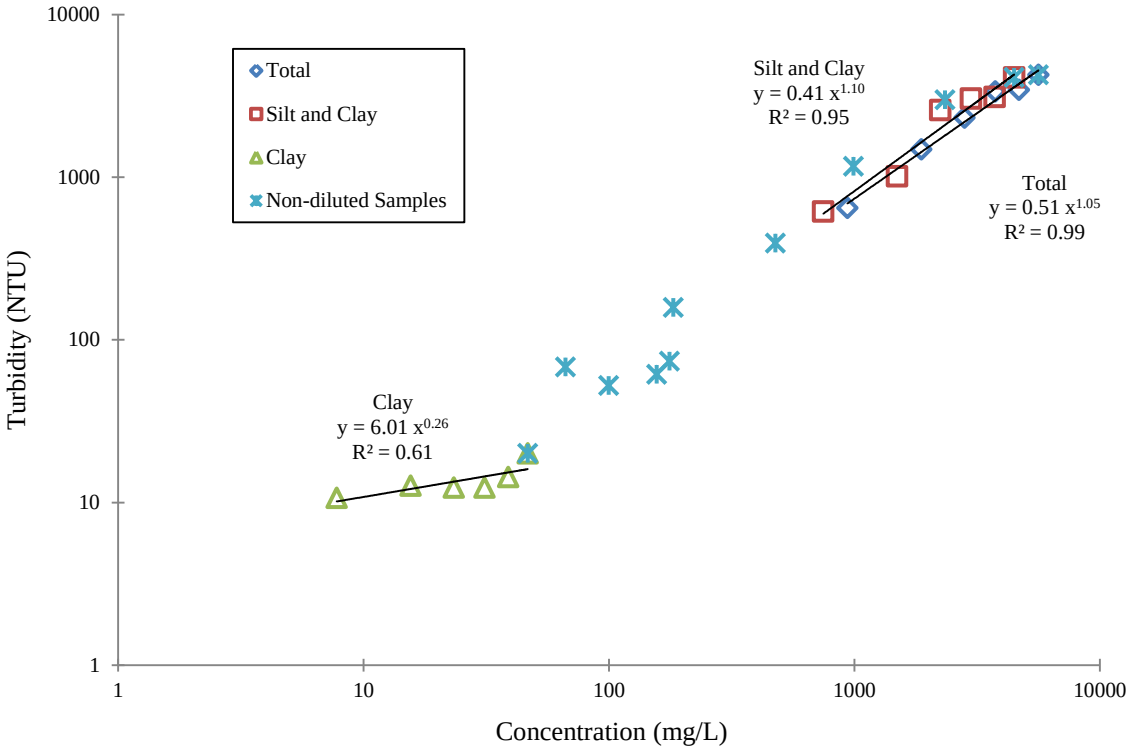

Figure F.1. AH - S Particle Settling

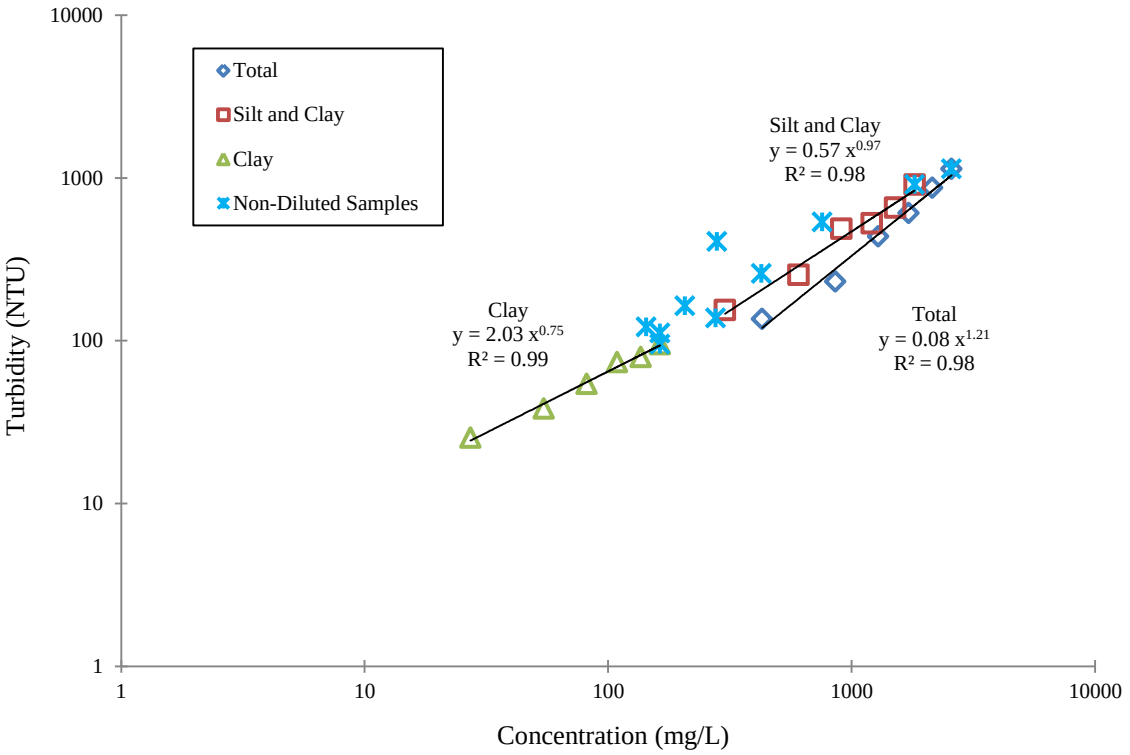

Figure F.2. AH - T (2) Particle Settling

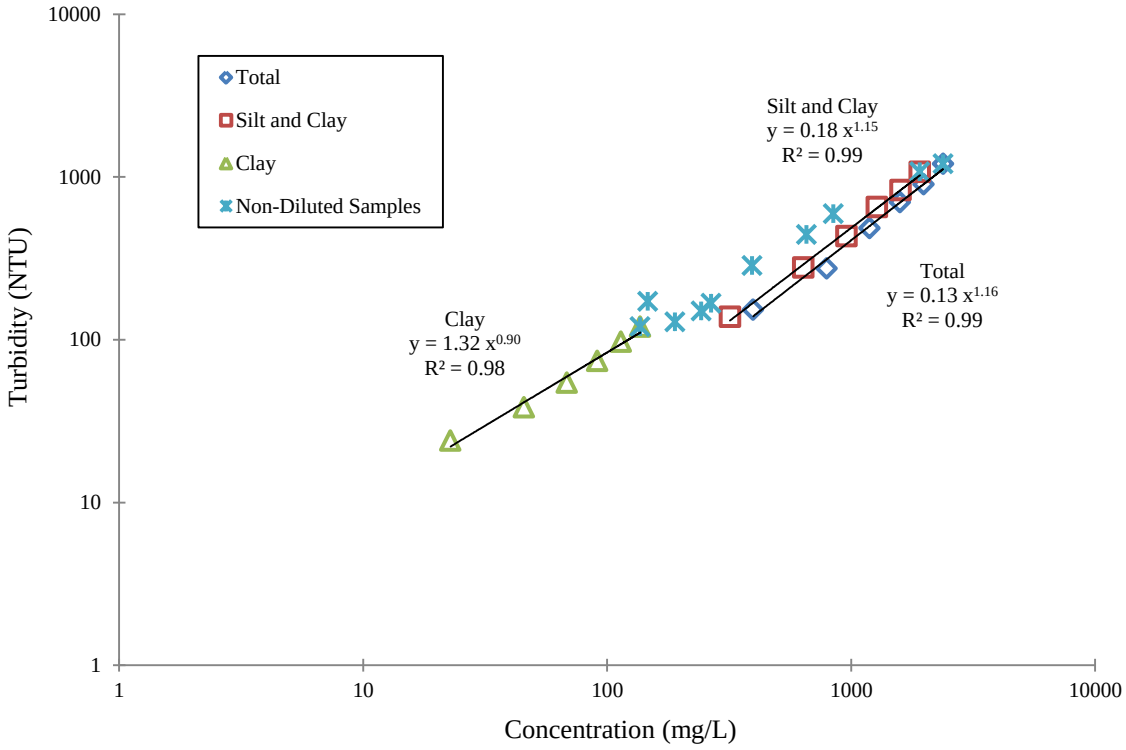

Figure F.3. AH - T (3) Particle Settling

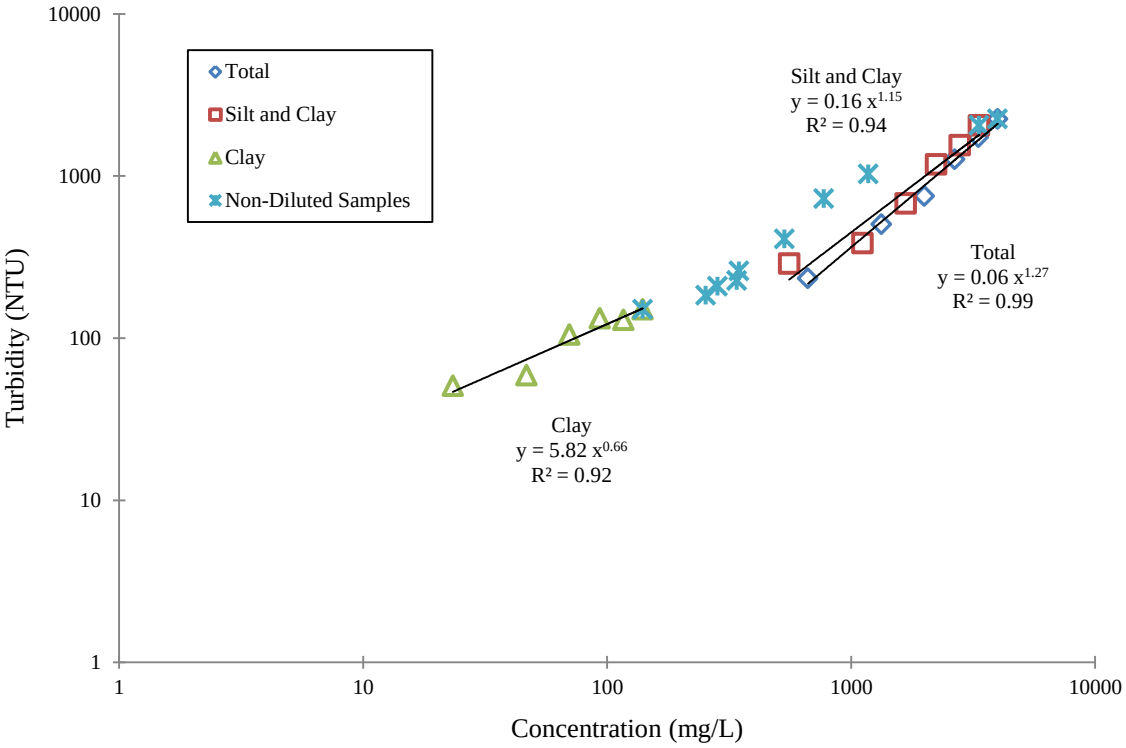

Figure F.4. AH - T (4) Particle Settling

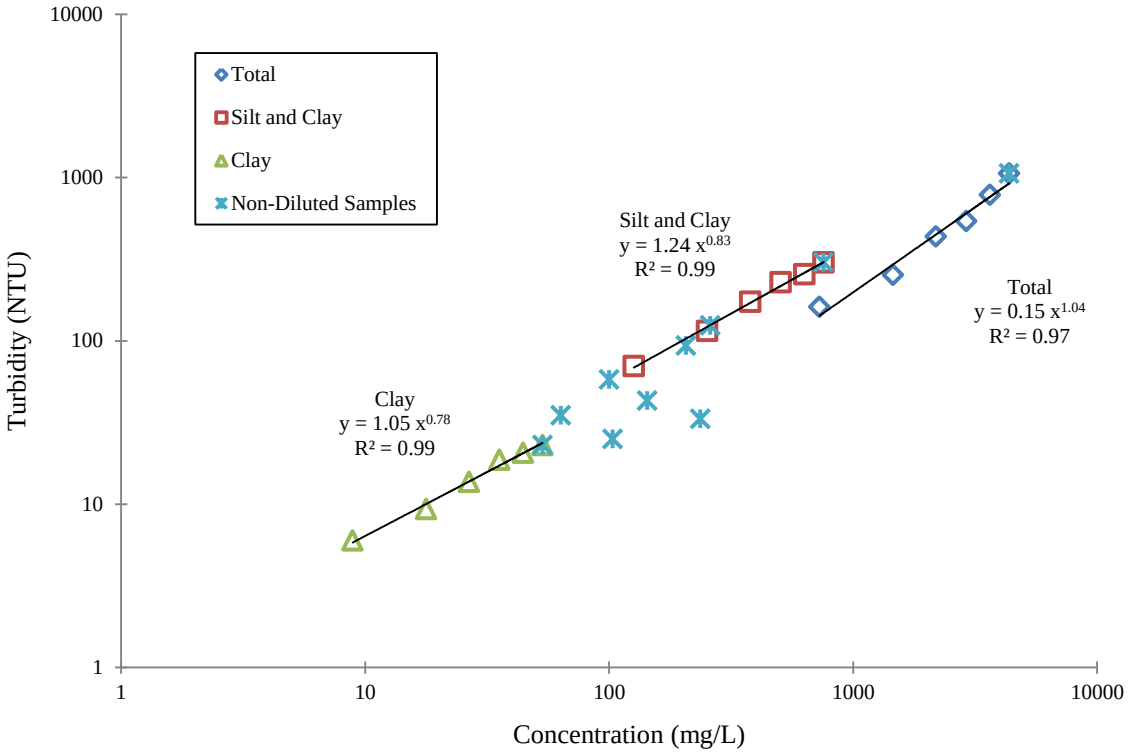

Figure F.5. AH - T (5) Particle Settling

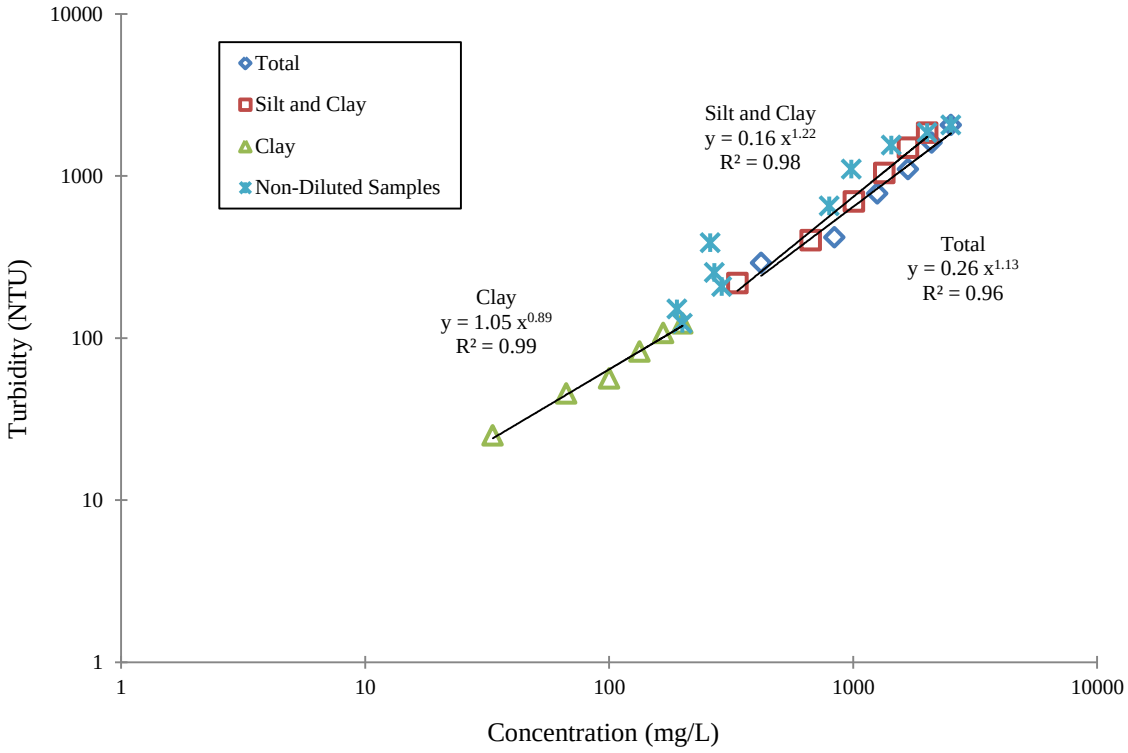

Figure F.6. CTY - S Particle Settling

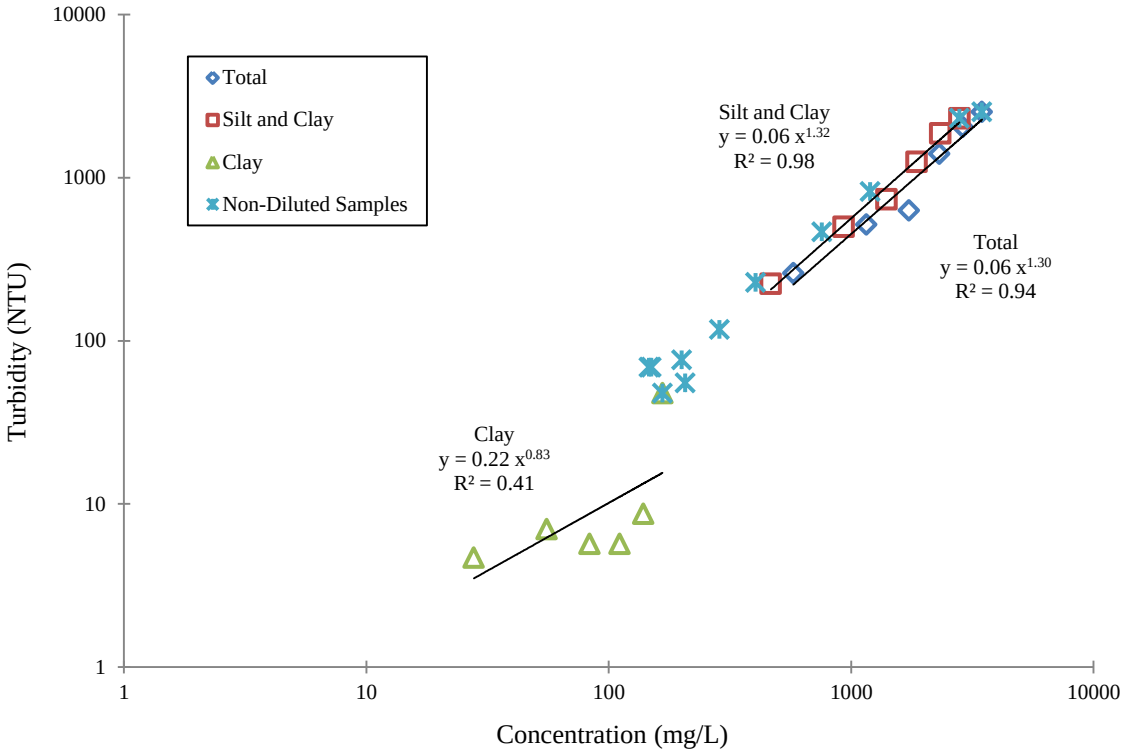

Figure F.7. CTY - T Particle Settling

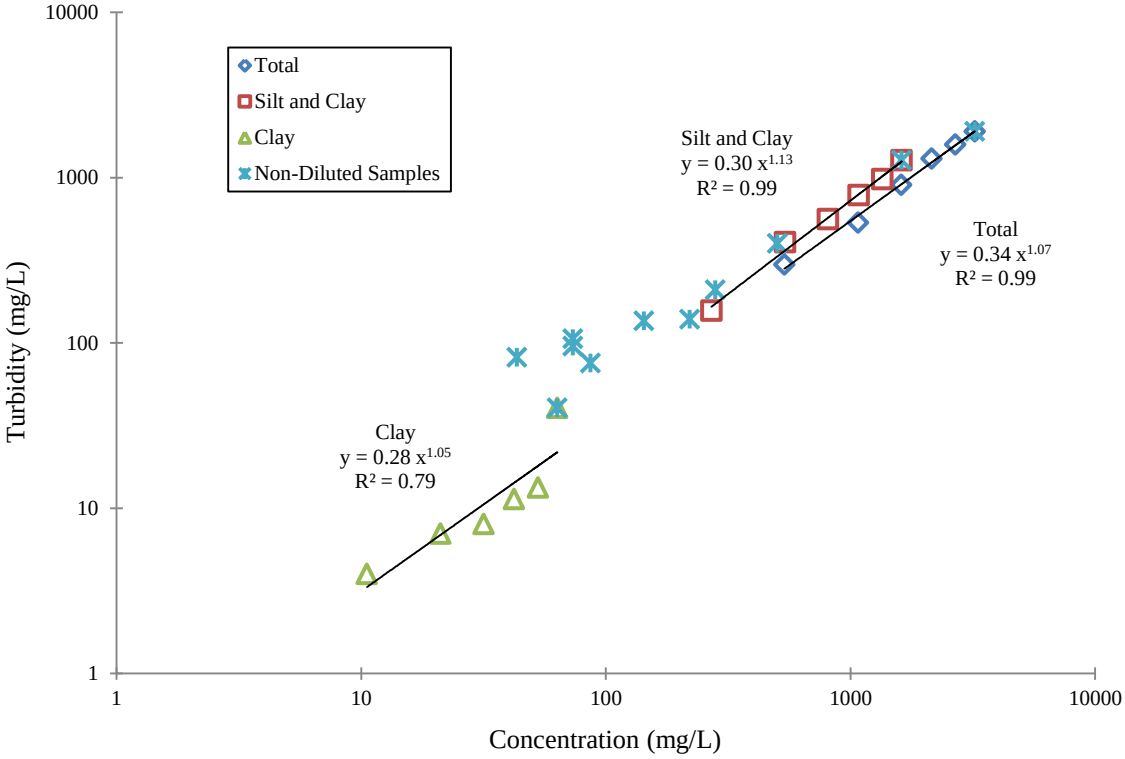

Figure F.8. Dul - S Particle Settling

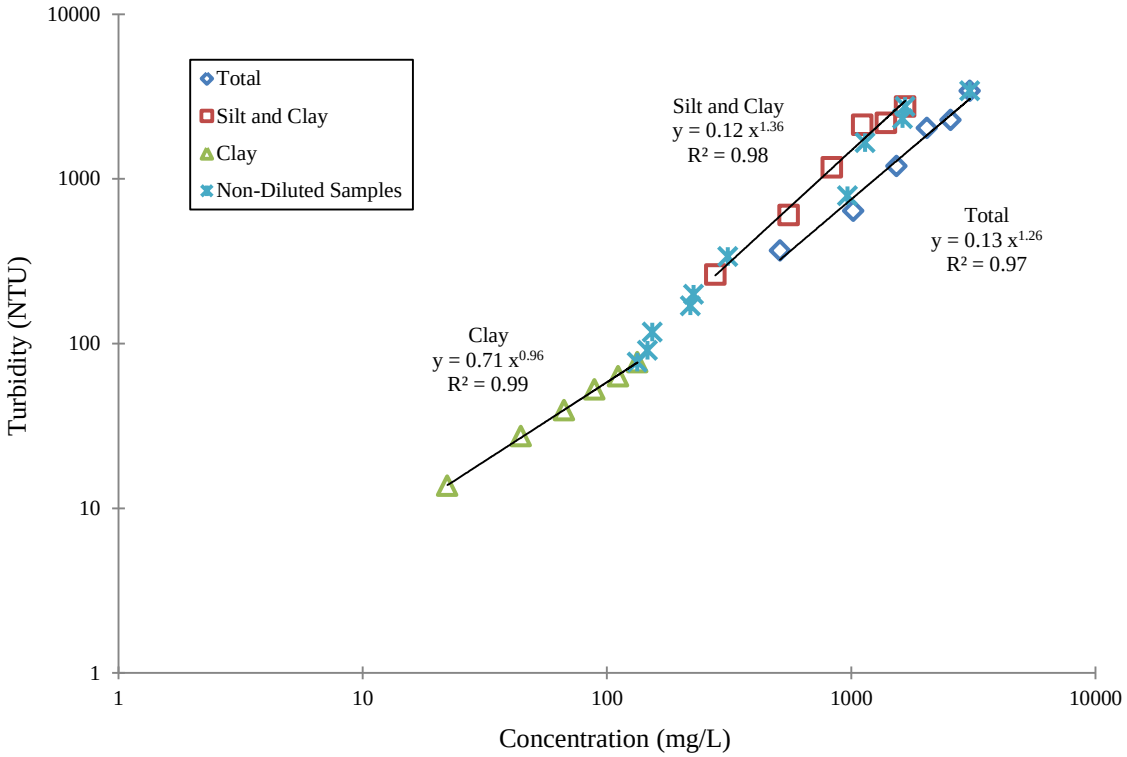

Figure F.9. Hast - S Particle Settling

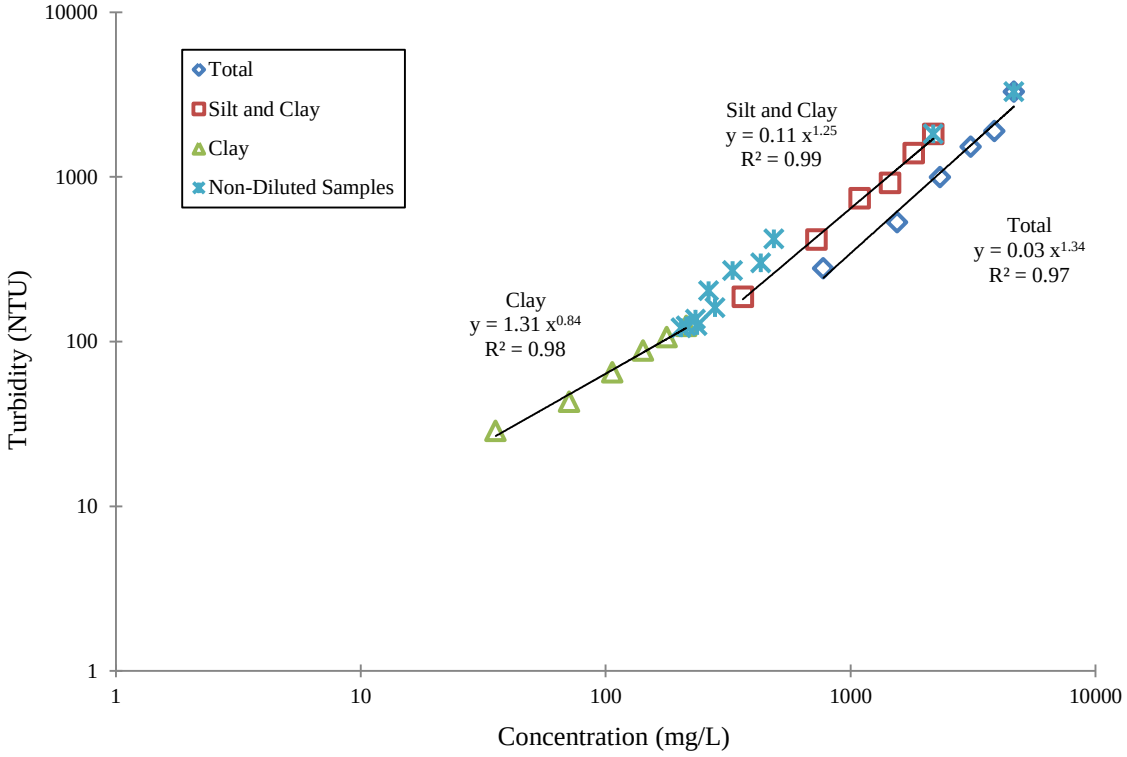

Figure F.10. Hast - T Particle Settling

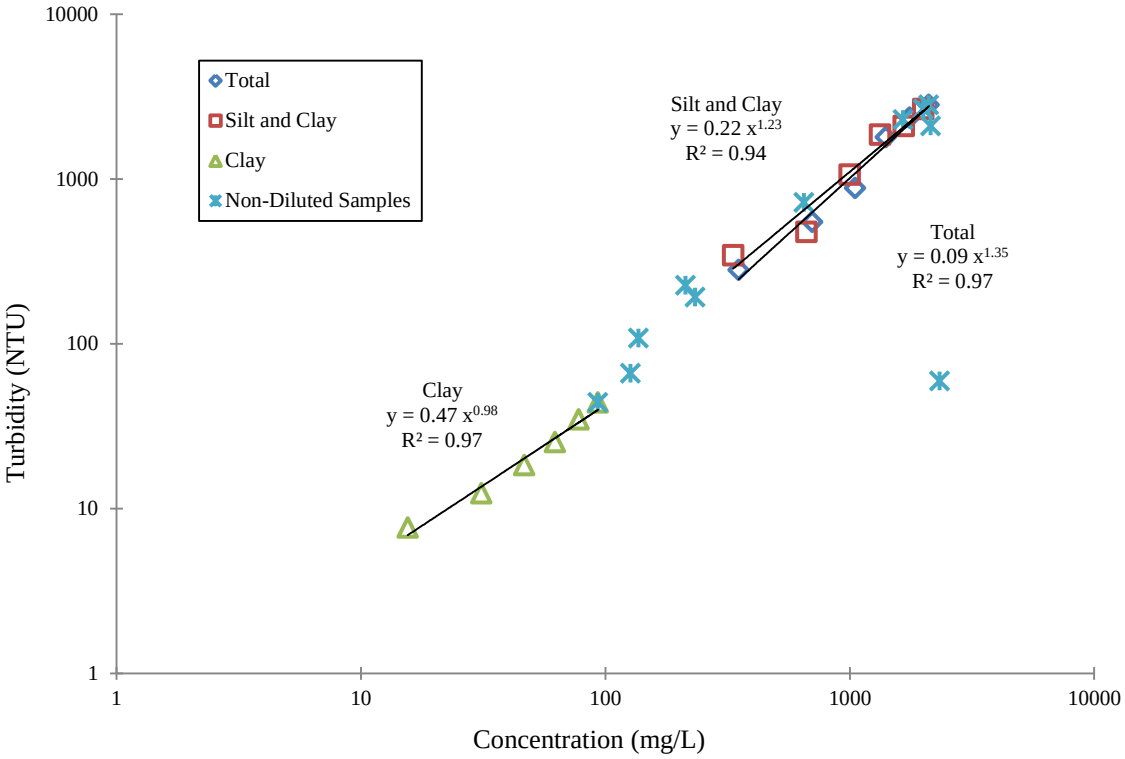

Figure F.11. OV - S Particle Settling

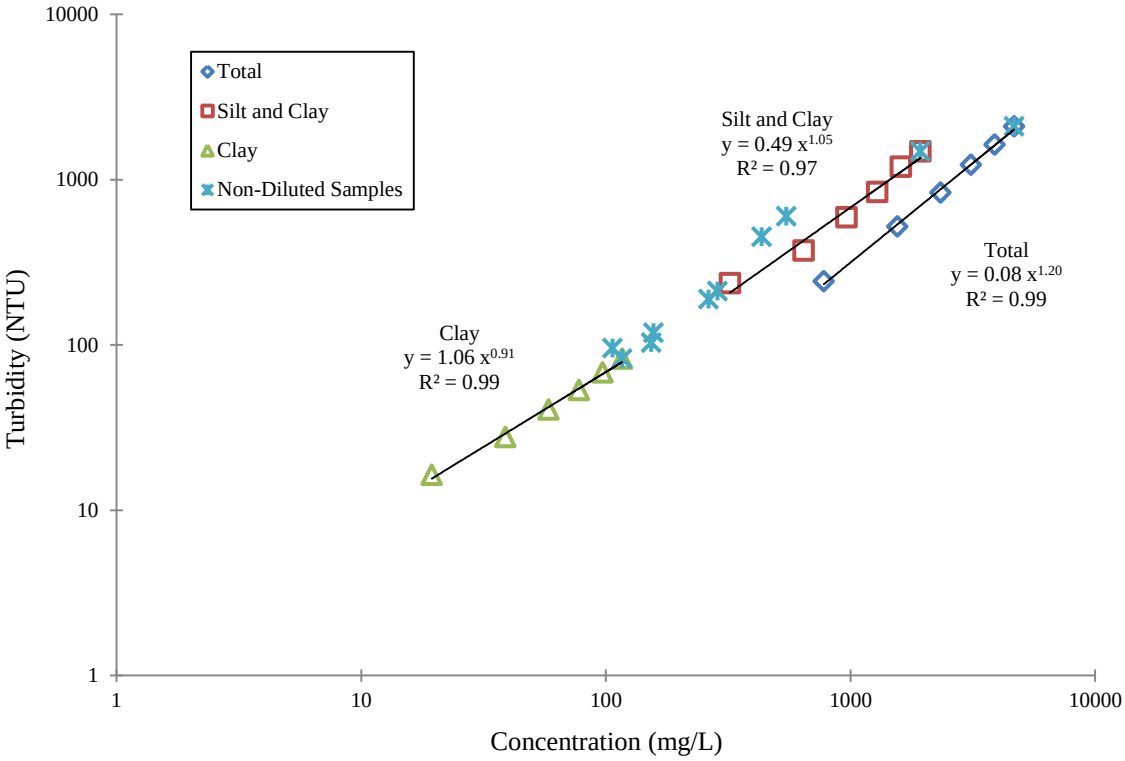

Figure F.12. Soil A Particle Settling

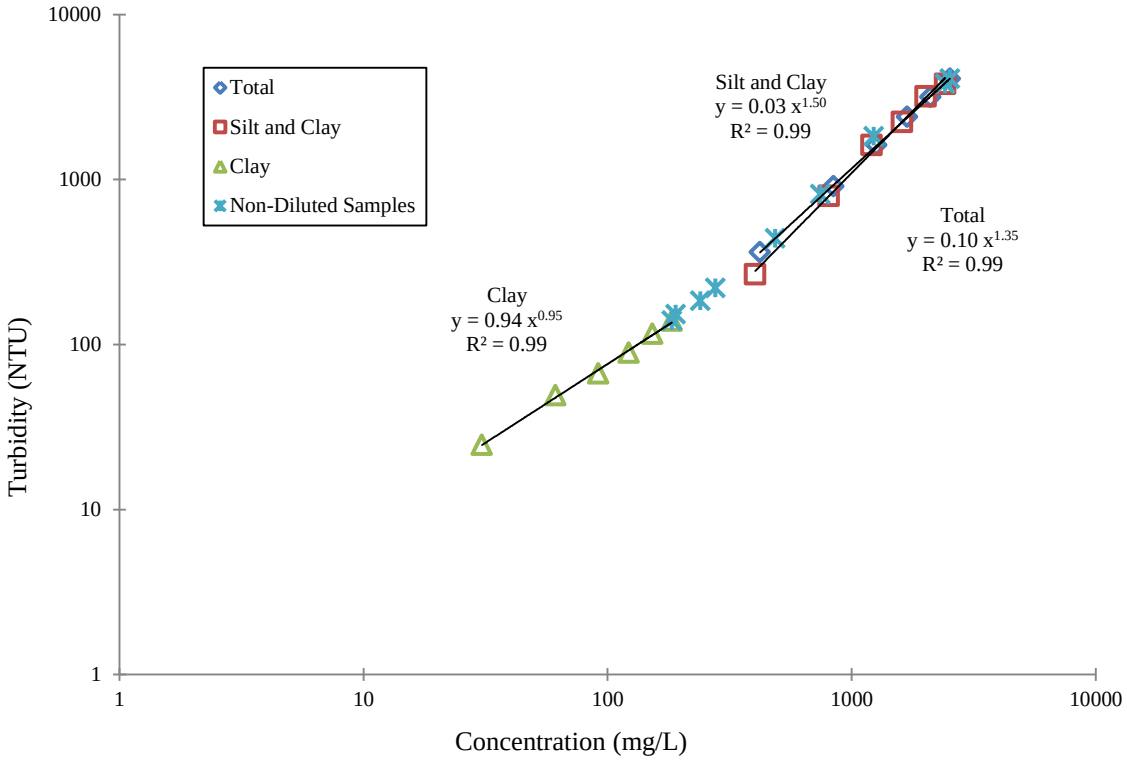

Figure F.13. Soil B Particle Settling

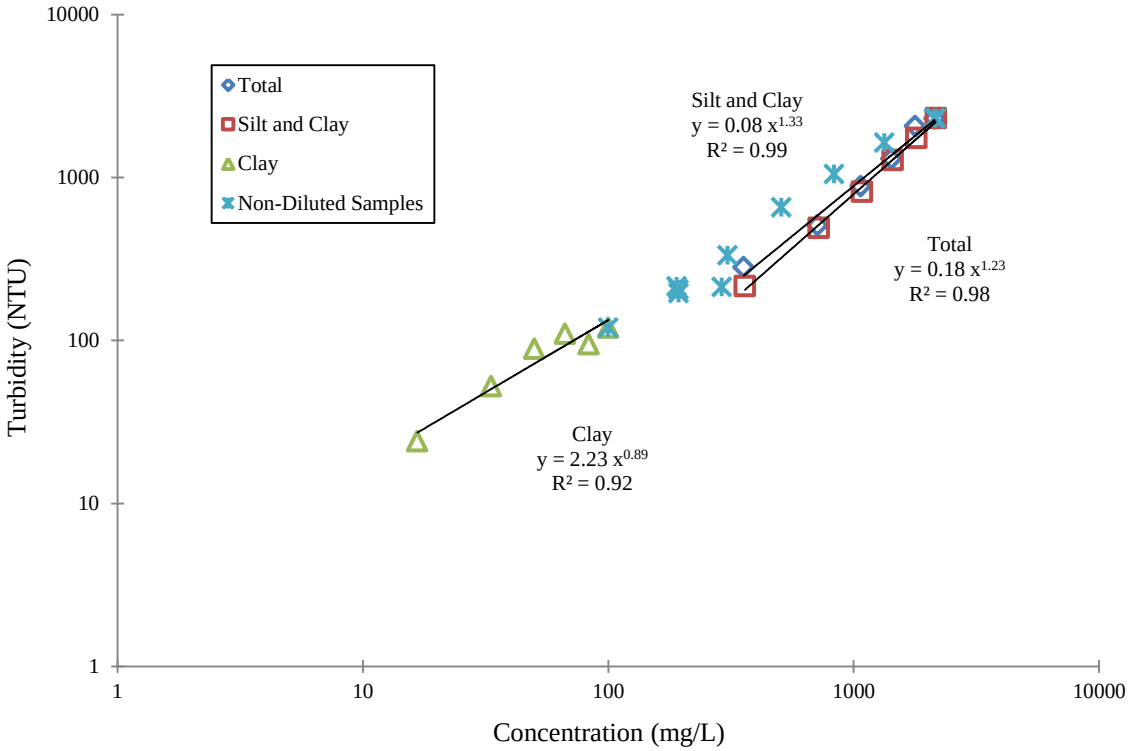

Figure F.14. TH - S Particle Settling

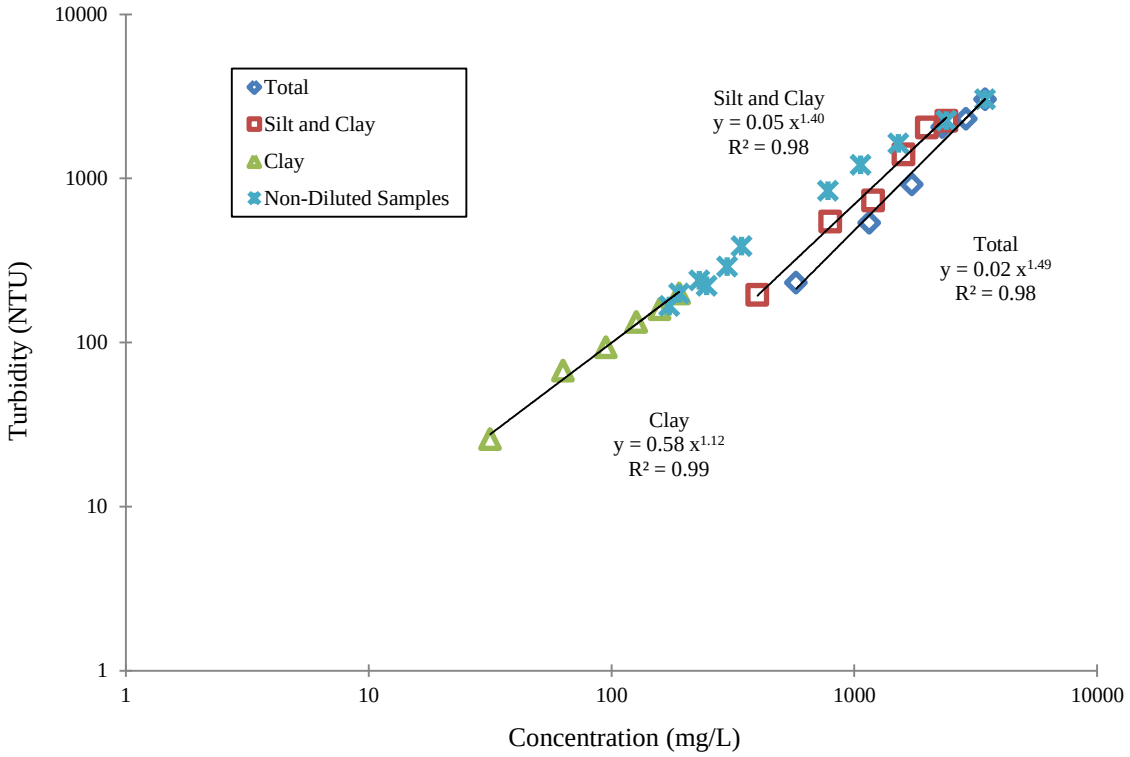

Figure F.15. TH - T Particle Settling

Table F.1. Particle settling data for each soil.

Row	Symbol	AHS	AHT 1	AHT 2	AHT 3	AHT 4	AHT 5	CTYS	CTYT
1	F_{total}	1.00	1.00	1.00	1.00	1.00	1.00	1.00	1.00
	F_{sc}	0.79	0.93	0.70	0.80	0.84	0.17	0.80	0.81
	F_c	0.007	0.037	0.063	0.057	0.029	0.012	0.079	0.048
	% Clay	0.675	3.659	6.347	5.742	2.858	1.221	7.947	4.808
2	T_{total}	4246.7	2605.0	1135.0	1201.3	2243.0	1058.7	2063.7	2528.3
	T_{sc}	4097.7	1900.3	911.0	1075.7	2046.3	302.0	1845.3	2311.7
	T_c	20.0	121.3	95.3	120.3	150.0	23.0	122.7	47.7
3	β_0	1.05	1.38	1.21	1.16	1.27	1.04	1.13	1.30
	α_0	0.514	0.047	0.080	0.133	0.057	0.148	0.262	0.057
4	ω_{total}	1.00	1.00	1.00	1.00	1.00	1.00	1.00	1.00
	ω_{sc}	0.98	0.99	0.97	0.98	0.98	0.84	0.98	0.98
	ω_c	0.55	0.70	0.75	0.74	0.68	0.60	0.77	0.73
5	ν_{total}	1.00	1.00	1.00	1.00	1.00	1.00	1.00	1.00
	ν_{sc}	1.22	1.07	1.35	1.20	1.16	4.44	1.21	1.20
	ν_c	70.36	16.70	10.45	11.38	20.60	42.47	8.63	13.23
6	T_{sand}	1227.4	338.5	434.2	344.9	515.9	777.7	615.4	676.7
	T_{silt}	3318.4	2185.5	605.4	774.0	1585.6	145.0	1220.2	1596.5
	T_{clay}	297.1	66.9	85.1	105.7	69.8	76.6	230.7	94.6
7	Actual	4246.7	2605.0	1135.0	1201.3	2243.0	1058.7	2063.7	2528.3
	Est.	4842.9	2590.9	1124.7	1224.6	2171.3	999.2	2066.3	2367.9
	Error	14.0	0.5	0.9	1.9	3.2	5.6	0.1	6.3
8	T_{sand}*	1.00	1.00	1.00	1.00	1.00	1.00	1.00	1.00
	T_{silt} *	0.80	0.89	0.66	0.79	0.79	0.24	0.79	0.74
	T_{clay}*	0.065	0.027	0.082	0.094	0.033	0.083	0.126	0.042
9	T_{sand}*	1.00	1.00	1.00	1.00	1.00	1.00	1.00	1.00
	T_{silt} *	0.96	0.96	0.90	0.94	0.93	0.95	0.94	0.91
	T_{clay}*	3.90	0.68	0.86	0.96	0.96	2.65	0.95	0.75
10	Sand	0	0	0	0	0	0	0	0
	Silt	20.7	7.7	34.8	19.4	18.3	297.0	19.5	22.7
	Clay	5860.6	2466.6	948.5	921.7	2791.8	3098.7	652.4	1706.7

Row	Symbol	DulS	HastS	HastT	OVS	Soil A	Soil B	THS	THT
1	F_{total}	1.00	1.00	1.00	1.00	1.00	1.00	1.00	1.00
	F_{sc}	0.50	0.54	0.47	0.95	0.41	0.96	1.00	0.69
	F_c	0.020	0.043	0.046	0.044	0.025	0.073	0.047	0.055
	% Clay	1.965	4.348	4.578	4.430	2.5	7.256	4.680	5.497
2	T_{total}	1902.7	3415.7	3284.3	2812.3	2094.0	4087.3	2304.3	3037.0
	T_{sc}	1270.3	2752.7	1818.7	2654.3	1483.0	3803.3	2312.7	2246.3
	T_c	40.3	77.0	124.0	44.0	82.3	139.7	119.7	198.7
3	β_0	1.07	1.26	1.34	1.35	1.20	1.35	1.33	1.49
	α_0	0.342	0.127	0.034	0.090	0.078	0.102	0.084	0.017
4	ω_{total}	1.00	1.00	1.00	1.00	1.00	1.00	1.00	1.00
	ω_{sc}	0.94	0.95	0.93	1.00	0.92	1.00	1.00	0.97
	ω_c	0.65	0.72	0.72	0.72	0.67	0.76	0.72	0.74
5	ν_{total}	1.00	1.00	1.00	1.00	1.00	1.00	1.00	1.00
	ν_{sc}	1.80	1.68	1.91	1.05	2.12	1.04	1.00	1.37
	ν_c	28.34	14.42	13.77	14.19	23.09	9.32	13.54	11.81
6	T_{sand}	1069.5	1785.1	1838.1	302.1	1378.2	470.9	94.7	1467.7
	T_{silt}	838.3	1285.5	836.9	2465.0	633.1	3620.0	2068.6	1585.9
	T_{clay}	169.7	151.6	82.0	105.0	82.0	207.4	94.2	63.1
7	Actual	1902.7	3415.7	3284.3	2812.3	2094.0	4087.3	2304.3	3037.0
	Est.	2077.4	3222.2	2757.0	2872.1	2093.3	4298.4	2257.4	3116.7
	Error	9.2	5.7	16.1	2.1	0.0	5.2	2.0	2.6
8	T_{sand}*	1.00	1.00	1.00	1.00	1.00	1.00	1.00	1.00
	T_{silt} *	0.53	0.47	0.34	0.93	0.36	0.94	1.00	0.54
	T_{clay}*	0.089	0.049	0.031	0.038	0.041	0.051	0.044	0.021
9	T_{sand}*	1.00	1.00	1.00	1.00	1.00	1.00	1.00	1.00
	T_{silt} *	0.90	0.81	0.74	0.97	0.80	0.98	1.00	0.81
	T_{clay}*	1.88	0.85	0.70	0.69	1.19	0.62	0.72	0.49
10	Sand	0	0	0	0	0	0	0	0
	Silt	70.6	74.0	115.9	4.9	124.3	4.5	0.0	49.3
	Clay	2014.4	1624.6	2189.2	1712.6	2820.8	1121.6	1544.5	2261.7

Table F.2. Row descriptions for Table F.1.

Row #	Description
1	Fraction finer values from laboratory concentration data
2	Laboratory turbidity values as each particle class is removed from suspenstion
3	α_0 and β_0 values from labortory data
4	ω estimated with fitted function: $\omega = 1 + 0.09*Ln(F)$
5	ν estimated with fitted function: $\nu = F^{-0.85}$
6	Turbidity of individual particle classes, found using estimated ω and ν (rows 6 and 8)
7	% Error between actual total turbidity and sum of turbidities found for each particle class
8	Dimensionless T*, found with concentration
9	Dimensionless turbidity, T*, found without concentration
10	% Error between T* using concentration and T* not using concentration

Appendix G
Field Data

The turbidity-concentration relationship is applied to field data in Chapter 6. Maps of the two field sites can be seen in Figure G.1 and Figure G.2.

The turbidity and concentration data for the field samples collected during the August 3 storm on the Arden Hills site are shown in Table G.1. The estimated turbidity values using Model 1 and Model 2 and the particle settling relationships are also shown in Table G.1. Table G.2 shows the estimated α values using Model 1 and Model 2. Table G.3 shows the estimated α and β values after particle settling occurs on the site.

Figure G.3 shows the rainfall data for the May 23 storm on the Bloomington site. The hydrograph for this storm was developed using the time of concentration and watershed area from Table G.4. The hydrograph for the storm (Figure 6.5) was developed assuming the runoff rate was equal to the rainfall excess at each time step.

Figure G.1. Map of Arden Hills construction site obtained from Google Maps.

Figure G.2. Map of Bloomington construction site obtained from Google Maps.

Table G.1. Field data used for Figure 6.3.

Sample #	Time (min)	Conc. (mg/L)	Turbidity (NTU)	Estimated Turbidity (NTU)		
				Model 1	Model 2	No Sand
1	0	4430	>4000	3468.1	3207.9	3052.9
2	5	8620	>4000	8807.2	8146.4	7362.4
3	10	6940	>4000	6501.7	6014.0	5527.4
4	15	5470	>4000	4659.2	4309.6	4034.8
5	20	4730	>4000	3801.3	3516.1	3329.3
6	25	3380	>4000	2374.7	2196.6	2134.8
7	30	9410	>4000	9957.5	9210.5	8267.5
8	35	10930	>4000	12279.9	11358.6	10077.9
9	40	9530	>4000	10135.7	9375.4	8407.3
10	45	8880	>4000	9181.3	8492.5	7657.4
11	50	8050	>4000	8002.8	7402.4	6725.6
12	55	6870	>4000	6410.1	5929.2	5453.8
13	60	7170	>4000	6805.4	6294.8	5770.9
14	65	6710	>4000	6202.1	5736.8	5286.5
15	70	6770	>4000	6279.9	5808.7	5349.1
16	75	6660	>4000	6137.5	5677.0	5234.4
17	80	6190	>4000	5539.8	5124.2	4751.6
18	85	5630	>4000	4851.1	4487.1	4191.6
19	90	5280	>4000	4434.2	4101.5	3850.6
20	95	4210	>4000	3229.4	2987.1	2854.1
21	100	4650	>4000	3711.6	3433.1	3255.0
22	105	3470	>4000	2463.7	2278.9	2210.3
23	110	3940	>4000	2943.2	2722.4	2614.6
24	115	3890	>4000	2891.0	2674.2	2570.8

Table G.2. Calculation of α with Model 1 and Model 2.

	Model 1	Model 2
% Silt	54	54
S	0.163	-
K_i	1.76E+06	-
α	0.028	0.025

Table G.3. Calculation of α and β with particle settling.

F_d	0.54
ν	1.689
ω	0.945
α	0.047
β	1.322

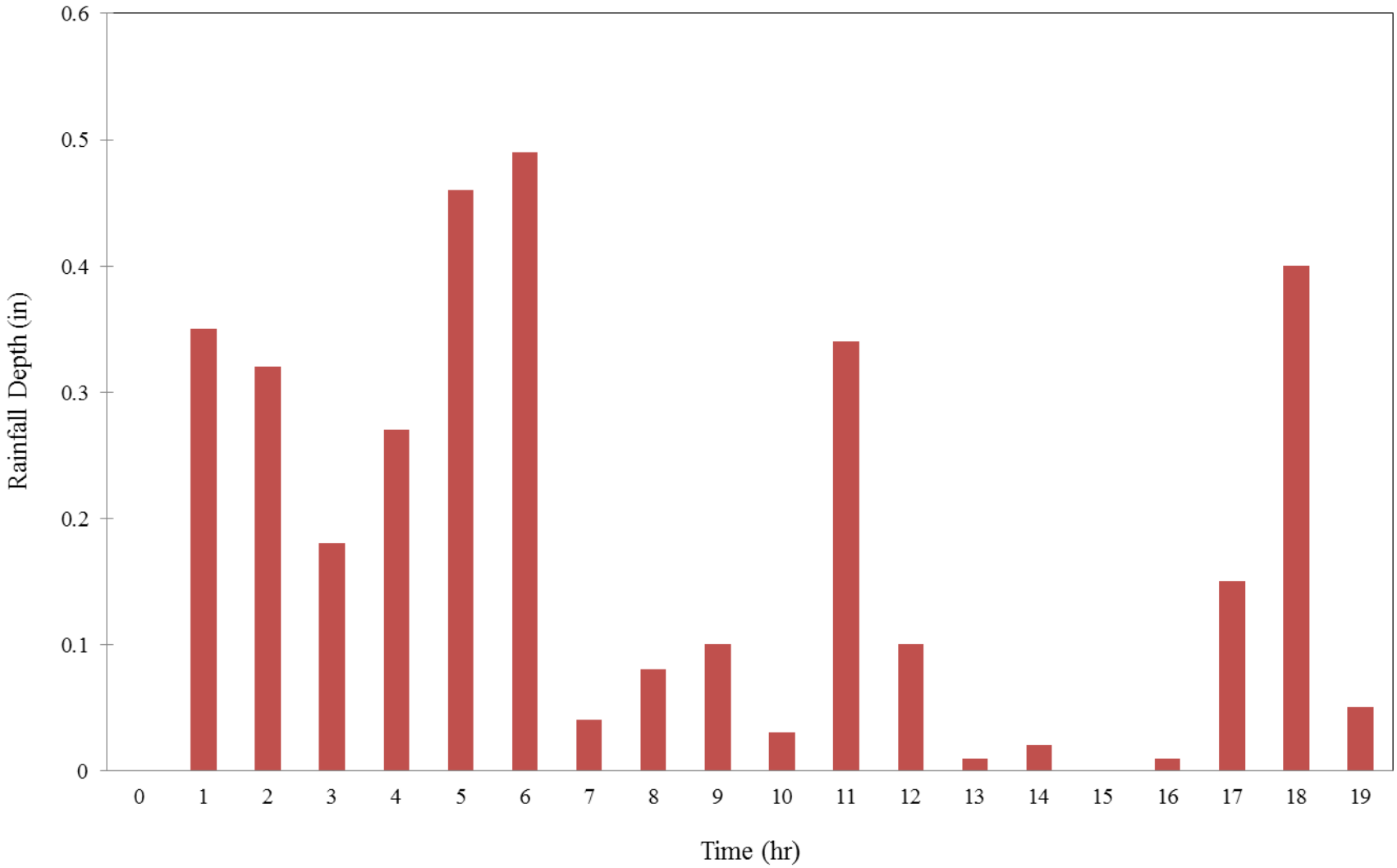

Figure G.3. Rainfall pattern for May 23 storm on Bloomington site.

Table G.4. Watershed information for Bloomington monitoring location.

	Ditch/Grass	Road	Total
Width (ft)	200	30	230
Length (ft)	1500	1500	3000
Slope	0.01	0.02	-
Area (ac)	6.89	1.03	7.92
Time of Concentration (min)	5.28	3.47	8.76